



AALBORG UNIVERSITY
DENMARK

Aalborg Universitet

Small Scale Harmonic Power System Stability

Yoon, Changwoo

DOI (link to publication from Publisher):
[10.5278/vbn.phd.engsci.00163](https://doi.org/10.5278/vbn.phd.engsci.00163)

Publication date:
2017

Document Version
Publisher's PDF, also known as Version of record

[Link to publication from Aalborg University](#)

Citation for published version (APA):
Yoon, C. (2017). *Small Scale Harmonic Power System Stability*. Aalborg Universitetsforlag.
<https://doi.org/10.5278/vbn.phd.engsci.00163>

General rights

Copyright and moral rights for the publications made accessible in the public portal are retained by the authors and/or other copyright owners and it is a condition of accessing publications that users recognise and abide by the legal requirements associated with these rights.

- Users may download and print one copy of any publication from the public portal for the purpose of private study or research.
- You may not further distribute the material or use it for any profit-making activity or commercial gain
- You may freely distribute the URL identifying the publication in the public portal -

Take down policy

If you believe that this document breaches copyright please contact us at vbn@aub.aau.dk providing details, and we will remove access to the work immediately and investigate your claim.

SMALL SCALE HARMONIC POWER SYSTEM STABILITY

**BY
CHANGWOO YOON**

DISSERTATION SUBMITTED 2017



AALBORG UNIVERSITY
DENMARK

SMALL SCALE HARMONIC POWER SYSTEM STABILITY

by

Changwoo Yoon



AALBORG UNIVERSITY
DENMARK

Dissertation submitted in 2017

Dissertation submitted: Jan. 2nd 2017

PhD supervisor: Prof. Claus Leth Bak
Aalborg University

Assistant PhD supervisor: Prof. Frede Blaabjerg
Aalborg University

PhD committee: Professor Birgitte Bak-Jensen (chairman)
Department of Energy Technology
Aalborg University

Professor Paolo Mattavelli
Department of Management and Engineering
University of Padova

Managing Director Dharshana Muthumuni
Manitoba HVDC Research Centre
Manitoba Hydro International Ltd.

PhD Series: Faculty of Engineering and Science, Aalborg University

ISSN (online): 2446-1636
ISBN (online): 978-87-7112-861-1

Published by:
Aalborg University Press
Skjernvej 4A, 2nd floor
DK – 9220 Aalborg Ø
Phone: +45 99407140
aauf@forlag.aau.dk
forlag.aau.dk

© Copyright: Changwoo Yoon

Printed in Denmark by Rosendahls, 2017



CV

Name Changwoo Yoon

Date of Birth 21st May 1984

Place of Birth Hwaseong-si, Gyeonggi-do, Rep. of KOREA

Citizen of Rep. of KOREA

Education 2003 – 2007 B.Sc. in Control and Instrumentation Engineering,
Seoul National University of Science and Technology, Korea

 2007 – 2009 M.Sc. in Control and Instrumentation Engineering,
Seoul National University of Science and Technology, Korea

 2013 – 2016 Ph.D. Studies at Aalborg University, Denmark

Work 2009–2013 Assistant Manager, Advanced Drive Technology Co.
Ltd., Anyang, Korea

ACKNOWLEDGEMENTS

There is no way I could have managed my study without many helps and supports from others. I am so thankful for dear my wife, Hyesun Jung, for enduring hardness well with me in a lonesome foreign place and for taking a full care of lovely son, Hongki.

Whenever I encountered worries in pursuing my study, there was a sincere support and an encouragement from supervisor Prof. Claus Leth Bak and I would like to loud his great supervisions to his students and to express my deepest appreciation to him.

I would also like to acknowledge with much appreciation my friend, Remus Beres, for the enormous time for reviewing all my articles and thesis with his utmost sincerity. From a trivial matter about music or at gym to a matter of great concern in life, his unconventionality and honesty guided me to come up with a better decision.

I was also fortunate to meet the Harmony project members: Tang Yi, Zhen Xin, Haofeng Bai, Miguel Angel, Minghui Lu, Dapeng Lu, Mohammadkazem, Esmaeil, Jun Bum Kwon and Xiongfei Wang. Also, I am thankful for the friends who shared their cultures and spent time with me many times: Hamid Soltani, Casper Vadstrup, Takaaki Tanaka, Qing Jung, Zian Qin, Yanbo Wang, Amir Bahman, Jorge Stark, Ruben Sanchez.

Pastor Lee Hanson, I cannot forget your care and the prayers for m\e and my family as well as your abiding help. My family wasn't able to stay in Denmark without your care and considerations.

Prof. Aniruddha Gole, I appreciate your offer that I could have a privilege to go a study abroad in University of Manitoba, Canada. I could meet such nice friends: Bob & Gale Dewbury, Jack & Miriam Duckworth and Yizhong Hu and other students.

Furthermore, I am thankful for the Korean family in Denmark: Niels Kofoed, Mikyung Sung and their two sons Jinbum Park and Jinsung Park. You cared and supported me as if I were their family member. I wasn't lonely at all with your love.

Lastly, I am also thankful for Prof. Frede Blaabjerg who gave me this opportunity to study in Denmark and Prof. Sewan Choi who recommended me to go Aalborg University as a good place to study.

ENGLISH SUMMARY

The conventional energy generation based on fossil fuels needs to be directed into a more secure and sustainable direction. Ever since the power electronics technology has been introduced, this paradigm has been changed substantially. The use of power electronics in renewable energy sources, such as photovoltaic cells and wind turbines, enables a full control and an efficient conversion of the electrical power. Thus, it facilitates the wide use of decentralized renewable energy generation all over the world.

However, as more renewable energy sources interfaced with power electronics based power units are connected in the existing distribution network, it may lead to a place with a great concentration of power electronics units in a small area. Under certain situations, unexpected abnormal operations may occur and it may create interactions among the installed power electronics units, which may result in a devastating fault in the utility network.

The interaction problem can be explained by the impedance relation at the point where the power electronics units are connected to. The impedance relation reveals the existence of the unstable poles and it can be investigated by the stability analysis tool, such as the Nyquist stability criterion. A case study shows several possible interaction problems that are created in locations with a high penetration of renewable energy generation. The resulted instabilities in the utility network are cleared out by changing the impedance of each power electronics unit, by adding passive damping, active damping or a specialized damping equipment.

In nowadays complex utility networks, it is required to introduce a more straightforward design method that can prevent eventual instabilities. An emerging method is passivity, which can prevent this instability issue by limiting and shaping the individual component impedance within a passive range. This results in a conservative design guideline. Additionally, it is a self-disciplinary design method that can reveal the potentially risky frequency range and it helps to solve the interaction problem efficiently. A simple example on how to use the rule of passivity in stabilizing a small-scale power electronics based power system is given.

Power losses in the system may be seen as a damping factor for stability analysis. Among many other losses in the system, the loss in the magnetic components that are present in harmonic filters may be significant and may create a mismatch between theory and practice. One of the most representative non-linearity exists in the filter inductor and is given by the magnetic hysteresis. By considering its behavior and the loss mechanism, it is investigated how the system damping changes and it reveals the limitation of the conventional linear model approach.

DANSK RESUME

Den konventionelle energiproduktion, baseret på fossilt brændsel, skal ændres til at blive mere sikker og bæredygtig. Siden indførelsen af effektelektronik teknologier har dette paradigme ændret sig betydeligt. Brugen af effektelektronik, i forbindelse med vedvarende energikilder som solceller og vindturbiner, giver fuld kontrol og en mere effektiv konvertering til elektrisk energi. Derfor fremmer det den udbredte brug af decentraliseret vedvarende energiproduktion over hele verden.

Men, når flere vedvarende energikilder med effektelektronik interface, bliver forbundet til det eksisterende distributionsnetværk, kan der opstå zoner med en høj koncentration af effektelektronik enheder inden for et lille område. I nogle specielle situationer, kan der opstå uventede unormale events og det kan medføre utilsigtet interaktion mellem enhederne. Dette kan resultere i ødelæggende fejl i forsyningsnetværket.

Problemet med utilsigtet interaktion kan forklares ved impedansrelationen i det punkt hvor effektelektronik enhederne er forbundne. Impedansrelationen afslører eksistensen af ustabile poler og dette kan undersøges med stabilitetsanalyse værktøjer, som 'Nyquist stabilitets kriterium'. Et casestudy viser flere mulige interaktionsproblemer, der opstår i områder med høj koncentration af vedvarende energikilder. Den resulterende ustabilitet i forsyningsnetværket, bliver afhjulpet ved at ændre impedansen på hver effektelektronik enhed, ved at tilføje passiv dæmpning, aktiv dæmpning eller et specialiseret dæmpningsudstyr.

Med nutidens komplekse forsyningsnetværk, kræves det at der introduceres mere ligetil designmetoder, som kan forhindre eventuel ustabilitet. En nyfremkommet metode er 'passivitet', som kan forhindre ustabilitet ved at begrænse og forme individuelle komponenters impedans indenfor et passivt område. Dette resulterer i en konservativ design guideline. Ydermere, er det en selvdisciplinerende metode, der kan afsløre det potentielt farlige frekvensområde. Dette hjælper med at afhjælpe interaktionsproblemet effektivt. Der gives et simpelt eksempel på, hvordan man bruger passivitetens regler, til at stabiliserer et mindre system, der anvender effektelektronik.

Tab af effekt i systemerne kan ses som en begrænsende faktor for brugen af stabilitets analyse. Blandt mange andre former for tab i systemerne, er tabet i de magnetiske komponenter, der findes i harmoniske filtre, betydeligt og kan give et misforhold mellem teori og praksis. En af de mest repræsentative former for ulinearitet, findes i filterspoler og er givet ved den magnetiske hysteres. Ved at overveje filterspolernes opførsel og mekanismen for tab, undersøges det hvordan systemets dæmpning ændres. Dette afslører begrænsningen i den konventionelle lineære model metode.

TABLE OF CONTENTS

Chapter 1. Introduction.....	13
1.1. Background and Motivation.....	13
1.2. Problem Formulation	15
1.3. Objectives.....	16
1.4. Limitations	17
1.5. Thesis Outline	17
1.6. Publications.....	18
Chapter 2. Network Modeling for Harmonic Studies	20
2.1. Network Components.....	20
2.2. Underground Distribution Cables	21
2.3. Loads.....	24
2.4. Grid-Connected VSC	25
2.4.1. Phase Locked Loop (PLL)	26
2.4.2. Current Control Loop.....	28
2.4.3. Harmonic Filters.....	30
2.5. Summary	31
Chapter 3. Analyzing Tools for Stability Assessment	32
3.1. Introduction.....	32
3.2. Time Domain Analysis Tool.....	33
3.2.1. Dommel’s Approach in PSCAD/EMTDC	33
3.2.2. Nodal Admittance Matrix Solution	34
3.3. Frequency Domain Stability Analysis.....	36
3.3.1. Impedance Based Stability Criterion.....	36
3.3.2. Passivity Stability Criterion	37
3.3.3. The Output Admittance of Grid-Connected VSC	37
3.3.4. Definition of the Non-Passive Range of the Converter Output Admittance	38
3.4. Example of Stability Analysis of Grid-Connected VSC	39
3.4.1. Influence of Pure Inductive Grid Impedance	40

3.4.2. Influence of Pure Capacitive Grid Impedance	41
3.5. Proposed IBSC Method for a Distribution Network with Multiple Connected VSC.....	42
3.5.1. Conditions for Stability	43
3.5.2. Proposed Sequential Stabilizing Procedure.....	44
3.5.3. Practical Example of Stability Analysis	45
3.6. Improved Stability Analysis Method to Deal with Complex Distribution Systems	51
3.6.1. The Minimal Entity Concept.....	51
3.6.2. Proposed Stability Analysis of the Complex Distribution system ^[C.5] ...	53
3.7. Summary	55
Chapter 4. Stabilization of Small Scale Power Systems.....	56
4.1. Stability Evaluation of Multiple Paralleled-Connected Converters	56
4.1.1. Impact of the Grid Impedance Variation.....	57
4.1.2. Influence of the Converters on Stability Analysis.....	60
4.2. Network Stabilization with Active Damping	62
4.2.1. Active and Passive Damping Methods.....	62
4.2.2. Converter Model with Active Damping	63
4.2.3. Network Model for the Load Admittance	64
4.2.4. Characterization of the Individual VSC	65
4.2.5. Stability Analysis of the Cigré Distribution System	66
4.2.6. Stabilization of the Network with Active Damping	67
4.2.7. Interactions between Converters	68
4.2.8. Stabilization of the Network with Reduced Active Damping Capability	69
4.3. Site Selection of Active Damper	71
4.3.1. Active Damper as a Stabilizer	71
4.3.2. Notch Filter Design for an Active Damper	72
4.3.3. Stability Analysis of the Cigré Distribution Network with Varying Grid Impedance	73
4.3.4. Active Damper Placement.....	77
4.4. Summary	80
Chapter 5. Extended Model for Harmonic Stability Study	81

5.1. Introduction.....	81
5.2. Description of Harmonic Instability.....	83
5.2.1. Filter Model.....	83
5.2.2. Controller Design.....	84
5.2.3. Evaluation of Stability Margin by Root Locus.....	85
5.3. Inductor Characterization.....	86
5.3.1. Loss in the Filter Inductors.....	86
5.3.2. Jiles-Atherton Model (JAH) for the Magnetic Hysteresis.....	86
5.3.3. Implementation of the Inductor Hysteresis in PSCAD/EMTDC.....	88
5.4. Harmonic Stability Scenario with Improved Inductor Model.....	89
5.4.1. Inductor Hysteresis Model Specifications.....	89
5.4.2. Influence of the Inductor Hysteresis Model on the Stability Analysis ...	91
5.4.3. Transient Response of the VSC with Hysteresis Model of the Filter Inductor.....	92
5.5. Summary.....	92
Chapter 6. Conclusions.....	94
6.1. Summary.....	94
6.2. Contributions.....	95
6.3. Future works.....	96
Literature list.....	97

TABLE OF FIGURES

Fig. 1.1 Typical PE based renewable power generation system.	13
Fig. 1.2 European LV distribution network benchmark application example [4]. ...	14
Fig. 2.1 Simplified electrical AC power transmission system with renewable energy source [16].	20
Fig. 2.2 Cigré benchmark case with balanced load condition [4].	21
Fig. 2.3 Geometry of underground lines of European LV distribution network benchmark [4].	22
Fig. 2.4 Full impedance magnitude of the underground cable UG1 [18].	24
Fig. 2.5 Simple structure of Grid-Connected VSC in Renewable Power Generation.	26
Fig. 2.6 Power flow vector diagram for: (a) Voltage drop across the line impedance (R_g , L_g); (b) PQ demand at the generator side; (c) Voltage relation and phase angle between V_{PCC} and V_g	26
Fig. 2.7 A merged vector diagram for V_{PCC} and θ calculation.	27
Fig. 2.8 Stationary Reference Frame PLL (SRF-PLL).	27
Fig. 2.9 A small signal representation of VSC control loop.	29
Fig. 3.1 (a) Electrical circuit of an inductor with series resistor; (b) Its equivalent model using the Dommel's approach [34].	33
Fig. 3.2 Exemplary circuits for obtaining network solution: (a) Voltage source based circuit; (b) Nodal admittance matrix with Dommel's modeling.	35
Fig. 3.3 Small-signal admittance representation of: (a) an interconnected system with current source; (b) the minor loop gain representation [J.1].	36
Fig. 3.4 The inverter output admittance Y_{CL} for two different designs of the LCL filter [J.1].	38
Fig. 3.5 Non-passive region of grid inverter derived from the numerator of $\Re(Y_c)$ [J.1].	39
Fig. 3.6 Stable and unstable region of grid inverter in pure inductive grid case: (a) $\omega d < \omega c$, (b) $\omega d > \omega c$ [J.1].	41
Fig. 3.7 Stable and unstable region of grid inverter in pure capacitive grid case: (a) $\omega d < \omega c$, (b) $\omega d > \omega c$ [J.1].	42
Fig. 3.8 Small-signal admittance representation of a small scale inverter-based power system [C.4].	42
Fig. 3.9 Passive component network (PCN) [C.4].	43
Fig. 3.10 The sequential stabilizing procedure: a) An inverter with passive component network; b) The second inverter with a stable admittance network; c) The proposed sequential stabilizing procedure [C.4].	45
Fig. 3.11 Nyquist diagram of the system at Step 1 for the initial condition (blue) and for the stabilized system with additional damping resistor R_d (green) [C.4].	46
Fig. 3.12 Time domain simulation of the converter voltages (upper) and currents (lower) at node R4 for Step 1: (a) Unstable case; (b) Stabilized case [C.4].	47

Fig. 3.13 Nyquist diagram of the system at Step 2 for the initial condition (blue) and for the stabilized system with increased damping resistor R_d (green) [C.4].	48
Fig. 3.14 Time domain simulation of the converter voltages (upper) and currents (lower) at node R4 for Step 2: (a) Unstable case; (b) Stabilized case [C.4].	48
Fig. 3.15 Nyquist diagram of the system at Steps 3 ~ 5 (only the initial condition) [C.4].	49
Fig. 3.16 Time domain simulation of the converter voltages (upper) and currents (lower) at node R4 for: (a) Step 3; (b) Step 4 ~ 5 [C.4].	50
Fig. 3.17 Simple model of the network: (a) Ideal grid with parallel admittance; (b) Ideal grid with series impedance and parallel admittance [C.5].	52
Fig. 3.18 Meaningless parallel compensation from the outside of the unstable node: (a) Full diagram (b) Equivalent diagram [C.5].	52
Fig. 4.1 Single line diagram of 3-phase distribution power system with five inverters in parallel [C.1].	56
Fig. 4.2 The Nyquist plots of the minor loop gain TMG with the different grid inductance LS and its moving trajectory as LS increases [C.1].	57
Fig. 4.3 The Nyquist plots for the marginally stable values of LS [C.1].	58
Fig. 4.4 Time-domain simulation for different values of LS at no-load condition of the PCC voltage (upper) and inverter currents (lower): (a) 155uH; (b) 165uH; (c) 200uH; (d) 260uH; (e) 275uH; (f) 400uH [C.1].	59
Fig. 4.5 The Nyquist plot of the minor loop gain TMA for different scenarios of the load admittances YLA [C.1].	61
Fig. 4.6 Time-domain simulation with full load condition of the converter showing the inverter phase currents (upper) and the PCC voltage (lower) [C.1].	61
Fig. 4.7 Averaged switching model of an inverter with active damping [C.2].	63
Fig. 4.8 PSCAD implementation of an inverter with active damping [C.2].	63
Fig. 4.9 Characteristics of the converters with the parameters given in Table 3.1 [C.2].	65
Fig. 4.10 Operation of the converters connected to an ideal grid voltage [C.2].	66
Fig. 4.11 Stability evaluation of the converters without damping [C.2].	67
Fig. 4.12 Individually stabilized inverters with active damping [C.2].	67
Fig. 4.13 Unstable converter w/o damping and stabilized w/ damping ($K_{AD,Inv.1} = 1$, $K_{AD,Inv.2} = 1$, $K_{AD,Inv.3} = 4$, $K_{AD,Inv.4} = 5$) [C.2].	68
Fig. 4.14 Unstable converters in the network without active damping [C.2].	68
Fig. 4.15 Output current of the converters in case of instability due to interaction between the converters [C.2].	69
Fig. 4.16 Stabilized converters with increased active damping gains ($K_{AD,Inv.1} = 1$, $K_{AD,Inv.2} = 1$, $K_{AD,Inv.3} = 10$, $K_{AD,Inv.4} = 12$) [C.2].	69
Fig. 4.17 Stabilized network by Inv.1 and Inv. 2 with active damping functions ($K_{AD,Inv.1} = 2$, $K_{AD,Inv.2} = 3$) [C.2].	70
Fig. 4.18 Minor loop gain of the stabilized converters with two active damping functions in the Inv. 1 and Inv. 2 [C.2].	70
Fig. 4.19 Active damper of distribution line (a) Single-line diagram of the active damper model; (b) Frequency dependent resistor [C.3].	72

Fig. 4.20 The response of the notch filter: (a) Bode plot; (b) Time domain response (upper) and its FFT (lower) [C.3].	73
Fig. 4.21 Stable and destabilized distribution system with varying grid impedance: (a) Rated grid impedance; (b) Three times higher grid impedance [C.3].	74
Fig. 4.22 Step by step procedure for analyzing the system stability in the weak grid condition [C.3].	75
Fig. 4.23 Stability assessment with different grid impedances (step 5) [C.3].	75
Fig. 4.24 Stability assessment with different grid impedances for individual converters [C.3].	76
Fig. 4.25 Simulated waveforms of the individual converters output current with increased grid impedances [C.3].	77
Fig. 4.26 Stability at node R4, when the active damper is placed at node R16 with different values of the resistance (from 1 Ω to 30 Ω) [C.3].	78
Fig. 4.27 Time domain simulations of the converters output current when: No active damper is connected (upper); The active damper is placed at node R18 (lower) [C.3].	79
Fig. 4.28 Time domain simulations of the converters output current when the active damper is placed at node R9 with the damping resistance value set to 17.5 Ω [C.3].	80
Fig. 5.1 Stability phenomena in power electronics based power system: (a) Circuit diagram of a power converter connected to the AC grid through an LCL filter, where L_1 and L_2 are the filter inductors on the converter and grid side, respectively and C accounts for the filter capacitance. The measured variables can be the converter and grid current (i_1 and i_2), converter modulated voltage (v_M), capacitor voltage (v_C) and the voltage at PCC (v_{PCC}); (b) Grid current waveforms (i_2) approaching instability [J.2].	82
Fig. 5.2 Single-phase small signal model of the grid inverter with LCL filter including its parasitic resistances [J.2].	83
Fig. 5.3 Root locus of the discretized T(s) in z-domain showing the stability margin of the power converter [J.2].	85
Fig. 5.4 Dommel's equivalence of an inductor: (a) Ideal inductor; (b) Practical inductor [J.2].	88
Fig. 5.5 B-H characteristics of the implemented inductor under: (a) Sinusoidal voltage excitation; (b) PWM voltage excitation [J.2].	90
Fig. 5.6 Actual damping effect of the inductor hysteresis on the grid current waveforms for the hysteresis and lumped model of the converter side inductor ($k_p = 6.2$) [J.2].	91
Fig. 5.7 Dynamic response of the grid-connected converter with hysteresis and lumped model of the converter side inductor ($k_p = 5$) [J.2].	92

CHAPTER 1. INTRODUCTION

1.1. BACKGROUND AND MOTIVATION

From the actual increment of global energy consumption, it is expected that the total amount to be doubled in 20 years, mostly in the form of electrical energy [1]. The conventional fossil fuel based energy system has a huge problem in meeting the goal of cutting 40% of the global greenhouse gas emission compared to 1990 level [2] and needs to be steered into a more secure and sustainable direction. An immediate alternative is to install renewable energy sources for increased sustainability of the energy sector. As it is targeted for 2030 by European Union (EU), the renewable energy is believed to take, at least, 27% share of total energy consumption [2]. The amount of money which has been committed to the renewable energy within the institutional framework of EU, has been on a gradually record-breaking process, even the competitive position of fossil fuel generation is still solid from the low oil price [3]. As a result of this massive investment, many renewable resources have been developed and deployed through the existing electrical grid and even it is expected to be installed much more to meet the future consumption expectancy.

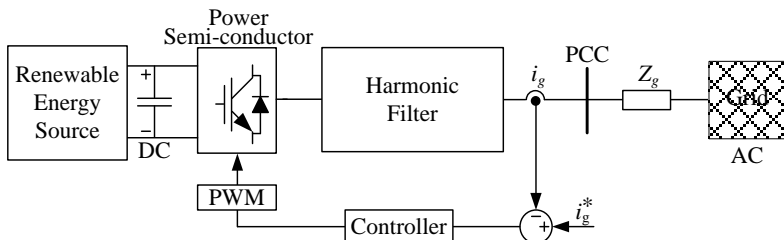


Fig. 1.1 Typical PE based renewable power generation system.

Traditionally, there have been large power generation plants, which are located at places where the geographical and environmental requirements are favorable, such as thermal, hydro and nuclear power plants. The energy sources were centralized, in order for the electricity operator to have full controllability of the power quality and to control the entire process, such as energy generation, transportation and utilization. Since power electronics (PE) technology has been introduced, this paradigm has been being changed substantially. PE can be seen as a key technology, which converts electrical energy into usable electrical form by using power semiconductor devices and harmonic filters. Fig. 1.1 shows a typical simplified PE based renewable power generation system. The energy supplied from Renewable Energy Sources (RES) is modulated by the Power Semiconductor device and filtered out by the Harmonic Filter. The Harmonic Filter output current i_g is adjusted by the Controller with its current reference i_g^* and is injected to utility Grid via the Point of

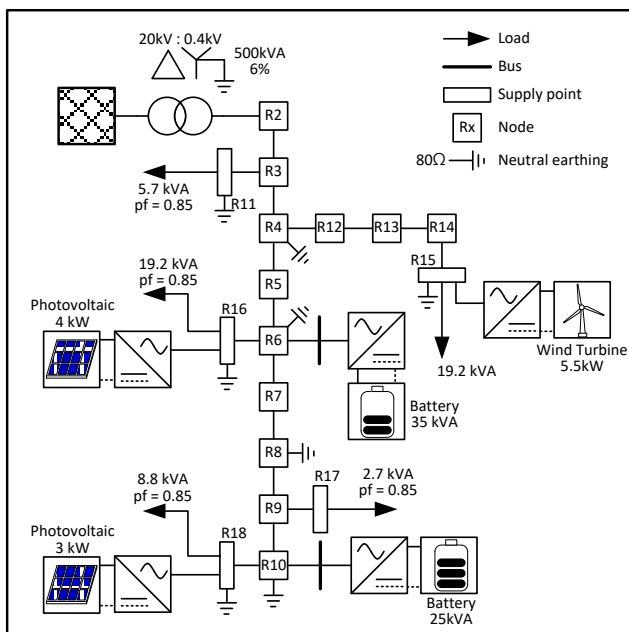


Fig. 1.2 European LV distribution network benchmark application example [4].

Common Coupling (PCC). Whenever the electrical energy is given in any form, the PE enables a full control and an efficient conversion of the electrical power, thus it facilitates the wide commercialization of renewable energy generation all over the world.

With increased share of renewables in the power system, the importance of the conventional centralized generation is relatively decreased and the decentralized power generation concept is gaining more attention [4]. Instead of having unidirectional power flow, the decentralized operation of the power system leads to bidirectional power flow and it has to be managed actively in order to have sustainable operation, regardless of the power generation condition [5], [6]. Therefore, the decentralized electrical power system is expected to become more complex, which makes it more difficult to manage the overall operation of the network at the same time. As an example, a benchmark case of an European low-voltage distribution network for studying distribution network performance in a residential area is depicted in Fig. 1.2 [4]. It contains energy storage battery units, photovoltaics (PV), a wind turbine and residential loads, which are expected to be frequently present in the future grid system. At the same time, those energy sources, which are interfaced with PE based power units and are connected via distribution lines, may be located near each other and there may lead to a place with a great concentration of PE based power units.

Recent reports [2], [3] shows how unexpected and severe problems may arise in the power distribution system with renewable energy sources. For example, it was Dutch networks with high penetration of PV generation that had showed that PV inverters, under certain circumstances, switched off undesirably, or exceeded the harmonic regulations [7]. Even when all the PV inverters individually satisfy harmonic output regulations, the power quality standards at PCC might be exceeded [7]. In a wind power plant (WPP) in China (Shanxi province), problems appears with 17th and 19th order harmonics that broke some components in the grid-connected inverters [8]. Also, large scale off-shore wind farms in Denmark and Germany have been experiencing unexpected automatic shutdowns from the underground power cable fault [9]–[12].

These accidents may be explained by resonating behaviors of the newly installed PE based power system components. Unlike the conventional power system, the PE based power components use high-frequency switching converters to improve performance and to reduce losses. The PE based power unit must include power filters, such as Inductor (L) filter, Inductor-Capacitor (LC) filter or Inductor-Capacitor-Inductor (LCL) filter, which are highly reasonable and may create potential resonance circuits in connection with the power system components. Since it has become very difficult to predict the potential problems [13], the influence of PE based power component in the existing power system has to be investigated thoroughly.

The motivation of this PhD study is to predict and to find potential problems, which are not fully identified and discussed until now for the upcoming decentralized and complex PE based power systems. Specifically, it is mainly about the analysis of the instability caused by high frequency resonances or interactions between PE based units in a given test system. It is required to derive a more simple method to predict problems and to find solutions by using some of the conventional stabilizing techniques.

This project is one of the sub-tasks of “HARMONY” project, which aim is to investigate the overall problem related to harmonics in power system of the future. It covers the full span of renewable power production, distribution and consumption, iterating towards a complete assessment and design methods for future power electronics based power systems.

1.2. PROBLEM FORMULATION

There has been a general agreement that those stability problems reported in some power systems, are closely related to the PE based power components which deployed in recent times. These include high frequency harmonic components, which may cause unpredictable behavior that makes even researchers to have very little progress towards understanding and preventing the stability issues associated

with PE based power components. Additionally, finding a more effective way to solve and prevent the problem during the design stage is also important.

1.3. OBJECTIVES

The main goal of this study is to answer the following questions.

- Is it possible to find the unstable condition in a PE based power system caused by the interactions between the interconnected PE units?

Firstly, the existence of the problem should be checked in the beginning. According to the practical parameter values in the European LV benchmark case [4], possible filter values and controller gains for PE units are investigated. From varying some of the parameters in the system, the unstable behavior may arise and can be found.

- Is it possible to analyze and predict those interactions by using an analytical tool?

According to the previous problematic cases, the problem may be reproduced by a mathematical model based tool. As the system is connected in the electrical domain, the only tool to model the overall system is its impedance/admittance based analysis method. Adopting a technique that enables the stability analysis based on impedance/admittance relation, the system stability can be investigated and can give us a design guide-line of the entire system.

- How those instabilities associated with PE based units can be stabilized?

There are several ways to stabilize the PE unit, by giving additional damping. The instability of the overall system also can be interpreted as some of the PE units in the network become unstable locally. By giving additional damping to the PE units or giving damping to the network may solve the instability issue and prevent the problem.

- Can we find a more effective way to stabilize the system? Or can we find a more suitable place to stabilize the system?

By adopting the impedance/admittance based stability analysis tool for a wide frequency range, the stability information of each node in the overall network can be obtained. Analyzing the distribution of the stability information, the optimal or the most effective location may be diagnosed.

- Can we get more accurate result?

By including the extended model of the components in the PE unit, the system stability margin may be changed and become more accurate.

1.4. LIMITATIONS

In this thesis, all the PE units in the distribution system are assumed to be Voltage Source Converter (VSC) with LCL filter which is the most typical structure for nowadays renewable energy generation system. The network is three phase four wire system of low voltage range (0.4 kV) and with balanced load condition. Hence, the positive sequence impedance of the cable is considered for each phase of the network. As the frequency range of interest is closely related to the natural resonance frequency of the PE units, which is in kilo hertz range due to the LCL filter resonance frequency, this study only focuses on that frequency region. Since the low frequency instability problems appears near to the fundamental frequency [14] or even lower than the line frequency [15] and is at least several decays lower than the LCL filter resonance frequency, they can be decoupled each other. Therefore, the influences of the Phase Locked Loop (PLL), power and voltage control loops are not considered.

1.5. THESIS OUTLINE

This thesis discusses about the interaction problems which might appear in the decentralized power generation system with high penetration of renewable energy resources. The main focus is to find the high frequency instability issues for a given network and to build models based on the impedance relation in order to assess the system stability. From the obtained impedance model, we can identify the problematic PE devices for a given small scale power distribution. These units should be taken into account for achieving a stable network. By scanning all nodes' damping margins, the stability map also can be found and effective nodes for solving the instability problem are found. All the procedures contain time domain simulation verification in PSCAD. Additionally, the effect of inductor hysteresis is addressed, since it can affect the stability of the system.

In the introduction chapter, it is briefly mentioned about the growing trend of decentralized power generation system with high share of renewable energy sources. Some of the problems that have occurred recently in networks with high share of PE based sources can reveal the importance of this study. To assess this issue practically, detailed objectives and limitations are presented.

In Chapter 2, constituent units of the distribution network for this study are explained. To focus more on the case and not to be confused by other reasons, the complexities of the model are investigated. Basically, the transmission line, the PE units and the grid impedance are discussed in this chapter.

In Chapter 3, the tools for system stability analysis are explained. Time domain simulation model of the network for PSCAD is explained as well as the principle operation of the Electro Magnetic Transient Program (EMTP). Mathematical model for frequency analysis is explained in this section which is called the Impedance Based Stability Criterion (IBSC). By expanding the IBSC we can further reach to a new concept called Passivity which can give a design guide-line for PE based units, which can guarantee the stable operation. Some other issues in implementing the IBSC are also mentioned.

In Chapter 4, the stability assessments for some case studies are given. Firstly, the unstable operations of the paralleled inverters are investigated and secondly, a more realistic benchmark case has been adopted and the analysis is performed. There are several ways to make the system stable by introducing damping in the system. Passive damping and active damping methods are discussed. If all nodes in the network are investigated, the most adequate location for the stabilization of the network can be found. This may show the risky index of the network.

In Chapter 5, the stability effect of the non-linear model is investigated. One of the most representative non-linearity exists in the filter inductor associated with the PE unit and is given by the magnetic hysteresis. By considering its behavior and the loss mechanism, we can investigate how the system damping changes and it can reveal the limitation of the conventional linear model.

In Chapter 6, the summary and future works are given. It enumerates the main contributions and overall conclusion of this study.

1.6. PUBLICATIONS

Journal publications

[J.1] : C. Yoon, H. Bai, R. N. Beres, X. Wang, C. L. Bak, and F. Blaabjerg, "Harmonic Stability Assessment for Multiparalleled, Grid-Connected Inverters," *IEEE Trans. Sustain. Energy*, vol. 7, no. 4, pp. 1388–1397, Oct. 2016.

[J.2] : C. Yoon, R. Beres, C. Leth Bak, F. Blaabjerg, and A. M. Gole, "Influence of inductor hysteresis on stability analysis of Power Electronics based Power system," *Electr. Power Syst. Res.* (under reviewing)

Conference Publications

[C.1] : C. Yoon, X. Wang, F. M. F. Da Silva, C. L. Bak, F. Blaabjerg, F. F. da Silva, C. Leth Bak, and F. Blaabjerg, "Harmonic stability assessment for multiparalleled, grid-connected inverters," in *2014 International Power Electronics and Application Conference and Exposition, 2014*, pp. 1098–1103.

[C.2] : C. Yoon, X. Wang, C. Leth Bak, and F. Blaabjerg, “Stabilization of Harmonic Instability in AC Distribution Power System with Active Damping,” in Proceedings of the 23rd International Conference and Exhibition on Electricity Distribution (CIRED), 2015.

[C.3] : C. Yoon, X. Wang, C. L. Bak, and F. Blaabjerg, “Site selection of active damper for stabilizing power electronics based power distribution system,” in 2015 IEEE 6th International Symposium on Power Electronics for Distributed Generation Systems (PEDG), 2015, pp. 1–6.

[C.4] : C. Yoon, X. Wang, C. Leth Bak, and F. Blaabjerg, “Stabilization of Multiple Unstable Modes for Small- Scale Inverter-Based Power Systems with Impedance- Based Stability Analysis,” in 2015 IEEE Applied Power Electronics Conference and Exposition - APEC 2015, 2015.

[C.5] : C. Yoon, H. Bai, X. Wang, C. L. Bak, and F. Blaabjerg, “Regional modeling approach for analyzing harmonic stability in radial power electronics based power system,” in 2015 IEEE 6th International Symposium on Power Electronics for Distributed Generation Systems (PEDG), 2015, pp. 1–5.

Co-authored Publications

[C.6] : Y. Tang, C. Yoon, R. Zhu, and F. Blaabjerg, “Generalized stability regions of current control for LCL-filtered grid-connected converters without passive or active damping,” in 2015 IEEE Energy Conversion Congress and Exposition (ECCE), 2015, pp. 2040–2047.

[C.7] : G. De Carne, G. Buticchi, M. Liserre, C. Yoon, and F. Blaabjerg, “Voltage and current balancing in Low and Medium Voltage grid by means of Smart Transformer,” in 2015 IEEE Power & Energy Society General Meeting, 2015, pp. 1–5.

CHAPTER 2. NETWORK MODELING FOR HARMONIC STUDIES

In general, the power grid is divided in three parts given by the power generators that produce electricity, the transmission lines that transport the electricity to the distribution system and finally the loads, which may include residential, commercial or industrial areas. Recently, more renewable energy sources are integrated in the existing power grid, which makes the concept of generation and transmission changing. It is moving from unidirectional power flow to bidirectional power flow and from a centralized power generation to multiple distributed generations. In order to consider these changes in the stability analysis, a benchmark network of the power distribution system is adopted. Then, each of the network components that contributes to the system stability are briefly described individually.

2.1. NETWORK COMPONENTS

The electrical power grid is highly inductive due to the large generators and transmission lines. The power grid, in the simplest form, can be composed of a voltage source connected to a series RL impedance (Resistive and Inductive) and the load, which is shown in Fig 2.1 [16]. The functionality of the power grid can be described by the KVL given by the generator voltage v_g , the voltage drop across the grid impedance v_{RL} and PCC voltage v_{pcc} . At the PCC, the load or the renewable energy source v_{renew} may be interfaced. By expanding this simple configuration, more complicated grid structure can be obtained.

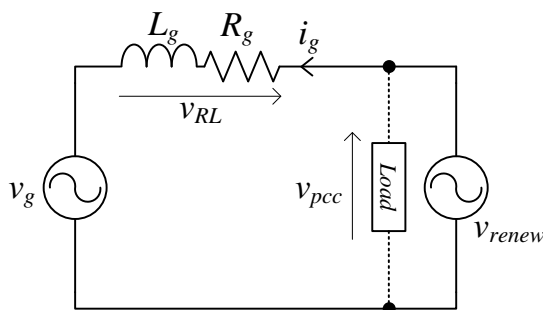


Fig. 2.1 Simplified electrical AC power transmission system with renewable energy source [16].

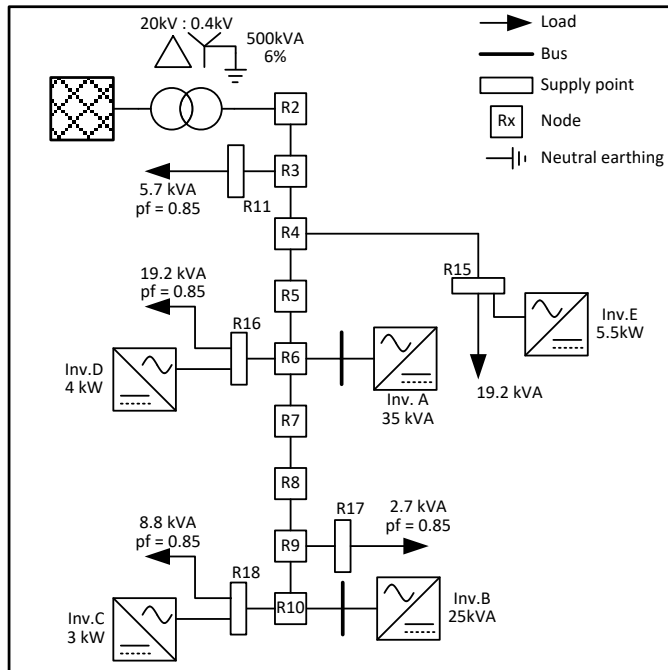


Fig. 2.2 Cigré benchmark case with balanced load condition [4].

Fig. 2.2 shows a Cigré benchmark network of a European LV distribution network with renewable energy sources. The LV distribution network is connected from a MV/LV transformer and is radial structured. It includes one or multiple line segments with the loads/generators connected along them radially. The test system for this study is a three-phase line to line 400 V with 50 Hz tied to the 20 kV feeder via a 500 kVA transformer. Originally, the benchmark network is aimed for microgrid operation [4]. As it is a residential area, the loads are mainly single phase, which may cause inherent load unbalance. Therefore, PE based battery energy storage units are used in order to diminish the load unbalance. Also, the distribution lines are underground cables, whose asymmetry may bring differences in the line impedances between the phases. Different from the original model, in this study, all unbalanced conditions are assumed to be balanced in order for the stability analysis not to be influenced by the unbalance condition. Hence, the stability analysis will focus only on the PE units and their controllers.

2.2. UNDERGROUND DISTRIBUTION CABLES

In order to show details of the underground cables that are used in the benchmark network, the geometry of the underground cables is depicted in Fig. 2.3. Their specifications and installation data are given in Table 2.1 and Table 2.2.

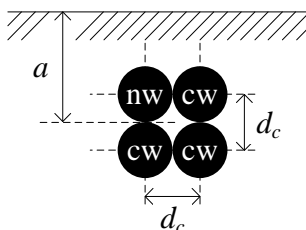


Fig. 2.3 Geometry of underground lines of European LV distribution network benchmark [4].

Table 2.1 Geometry of underground lines of European LV distribution network benchmark [4].

Conductor ID	Type	Cross-sectional Area [mm ²]	Number of strands	R per phase [Ω/km]	d_c [cm]	GMR* [cm]	a [m]
UG1	NA2XY	240	37	0.162	1.75	0.671	0.1
UG2	NA2XY	150	37	0.265	1.38	0.531	0.1
UG3	NA2XY	120	37	0.325	1.24	0.475	0.1
UG4	NA2XY	25	1	1.54	0.564	0.22	0.1
UG5	NA2XY	35	1	1.11	0.668	0.26	0.1
UG6	NA2XY	70	1	0.568	0.944	0.368	0.1

*GMR : Geometric mean radius

Table 2.2 Line parameters of residential feeder of European LV distribution network benchmark [4].

Line segment	Node from	Node to	Conductor ID	R'ph [Ω/km]	X'ph [Ω/km]	l [m]	Installation
1	R1	R2	UG1	0.163	0.136	35	UG 3-ph
2	R2	R3	UG1	0.163	0.136	35	UG 3-ph
3	R3	R4	UG1	0.163	0.136	35	UG 3-ph
4	R4	R5	UG1	0.163	0.136	35	UG 3-ph
5	R5	R6	UG1	0.163	0.136	35	UG 3-ph
6	R6	R7	UG1	0.163	0.136	35	UG 3-ph
7	R7	R8	UG1	0.163	0.136	35	UG 3-ph
8	R8	R9	UG1	0.163	0.136	35	UG 3-ph
9	R9	R10	UG1	0.163	0.136	35	UG 3-ph
10	R3	R11	UG4	1.541	0.206	30	UG 3-ph
11	R4	R12	UG2	0.266	0.151	35	UG 3-ph
12	R12	R13	UG2	0.266	0.151	35	UG 3-ph
13	R13	R14	UG2	0.266	0.151	35	UG 3-ph
14	R14	R15	UG2	0.266	0.151	30	UG 3-ph
15	R6	R16	UG6	0.569	0.174	30	UG 3-ph
16	R9	R17	UG4	1.541	0.206	30	UG 3-ph
17	R10	R18	UG5	1.111	0.195	30	UG 3-ph

Finally, the equivalent positive sequence impedances of the line segments are calculated according to their line length and installation type as shown in Table 2.3.

Table 2.3 Line parameters of residential feeder [4].

Line segment	Node from	Node to	Calculated phase conductor resistance [m Ω]	Calculated phase conductor inductance [μ H]
1	R1	R2	2.85	7.58
2	R2	R3	2.85	7.58
3	R3	R4	2.85	7.58
4	R4	R5	2.85	7.58
5	R5	R6	2.85	7.58
6	R6	R7	2.85	7.58
7	R7	R8	2.85	7.58
8	R8	R9	2.85	7.58
9	R9	R10	2.85	7.58
10	R3	R11	23.12	9.84
11	R4	R12	4.66	8.41
12	R12	R13	4.66	8.41
13	R13	R14	4.66	8.41
14	R14	R15	3.99	7.21
11-14	R4	R15	17.96	32.44
15	R6	R16	8.54	8.31
16	R9	R17	23.12	9.84
17	R10	R18	16.67	9.31

The impedance of the MV/LV transformer is given in Table 2.4.

Table 2.4 Transformer parameters of European LV distribution network benchmark [4].

Primary Voltage [kV, line to line]	Secondary Voltage [kV, line to line]	Connection	Transformer impedance based on sec. side [Ω]	S_{rated} [kVA]
20	0.4	3-ph Δ - Y ground	$0.0032 + j0.0128$	500

In this study, only the positive sequence impedance of the cables is used for considering balanced load condition to reduce the complexity of the analysis. And the capacitive impedance of cable is neglected since the distance of the distribution line is short enough [17]; the capacitive impedance may bring unexpected resonance in the network [9]–[12], but in this case, the frequency of interest is significantly lower than the cable resonance frequency as shown in Fig. 2.4 which is about the worst case resonance behavior of the cable UG1 [18]. The resonance appears around

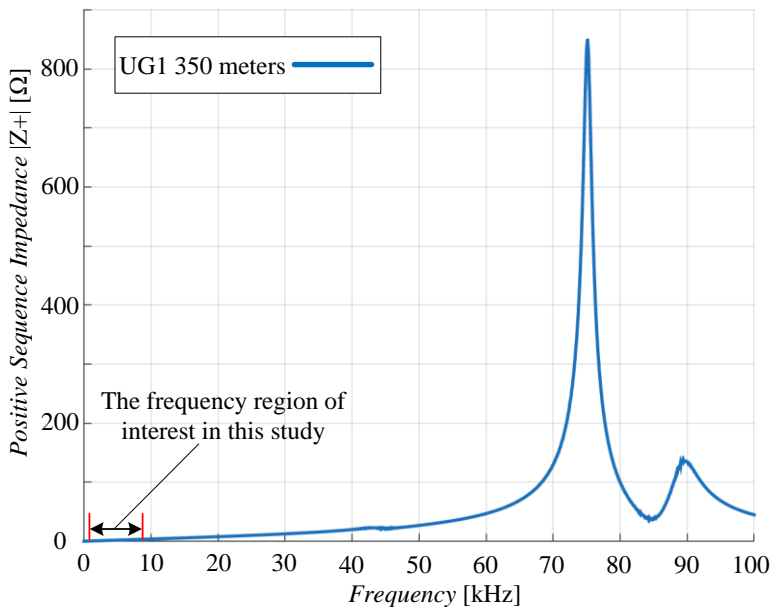


Fig. 2.4 Full impedance magnitude of the underground cable UG1 [18].

75 kHz while the frequency of interest resides within the few kHz range and the resonance frequency is higher when the distance of cable is segmented into several pieces.

2.3. LOADS

In a residential area, there might be nonlinear loads [19], such as diode rectifiers with capacitive load, which makes the impedance of the network to be frequency dependent. This makes the stability analysis of the system more complicated. To focus more on the interactions of the power inverters, all the loads are assumed to be passive and they are characterized by their apparent power and power factor. The relations among the applied voltage V_{Load} , apparent power S , power factor pf , load resistance R_{Load} and load reactance X_{Load} are as follows.

$$\begin{cases} pf = \frac{R_{Load}}{\sqrt{R_{Load}^2 + X_{Load}^2}} \\ S = \frac{V_{Load}^2}{\sqrt{R_{Load}^2 + X_{Load}^2}} \end{cases} \quad (2.1)$$

By solving (2.1) with respect to $\{X_{Load}, R_{Load}\}$ result in,

$$\left\{ \begin{array}{l} R_{Load} = \frac{pf V_{Load}^2}{S} \\ X_{Load} = \begin{cases} \frac{\sqrt{1-pf^2} V_{Load}^2}{S}, & \text{Inductive reactance} \\ -\frac{\sqrt{1-pf^2} V_{Load}^2}{S}, & \text{Capacitive reactance} \end{cases} \end{array} \right. \quad (2.2)$$

For the inductive load case, L_{Load} is calculated as follows:

$$L_{Load} = \frac{X_{Load}}{2\pi f} \quad (2.3)$$

where f is the fundamental frequency of the network.

All loads parameters that are used in the benchmark network are calculated and shown in Table 2.5.

Table 2.5 Load Parameters.

Loads [kVA]	Power Factor [pf]	R_{Load} [Ω]	X_{Load} [Ω]	L_{Load} at 50Hz [mH]
2.7	0.85	16.653	10.321	32.852
5.7	0.85	7.888	4.888	15.561
8.8	0.85	5.109	3.166	10.079
19.2	0.85	2.341	1.451	4.619

2.4. GRID-CONNECTED VSC

Fig. 2.5 shows one simple example of a three-phase grid-connected VSC with LCL filter (single line diagram). The aim for this VSC is to convert DC voltage v_{dc} from renewable energy sources to the AC grid voltage v_{PCC} in order to deliver the generated power to the AC grid. It utilizes modulation techniques [20] via the switching semiconductors, which result in high frequency pulsation voltage v_M that has to be filtered out by the harmonic filter, while maintaining the fundamental frequency information of the v_{PCC} . The harmonic filter should also ensure that the grid current i_g is within the permissible harmonics emission range [21].

By governing i_g , the amount of active power P and reactive power Q generation can be controlled and it enables the 4-quadrant operation, which ensure the bidirectional control of the current [22].

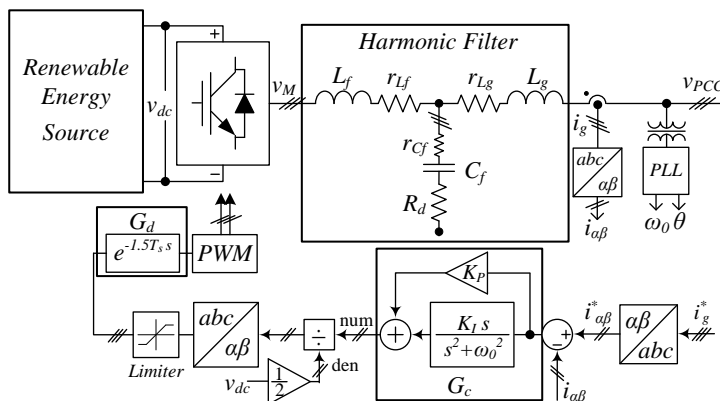


Fig. 2.5 Simple structure of Grid-Connected VSC in Renewable Power Generation.

There are three major parts of the VSC in respect to the stability analysis of the interconnected system. One is the Phase Locked Loop (PLL), which is used for synchronization of the VSC with the grid voltage. The second is the current control loop that enables the 4-quadrant operation of the VSC. Lastly, the impedance of the harmonic filters is another factor that contributes to the VSC stability.

2.4.1. PHASE LOCKED LOOP (PLL)

In order to transfer power in an AC system, the phase angle and the magnitude of voltage and currents at each node should be controlled accordingly to the node power demand. Fig. 2.6 shows three important vector diagrams for relating the power flow from the node voltages and the phase angles as shown in the simple power transmission system diagram illustrated in Fig. 2.1.

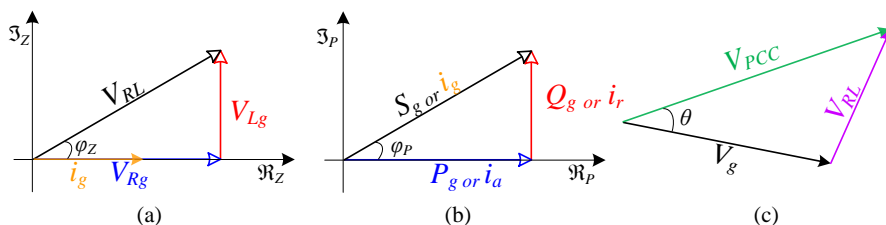


Fig. 2.6 Power flow vector diagram for: (a) Voltage drop across the line impedance (R_g, L_g); (b) PQ demand at the generator side; (c) Voltage relation and phase angle between V_{PCC} and V_g .

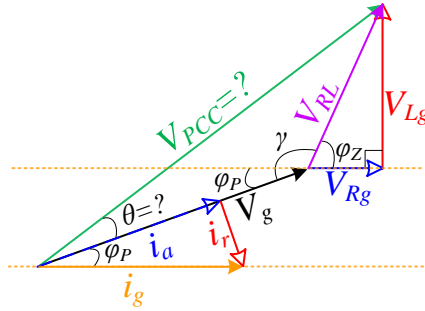


Fig. 2.7 A merged vector diagram for V_{PCC} and θ calculation.

These three relations can be merged into one unified vector diagram. Line current i_g can be synthesized by the active current i_a and reactive current i_r , which are calculated by the power demands P_g and Q_g at the node voltage V_g . By using the alternating angle φ_P and the line impedance angle φ_Z , the angle γ can be found in order for the required voltage V_{PCC} and the phase angle θ to be calculated (2.4).

$$\begin{cases} V_s = \sqrt{V_g^2 + V_{RL}^2 - 2V_{RL}V_g \cos(\gamma)} \\ \theta = \text{asin}\left(\frac{V_{RL}}{V_s} \sin(\gamma)\right) \end{cases} \quad (2.4)$$

In order to deliver the active and reactive power accurately, the phase angle θ has to be accurately applied. The angle information is typically measured and extracted by PLL in the VSC controller and used to control output voltage to be synchronized with the PCC voltage. Fig. 2.8 shows a block diagram for the Stationary Reference Frame PLL (SRF-PLL) [23], which is widely used in the three phase AC system for its simplicity.

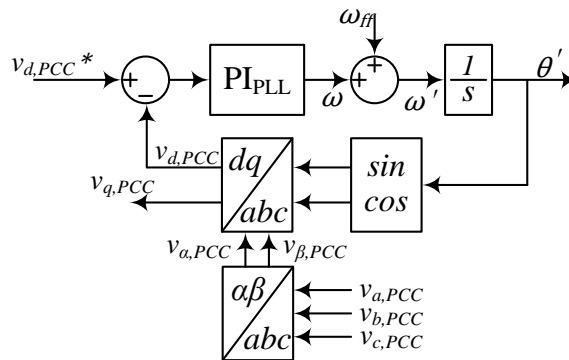


Fig. 2.8 Stationary Reference Frame PLL (SRF-PLL).

As it is an inherently negative feedback system, which is designed for the fundamental frequency tracking (50 or 60 Hz), the bandwidth of the PLL should not be too fast in order not to be affected by noise from the grid or voltage transients such as line notching, frequency variation or harmonics. The closed loop transfer function and the PLL bandwidth can be calculated by the forward loop elements PI_{PLL} and $1/s$ [24].

$$PI_{PLL} = K_p \left(1 + \frac{1}{T_i s}\right) \quad (2.5)$$

The closed-loop phase transfer function is:

$$\frac{\theta'}{v_{d,PCC}^*} = \frac{K_p s + \frac{K_p}{T_i}}{s^2 + K_p s + \frac{K_p}{T_i}} = \frac{2\zeta\omega_n s + \omega_n^2}{s^2 + 2\zeta\omega_n s + \omega_n^2} \quad (2.6)$$

where, $\omega_n = \sqrt{\frac{K_p}{K_i}}$ is the natural frequency and $\zeta = \frac{\sqrt{K_p T_i}}{2}$ is the damping factor.

The -3 dB bandwidth of the system becomes:

$$\omega_{-3dB} = \omega_n \left(1 + 2\zeta^2 + \sqrt{(1 + 2\zeta)^2 + 1}\right)^{\frac{1}{2}} \quad (2.7)$$

By applying the default value of the PI controller gain in the PLL block of PSCAD/EMTDC, the bandwidth of the PLL can be calculated as:

$$\begin{aligned} \omega_{-3dB} &= 68.65 \text{ rad/sec} \begin{cases} K_p = 50 \\ K_i = 900 \\ T_i \end{cases} \\ &= 10.92 \text{ Hz} \end{aligned} \quad (2.8)$$

Generally, in this small scale residential power distribution system, the bandwidth of the PLL is several decades slower than harmonics caused by the harmonic interactions [25]. Therefore, in this study, the instability caused by the effect of the PLL is not considered [25], [26] and it only focuses on instabilities caused by the filter resonance together with its controller [27].

2.4.2. CURRENT CONTROL LOOP

To control the current i_g from a given outer loop active power reference P_g and reactive power reference Q_g , the closed loop current control routine is adopted. Fig. 2.9 shows a small signal representation of the VSC control loop. There are two inputs, one is the current reference i_g^* from the higher lever controller such as the voltage control or power control and the other one is the disturbance input of the fluctuating voltage v_{PCC} . By using the superposition principle and the linear

characteristic of the small signal modeling, the combined dual-input single-output system can be decoupled as shown in Fig. 2.9.

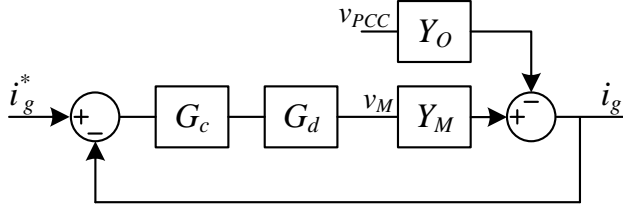


Fig. 2.9 A small signal representation of VSC control loop.

Basically, in this case, the three phase VSC is controlled in the stationary reference frame with Proportional+Resonant (P+R) current controller G_c , together with the time delay G_d , which can be written in an exponential form that takes into account the digital computation delay and its modulation effect [28]. The switching patterns are determined by the Sinusoidal Pulse Width Modulation (SPWM) method and the normalized gain $1/2v_{dc}$ (modulation index) as was illustrated in Fig. 2.4. G_c and G_d are given as:

$$G_c = K_p + \frac{K_I}{s^2 + \omega_0^2} \quad (2.9)$$

$$G_d = e^{-1.5 T_s s} \quad (2.10)$$

where, the K_p and K_I are the proportional and integral gains of PR controller; ω_0 is the grid synchronization frequency and T_s is the sampling time of the VSC, which is the inverse of the switching frequency f_s .

In Fig. 2.9, Y_M represents the transfer function from the modulated voltage v_M to the filter output current i_g , while Y_O represents the transfer function from the voltage deviation in v_{PCC} to the output current in a opposite direction $-i_g$:

$$Y_M = \left. \frac{i_g}{v_M} \right|_{v_{PCC}=0} = \frac{Z_{cf}}{Z_{cf}Z_{Lf} + Z_{Lg}Z_{Lf} + Z_{cf}Z_{Lg}} \quad (2.11)$$

$$Y_O = \left. \frac{-i_g}{v_{PCC}} \right|_{v_M=0} = \frac{Z_{Lf} + Z_{cf}}{Z_{cf}Z_{Lf} + Z_{Lg}Z_{Lf} + Z_{cf}Z_{Lg}} \quad (2.12)$$

where, the impedances Z_{cf} , Z_{Lf} and Z_{Lg} are defined as follows:

$$Z_{cf} = r_{cf} + \frac{1}{sC_f} + R_d, Z_{Lf} = r_{Lf} + sL_f, Z_{Lg} = r_{Lg} + sL_g$$

The open loop transfer function T of the VSC is determined as follows:

$$T = G_c G_d Y_M \quad (2.13)$$

The control to output transfer function and G_{CL} and disturbance to output current transfer function Y_{CL} , which is called the output admittance, are determined as:

$$G_{CL} = \left. \frac{i_g}{i_g^*} \right|_{v_{PCC}=0} = \frac{T}{1+T} \quad (2.14)$$

$$Y_{CL} = \left. \frac{-i_g}{v_{PCC}} \right|_{i_g^*=0} = \frac{Y_O}{1+T} \quad (2.15)$$

where, the open loop gain T can be used for small-signal stability analysis of the VSC; the closed loop transfer function G_{CL} can be used for designing the controller bandwidth and the output response of the VSC, while Y_{CL} can be used for analyzing the interaction problems of the grid-connected converter with the utility grid impedance [31], [32].

2.4.3. HARMONIC FILTERS

Several types of harmonic filters exist in practice, from a simple filter inductor (L) to a more complicated high order filter such as the inductor-capacitor-inductor (LCL) filter. The effectiveness in harmonic attenuation by having low volume and lower cost in the passive components, enables the LCL filter to be the most used filter topology in nowadays power electronics based power system [16], [28], [29]. The passive components of the LCL filter can be categorized as:

- Converter side inductor
- Grid side inductor
- Shunt capacitor
- Damping circuit

The base ratings of the VSC can be used to refer the ratings of the harmonic filter passive components to that of the VSC system, as given by:

$$Z_b = \frac{3V_{PCC}^2}{S_{VSC}} \quad L_b = \frac{Z_b}{\omega_1} \quad C_b = \frac{1}{\omega_1 Z_b} \quad I_b = \frac{S_{VSC}}{3V_{PCC}} \quad (2.16)$$

where Z_b , L_b , C_b and I_b are the base impedance, base inductance, base capacitance and base current, respectively; V_{PCC} is the rms line to neutral voltage at the PCC, S_{VSC} is the apparent power of the VSC and ω_1 is the fundamental frequency of the grid.

The converter side inductor is the main design limitation of the LCL harmonic filter, since the inductor is excited with high frequency rectangular voltages from the

PWM [29], which may lead to significant losses in the core [30] depending on the magnetic material [31] and current ripple specifications [32]. In distribution networks, the VSC are of relatively low power, which implies the use of switching frequencies above 8 kHz. For these frequencies, the ratings of the harmonic filter inductances are within 5 % of the base inductance value of the VSC, while the filter capacitor should be limited in the same range [33]. For optimized low cost harmonic filters, is possible to decrease the filter inductances and increase the filter capacitors.

The final selection of the harmonic filter parameters should ensure the proper attenuation of the switching harmonics, as indicated by the utility operator. The total harmonic distortion and individual harmonic distortion of the current and voltage at PCC should be used correspondingly in the filter design. The resonance of the harmonic filter may require the use of a damping resistor in series with the filter capacitor, whose ratings should be less than 30 % of the VSC base impedance. To limit the power losses associated with the dissipative elements, different combinations of RLC components with significant lower ratings than that of the main filter components can be adopted [33].

2.5. SUMMARY

Before proceeding to the main instability issues, each element in the benchmark network was explained. The aim was to focus more on the instability issues related to the connection of multiple VSCs in the distribution network only, and not to be mixed or coupled with other factors, such as subharmonic oscillation or imbalanced loading condition. The three phase load is assumed to be balanced load and the only the positive sequence impedance of the transmission line (cable) is considered. The essential parts of the VSC are included in the model such as PLL, current controller and harmonic filters.

CHAPTER 3. ANALYZING TOOLS FOR STABILITY ASSESSMENT

This chapter is based on publications [J.1], [C.4], [C.5].

The principle of time domain analysis in the PSCAD/EMTDC simulation tool is given in this chapter. The network solutions at each time step Δt are revealed by the Nodal Admittance Matrix, which is calculated from the equivalent network equations obtained with the Dommel's approach. The Laplace transformation technique, which contains all the frequency information is adopted for describing the complex dynamic behavior of the system, represented with concise algebraic fractional function called "transfer functions" with the variable ' s '. Afterwards, the system stability is simply measured by finding the location of the roots in the transfer function, either by the impedance based stability criterion (IBSC) or by the passivity theorem.

3.1. INTRODUCTION

The time domain analysis describes all the measured variables and their status changes into mathematical functions as a function of the time t . It measures and stores the changes in the measured variables while increasing its time t [34].

The frequency domain analysis assumes a linear system with small variations in the input signal at their operating points. All the frequency information is revealed with the use of the Laplace transformation technique [35], where the complex dynamic behaviors of the system can be represented with concise algebraic fractional function, called "transfer functions" with the variable ' s '. Then, the system stability is simply measured by finding the location of the roots in the transfer function.

To understand the stability of the system, it must be obtained quantitative mathematical models of the system variables, such as the important physical quantities as voltages and currents. The relation between the voltage and current is called impedance or admittance, which is a mathematical model containing differential equations to model system dynamics. The impedance or admittance of respective parts of the network could be written in simple algebraic equations that helps to investigate the system characteristics, where the interconnected impedance relation could be related to the stability criteria [36]. The stability of the system can be evaluated by the impedance based stability analysis of the interconnected impedance at a given node in the network [37]. Afterwards, the passivity criterion

[38] is an emerging method that can prevent this instability issue by shaping the impedance/admittance. However, it is required to introduce a more straightforward stability assessment method that can prevent eventual instabilities in complex networks, such as nowadays decentralized power system with high share of renewable energy sources.

3.2. TIME DOMAIN ANALYSIS TOOL

The main tool for solving the network solution in PSCAD/EMTDC is the Nodal Admittance Matrix, which makes use of the Dommel's approach to model the equivalent network components. However, more advanced calculation methods like the Modified Nodal Analysis has the advantage of giving automated solutions [39].

3.2.1. DOMMEL'S APPROACH IN PSCAD/EMTDC

The linear components of the network can be converted into a suitable form that can be used further for computation in computer programs such as the PSCAD/EMTDC. The equivalent models are obtained by the Dommel's approach [34], which uses the trapezoidal rule to connect the differential equation and the difference equation for a given time step that addresses the digital computation.

In Fig. 3.1 it is shown an example of the equivalent circuit of an inductor using the Dommel's approach, that can be used further for the network solution calculation. For example, the voltage across the two components of the inductor (L_x and R_x) is $v_x(t)$, while the current is $i_x(t)$. Then, the Dommel's equivalent that is needed to obtain the network solution contains the equivalent conductance G_x and the history term $I_x(t - \Delta t)$.

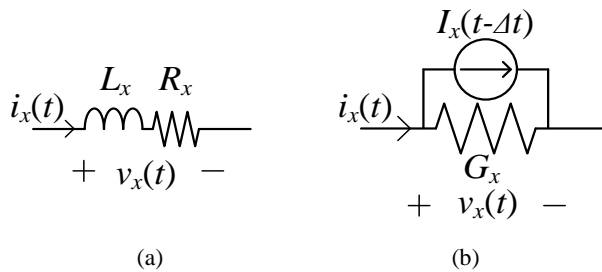


Fig. 3.1 (a) Electrical circuit of an inductor with series resistor; (b) Its equivalent model using the Dommel's approach [34].

The ordinary differential equation (ODE) of the inductor from Fig. 3.1(a) is:

$$v_x(t) = R_x i_x(t) + L_x \frac{di_x(t)}{dt} \quad (3.1)$$

By applying the trapezoidal rule with the time step Δt in (3.1), the voltage equation can be rearranged as function of the time instants (t) and $(t - \Delta t)$ [34], [40] as:

$$\frac{v_x(t) + v_x(t - \Delta t)}{2} = R_x \frac{i_x(t) + i_x(t - \Delta t)}{2} + L_x \frac{i_x(t) - i_x(t - \Delta t)}{\Delta t} \quad (3.2)$$

Then, the voltage equation as function of the lumped impedances Z_x and Z_{x1} can be written as:

$$v_x(t) = Z_x i_x(t) + Z_{x1} i_x(t - \Delta t) - v_x(t - \Delta t) \quad (3.3)$$

$$\text{where, } Z_x = R_x + \frac{2L_x}{\Delta t}, \quad Z_{x1} = R_x - \frac{2L_x}{\Delta t}.$$

From (3.3), the inductor current can be written as function of the conductance term G_x and the history term $I_x(t - \Delta t)$ [40] as:

$$\begin{aligned} i_x(t) &= \frac{1}{Z_x} v_x(t) + \frac{1}{Z_x} v_x(t - \Delta t) - \frac{Z_{x1}}{Z_x} i_x(t - \Delta t) \\ &= G_x v_x(t) + G_x v_x(t - \Delta t) - G_x Z_{x1} i_x(t - \Delta t) \\ &= G_x v_x(t) + I_x(t - \Delta t) \end{aligned} \quad (3.4)$$

$$\text{where, } G_x = \frac{1}{Z_x}, \quad I_x(t - \Delta t) = G_x v_x(t - \Delta t) - G_x Z_{x1} i_x(t - \Delta t).$$

This Dommel's representation can transform the ODE into a simple conductance and current source model, which enables the overall network to be represented only with conductances and current sources.

3.2.2. NODAL ADMITTANCE MATRIX SOLUTION

The network solution can be calculated with the conductance and history terms obtained in the previous chapter. For example, a more complex circuit is presented in Fig. 3.2. By converting all the voltage sources into Norton current sources and all network components into Dommel's equivalents, the linear circuit from Fig. 3.2(a) can be converted into the Dommel model illustrated in Fig. 3.2(b).

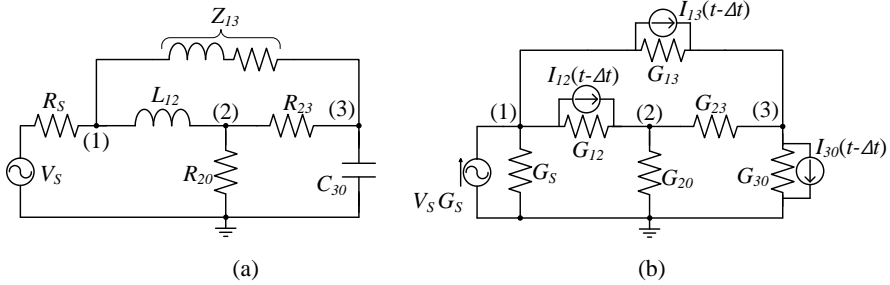


Fig. 3.2 Exemplary circuits for obtaining network solution: (a) Voltage source based circuit; (b) Nodal admittance matrix with Dommel's modeling.

The nodal admittance can be formulated from the KCL of the respective node as:

$$KCL_1: (G_S + G_{12} + G_{13})V_1 - G_{12}V_2 - G_{13}V_3 = V_S G_S - I_{12}(t - \Delta t) - I_{13}(t - \Delta t)$$

$$KCL_2: -G_{12}V_1 + (G_{20} + G_{12} + G_{23})V_2 - G_{23}V_3 = I_{12}(t - \Delta t)$$

$$KCL_3: -G_{13}V_1 - G_{23}V_2 + (G_{13} + G_{23} + G_{30})V_3 = I_{13}(t - \Delta t) - I_{30}(t - \Delta t)$$

or in a matrix form:

$$[V(t)] = [G]^{-1}[I(t)] \quad (3.5)$$

$$\text{where, } [G] = \begin{bmatrix} G_S + G_{12} + G_{13} & -G_{12} & -G_{13} \\ -G_{12} & G_{20} + G_{12} + G_{23} & -G_{23} \\ -G_{13} & -G_{23} & G_{13} + G_{23} + G_{30} \end{bmatrix},$$

$$[V(t)] = \begin{bmatrix} V_1(t) \\ V_2(t) \\ V_3(t) \end{bmatrix}, [I(t)] = \begin{bmatrix} V_S(t)G_S - I_{12}(t - \Delta t) - I_{13}(t - \Delta t) \\ I_{12}(t - \Delta t) \\ I_{13}(t - \Delta t) - I_{30}(t - \Delta t) \end{bmatrix}.$$

The node voltage vector $[V(t)]$ is calculated by solving $[G]^{-1}[I(t)]$ via the LU decomposition method [40]. At each time step, all the history terms and sources in $[I(t)]$ are updated before performing the LU decomposition. If there is no change in the conductance matrix $[G]^{-1}$, the previous results can be preserved for the next calculation, which it may drastically reduce the number of calculations.

3.3. FREQUENCY DOMAIN STABILITY ANALYSIS

3.3.1. IMPEDANCE BASED STABILITY CRITERION

In 1976, R. D. Middlebrook first used the impedance relation to design the input filter of a DC-DC converter [36] and he explained the role of the closed loop system (mainly of the minor loop), that influences the converter stability [37] [41]. For example, in Fig. 3.3 it is shown the admittance relation, which is adapted for an AC power distribution system, where Y_S is the source admittance and Y_L is the load admittance.

The source admittance may be referred to, as a grid connected VSC with its corresponding current control structure and the load admittance may be referred to, as the grid impedance seen from the PCC.

The relation between voltage and current can be written as:

$$I_S = V_{PCC}(Y_S + Y_L) \quad (3.6)$$

which can be converted into a series connected negative feedback block as shown in Fig. 3.3(b). The feedback loop gain, called the minor loop gain T_M , becomes the loop gain of the closed loop transfer function, which can be obtained from the two admittances as:

$$T_M = \frac{Y_S}{Y_L} \quad (3.7)$$

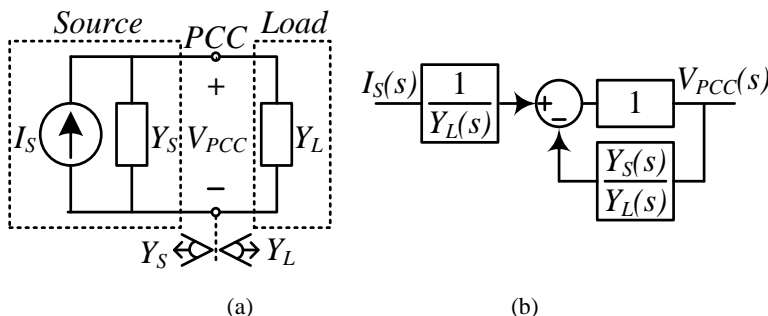


Fig. 3.3 Small-signal admittance representation of: (a) an interconnected system with current source; (b) the minor loop gain representation [J.1].

By analyzing the loop gain of the system, the possible unstable poles of the system can be investigated by using some stability analysis tools, such as the Nyquist stability criterion or root locus [35]. Therefore, the inter-connected system stability can be evaluated.

3.3.2. PASSIVITY STABILITY CRITERION

The concept of passivity was originated in the control theory field [42] and recently, it is gaining attention also in the power electronics and power system field [43]–[45]. It helps to mitigate the interaction problems between the grid connected VSC units [26]. The passivity can deal with large electrical systems, provided that the frequency response requirements for each individual subsystem do not affect the rest of the system. That means that the frequency response of a subsystem should be ranged within a certain phase angle margin given by $[-90^\circ, +90^\circ]$, in order not to affect the other passive subsystems [26]. A necessary and sufficient condition that a linear network is passive if its impedance is a positive real function. More accurate formulation was followed thereafter; that is, $\text{Re}\left(\int_{-\infty}^t v^*(\tau)i(\tau)d\tau\right) \geq 0$ for all $t > -\infty$, where v , i and $*$ are the stimulus voltage, output current and complex conjugate respectively [46]. Because the total energy delivered to the network is $\frac{1}{\pi} \int_0^{+\infty} \text{Re}[Z(j\omega)] \|I(j\omega)\|^2 d\omega$ and it greater than 0, this will impose that $\text{Re}[Z(j\omega)] \geq 0$ at each frequency [47], which guarantees the phase angle of the impedance $Z(s)$ to be in a passive range, given by $[-90^\circ, +90^\circ]$. Since complex networks are composed by a large number of sub-systems, the stability of the overall system can be achieved by making each sub-system passive. This means that the output admittance of grid-connected converters should be passive in order for the phase angle of the interconnected system to be in the $[-180^\circ, +180^\circ]$ range. This will ensure that the $(-1, j0)$ point in the Nyquist plot will never be encircled, resulting in a stable system in all conditions [48].

3.3.3. THE OUTPUT ADMITTANCE OF GRID-CONNECTED VSC

Typical Bode diagrams of the output admittance of a grid current controlled inverter for two different possible designs of the LCL filter are shown in Fig. 3.4. The filter designs are made according to the placement of the LCL filter resonance frequency ω_{res} as function of the dip (anti-resonance) frequency ω_d of the output admittance, mainly given by:

$$\omega_{res} = \sqrt{\frac{L_f + L_g}{L_f L_g C_g}} \quad (3.7)$$

$$\omega_d = \sqrt{C_f L_f}^{-1} \quad (3.8)$$

Additionally, the critical frequency of the inverter ω_c is defined as:

$$\omega_c = \frac{\pi}{3T_s} \quad (3.9)$$

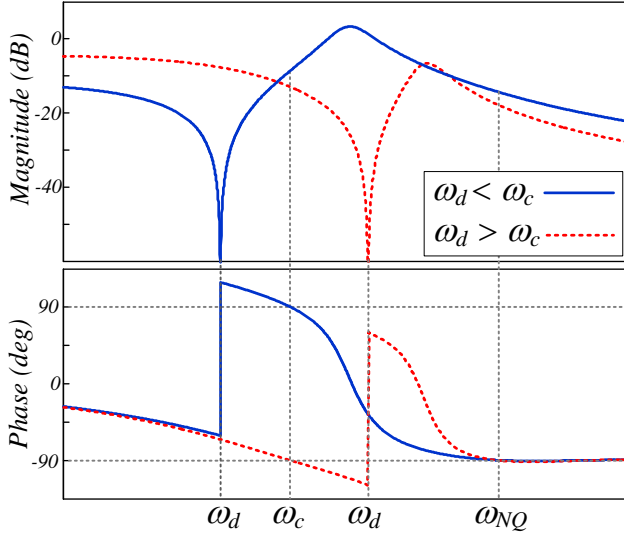


Fig. 3.4 The inverter output admittance Y_{CL} for two different designs of the LCL filter [J.1].

The critical frequency of the inverter ω_c is one-sixth of the sampling frequency given by T_s , while the Nyquist frequency ω_{NQ} is defined as the half of the sampling frequency.

The inverter does not need resonance damping for its stand-alone stable operation if $\omega_{res} > \omega_c$ is satisfied [49]. The locations of the anti-resonance frequency ω_d in respect to ω_c result in two distinctive ways of classifying the non-passive region in Fig. 3.4, given by $\omega_d > \omega_c$ and $\omega_d < \omega_c$. The phases of the two admittances exceed the passive range $[-90^\circ, +90^\circ]$ in the interval of (ω_d, ω_c) or (ω_c, ω_d) , respectively, even though the inverter is designed stable as stand-alone. The phase angle degradation is introduced by the time delay term G_d until ω_d , where the 180° phase jump occurs. It can be concluded that the time delay and the parallel resonance frequency ω_d are the main reason of passivity violation of the grid-connected converter.

3.3.4. DEFINITION OF THE NON-PASSIVE RANGE OF THE CONVERTER OUTPUT ADMITTANCE

The passivity violation can be identified by evaluation of the negative value of the output admittance real part [48], mainly given by:

$$\Re(Y_C(j\omega)) = \frac{K \cos(1.5T_s\omega) (1 - \omega^2 C_f L_f)}{(K \sin(1.5T_s\omega) + \omega(\omega^2 C_f L_f L_g - L_f - L_g))^2 + (K \cos(1.5T_s\omega))^2} \quad (3.10)$$

From (3.10) it can be noticed that the only functions which can be negative are the cosine function (that is resulted from the time delay G_d) and the anti-resonance term ω_d [43]. Therefore, the non-passive region of the inverter is defined by these two terms, which are illustrated in Fig. 3.5 together with their combined polarities. The polarity of the cosine term changes at ω_c and at the Nyquist frequency ω_{NQ} . The $(1 - \omega^2 C_f L_f)$ term has three different ranges depending on the different values of ω_d given by:

- ω_d is smaller than ω_c , the non-passive region becomes $[\omega_d, \omega_c]$
- ω_d is larger than ω_c , the non-passive region becomes $[\omega_c, \omega_d]$
- ω_d is equal to ω_c , the non-passive region disappears and the system becomes stable for all passive network admittance [50]

In this work, the frequency range for harmonic analysis is limited to the Nyquist sampling frequency ω_{NQ} . Above the Nyquist frequency, there may be other issues, which needs to be investigated [51] and are omitted here.

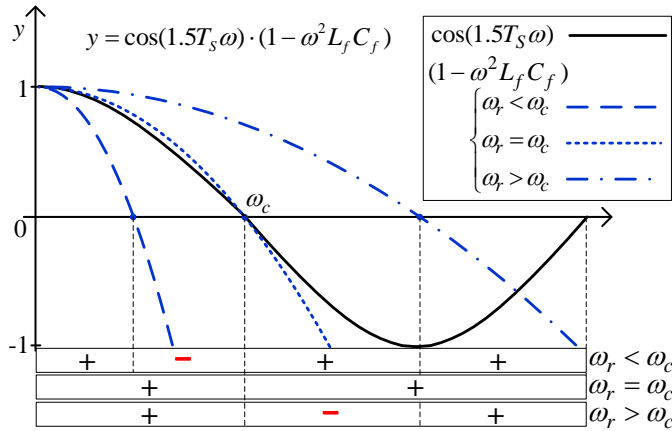


Fig. 3.5 Non-passive region of grid inverter derived from the numerator of $\Re(Y_C)$ [J.1].

3.4. EXAMPLE OF STABILITY ANALYSIS OF GRID-CONNECTED VSC

The stability regions of the converter output admittance Y_{CL} with different grid admittance Y_G can be described by using the graphical interpretation of IBSC, while the non-passive region of the converter can provide possible forbidden regions for the passive grid admittances. It makes possible to find out the critical grid admittance that may trigger the power converter instability. Based on the minor loop gain definition T_M in (3.7), the source admittance Y_{CL} which is the output admittance

of the VSC and the load admittance which is in this case the grid admittances Y_G are used to find out the interconnected system stability as shown in Fig. 3.3 [36].

$$T_M = \frac{Y_{CL}}{Y_G} \quad (3.11)$$

According to the passivity theorem, the VSC stability is satisfied if $|Y_{CL}| > |Y_G|$ and $\angle Y_{CL} - \angle Y_G = -\pi \pm 2\pi N$ [35].

3.4.1. INFLUENCE OF PURE INDUCTIVE GRID IMPEDANCE

The graphical interpretation of IBSC requires knowledge of both Y_{CL} and Y_G . For a pure inductive grid, Y_G is:

$$Y_G(j\omega) = \frac{1}{j\omega L_g} \quad (3.12)$$

Then, the grid and output converter admittances are illustrated in Fig. 3.6 for two designs of the LCL filter. Since the grid impedance is passive, the frequency range of concern is limited to the non-passive range of the inverter given by a phase difference larger than 180° , which occurs between ω_d and ω_c . Therefore, the magnitude condition has to be evaluated in order to calculate the critical grid impedance that may lead to instability as follows:

- $\omega_d < \omega_c$: the increase in the grid impedance $|Y_G|$ (color line) makes the magnitude condition area $|Y_{CL}| > |Y_G|$ to be broadened. Then, the frequency where the negative crossover takes place is ω_c and is given by $(\angle Y_{CL} - \angle Y_G = -\pi \pm 2\pi N)$. The critical inductance value of the grid L_G can be calculated by equating the grid admittance (3.12) to the output admittance of the converter Y_{CL} at the critical frequency ω_c , which results in:

$$L_G = \frac{\sqrt{K^2 \cos(1.5T_s \omega_c)^2 + (K \sin(1.5T_s \omega_c) + \omega_c(\omega^2 C_f L_f L_g - L_f - L_g))^2}}{\omega_c |1 - \omega_c^2 C_f L_f|} \quad (3.13)$$

- $\omega_d > \omega_c$: the converter is stable since the phase difference is less than 180°

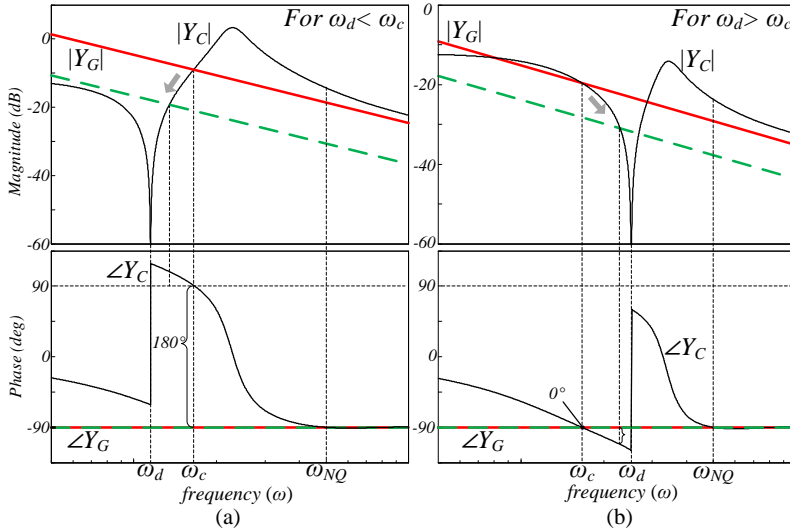


Fig. 3.6 Stable and unstable region of grid inverter in pure inductive grid case: (a) $\omega_d < \omega_c$, (b) $\omega_d > \omega_c$ [J.1].

3.4.2. INFLUENCE OF PURE CAPACITIVE GRID IMPEDANCE

Similarly, the critical frequency is evaluated for the capacitive grid, which may occur if the converter is connected with the grid through long underground cables. The stability analysis for variable grid capacitance C_G is opposite to that of the L_G as it is illustrated in Fig. 3.7. The frequency dependent pure capacitive grid can be characterized by:

$$Y_G(j\omega) = j\omega C_g \quad (3.14)$$

The magnitude condition evaluation reveals the following:

- $\omega_d < \omega_c$: the converter is stable since the phase difference is less than 180°
- $\omega_d > \omega_c$: the decrease in the grid impedance $|Y_G|$ (color line) makes the magnitude condition area $|Y_{CL}| > |Y_G|$ to be broadened. Then, the frequency where the negative crossover takes place is ω_c . A capacitance value smaller than the critical capacitance value of the grid C_G would make the converter unstable as given by:

$$C_G = \frac{|1 - \omega_c^2 C_f L_f|}{\omega_c \sqrt{K^2 \cos(1.5T_s \omega_c)^2 + (K \sin(1.5T_s \omega_c) + \omega_c (\omega^2 C_f L_f L_g - L_f - L_g))^2}} \quad (3.15)$$

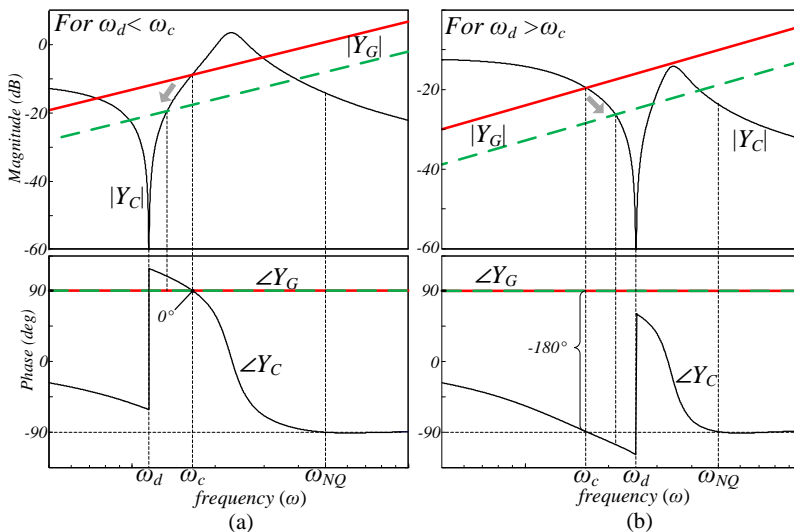


Fig. 3.7 Stable and unstable region of grid inverter in pure capacitive grid case: (a) $\omega_d < \omega_c$, (b) $\omega_d > \omega_c$ [J.1].

3.5. PROPOSED IBSC METHOD FOR A DISTRIBUTION NETWORK WITH MULTIPLE CONNECTED VSC

In a practical situation, there are multiple converters connected to the distribution network as illustrated in Fig. 3.8. For this scenario, the source admittance is given by the converter admittance of the analyzed converter. However, the load admittance Y_L will contain all the other converter admittances Y_{Sx} connected to the network and the impedances in the network given by the passive components such as resistors, inductors and capacitors (from the distribution lines and transformers). Additionally,

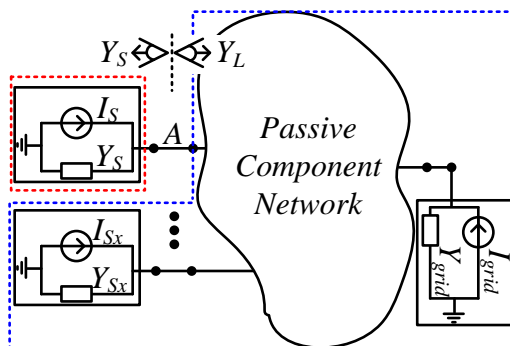


Fig. 3.8 Small-signal admittance representation of a small scale inverter-based power system [C.4].

the grid admittance Y_{grid} from the upper level network, such as medium-voltage network, also needs to be taken into account.

However, the problem may appear in the load admittance Y_L . Even all of the converters which make up Y_L are stable stand-alone and they only have LHP poles in their output admittance, the resulted impedance $1/Y_L$ can turn into unstable state, i.e. caused by non passive behavior of each converter output admittance Y_{Sx} , as a result of the interaction between the converters. All the individual converter admittances are aggregated and hidden into the transfer function Y_L , the use of the IBSC is still not intuitive. Even all of the converters present in the load admittance are planned to be operated stable, the stability of the combined load admittance still remains unknown [7], [52].

3.5.1. CONDITIONS FOR STABILITY

In order to apply the Nyquist stability criterion to the minor loop gain given by the admittance ratio, the stability of the current source I_S and of the load admittance Y_L needs to be procured individually. For example, the stability at node A can be analyzed by the admittance ratio T_{MA} given by:

$$T_{MA} = \frac{Y_{SA}}{Y_{LA}} \quad (3.16)$$

Let's assume first that there is only one connected converter to the Passive Component Network (PCN), while detaching all the other active PE units from the network as shown in Fig. 3.9. In this case, the load admittance Y_{LA} contains only passive components without having negative real parts, so there is no way to induce right half plane poles (RHP) and zeros (RHZ) into the PCN. If the current source I_{SA} is stable from the beginning and the inverse of the load admittance $1/Y_{LA}$ has no RHP pole, then the IBSC requirements are satisfied. This means that (3.16) satisfies the Nyquist stability criterion and the voltage on node A is stable with respect to the current source I_{SA} [C.4].

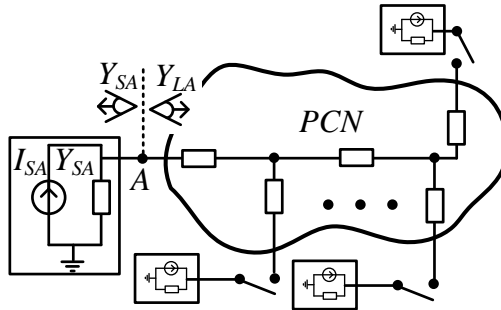


Fig. 3.9 Passive component network (PCN) [C.4].

If the stable operation is achieved on the node A , all the nodes which are in PCN is stable and the other inverters can be connected sequentially to inspect further.

At this point, it needs to be defined a set of statements which will be used when it comes to extending this stability evaluation procedure for the entire distribution network such as:

- “ 1. The network with only passive components is always stable
 2. The arbitrary node in the PCN is stable when all active components connected nodes are stable ” [C.4]

Statement 2 gives an essential condition that enables to extend the IBSC analysis for all nodes in the distribution network sequentially. But, still the contribution of each active component on the system stability is not straightforward, as the load system stability is determined by how Y_{LA} is grouped in the beginning: the participation of the network components also decides the system stability [C.1], [25].

3.5.2. PROPOSED SEQUENTIAL STABILIZING PROCEDURE

The proposed sequential stabilizing method collects all the stable load admittances that contain all the converters in the network as illustrated in Fig. 3.10 (a) and (b). An absolutely stable load admittance of the PCN is expanded sequentially to include the whole network by adding each of the converters one by one. The system stability is evaluated by the Nyquist stability criterion at each iteration. If the connection of one of the converters turns out to be unstable, then stabilizing functions such as damping resistors or active damping methods should be considered. The procedure ends when the networks with all connected converters are evaluated and the network is stabilized if necessary. The flowchart of the proposed sequential stabilizing procedure for networks with multiple connected converters is shown in Fig. 3.10 (c).

The Nyquist stability criteria can be adopted with any of the converters output admittance Y_{S1} and its corresponding PCN admittance Y_{L1} seen from the arbitrary node A , as shown in Fig. 3.10 (a). The terminology chosen here is arbitrary and the equivalent admittance Y_{PCN} is determined by the location where it is measured as it will have a different value for each node. If the stability between the connected system Y_{S1} and Y_{L1} is guaranteed on the node A , it can be extended to the next node B as shown in Fig. 3.10 (b). The new stable load admittance Y_{L2} seen from the node B will contain also Y_{S1} . Then, the stability can be evaluated on node B for the unidentified source admittance Y_{S2} with respect to the new stable load admittance Y_{L2} obtained from the previous step [C.1].

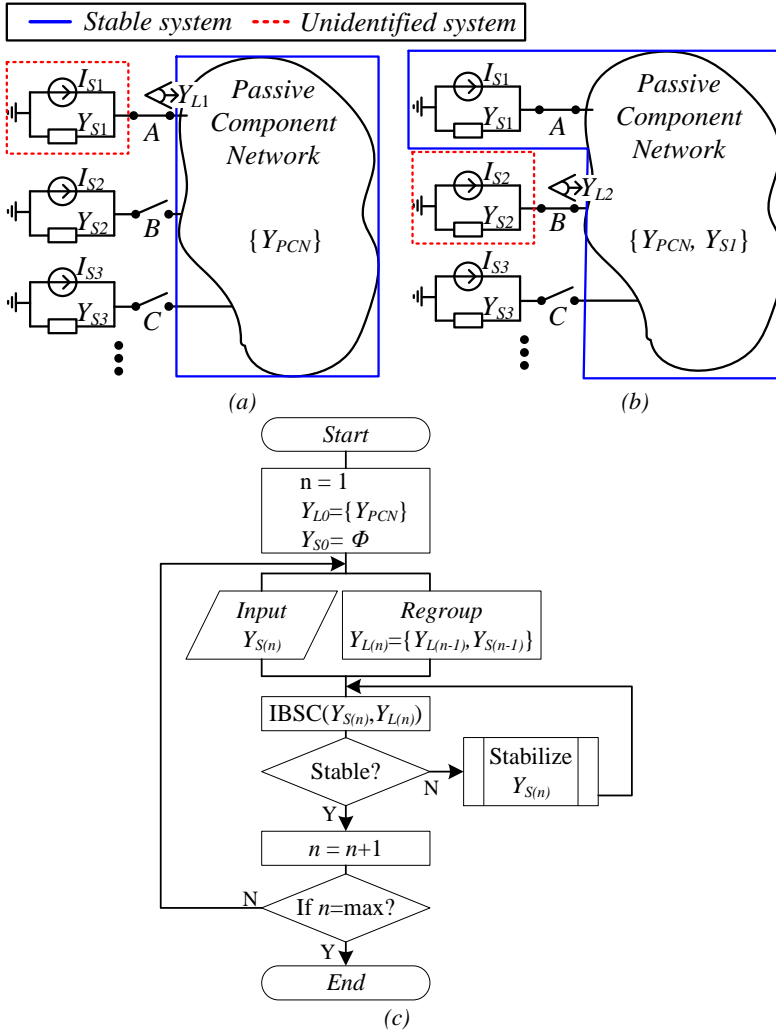


Fig. 3.10 The sequential stabilizing procedure: a) An inverter with passive component network; b) The second inverter with a stable admittance network; c) The proposed sequential stabilizing procedure [C.4].

3.5.3. PRACTICAL EXAMPLE OF STABILITY ANALYSIS

To application of the proposed sequential stabilizing procedure for the small-scale distribution system shown in Fig. 2.2 is presented in the following. The ratings of the system are given in Table 3.1.

Table 3.1 The Ratings of the Grid-Connected Converters [C.4].

		Converter name				
		Inv. 1 (Inv. A)	Inv. 2 (Inv. B)	Inv. 3 (Inv. C)	Inv. 4 (Inv. D)	Inv. 5 (Inv. E)
Power rating [kVA]		35	25	3	4	5.5
Base Frequency, f_0 [Hz]		50				
Switching Frequency, f_s [kHz] (Sampling Frequency)		10		16		
DC-link voltage, v_{dc} [kV]		0.75				
Harmonic regulations for LCL filters		IEEE519-1992				
Filter values	L_f [mH]	0.87	1.2	5.1	3.8	2.8
	C_f [μ F]/ R_d [Ω]	22/0	15/1	2/7	3/4.2	4/3.5
	L_g [mH]	0.22	0.3	1.7	1.3	0.9
Parasitics values	r_{L_f} [m Ω]	11.4	15.7	66.8	49.7	36.7
	r_{C_f} [m Ω]	7.5	11	21.5	14.5	11
	r_{L_g} [m Ω]	2.9	3.9	22.3	17	11.8
Controller gain	K_p	5.6	8.05	28.8	16.6	14.4
	K_I	1000	1000	1500	1500	1500

Considering the sequential stabilizing procedure given in Fig. 3.10 (c), the iterative stability assessment is performed as follows:

Step 1: The output admittance of the Inv.1 at node R6 given by Y_{S1} is obtained from (2.15). The load admittance Y_{L1} at node R6 containing only the passive component network without any converters is calculated. The minor loop gain for the node R6 can be written as:

$$T_{M1} = \frac{Y_{S1}}{Y_{L1}} \quad (3.17)$$

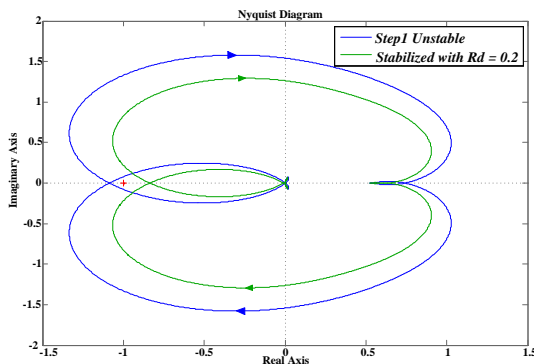


Fig. 3.11 Nyquist diagram of the system at Step 1 for the initial condition (blue) and for the stabilized system with additional damping resistor R_d (green) [C.4].

In Fig. 3.11 is shown the Nyquist plot of the minor loop gain from (3.17). It reveals that the Inv. 1 connected to the network is unstable (blue) as it encircles $(-1, 0j)$. Since Y_{L1} is always stable from statement 1, then Y_{S1} can be modified to suffice the stability condition. A damping resistor R_d is added in the harmonic filter of the Inv.1,

which can reshape the output admittance Y_{S1} in order to stabilize the system. The time domain results are shown in Fig. 3.12(a) and Fig. 3.12(b).

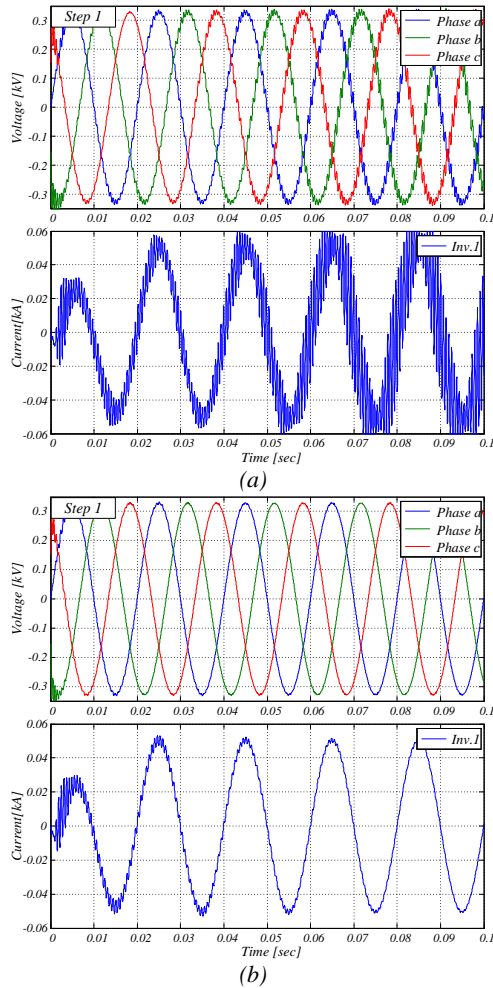


Fig. 3.12 Time domain simulation of the converter voltages (upper) and currents (lower) at node R4 for Step 1: (a) Unstable case; (b) Stabilized case [C.4].

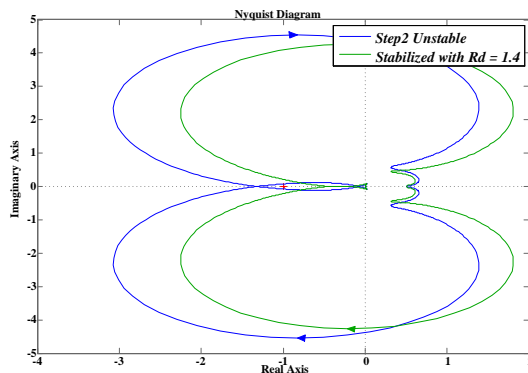
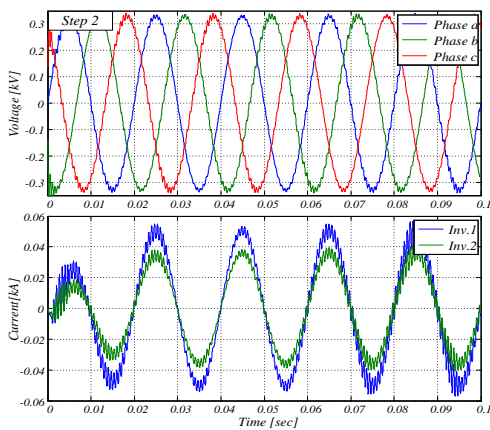
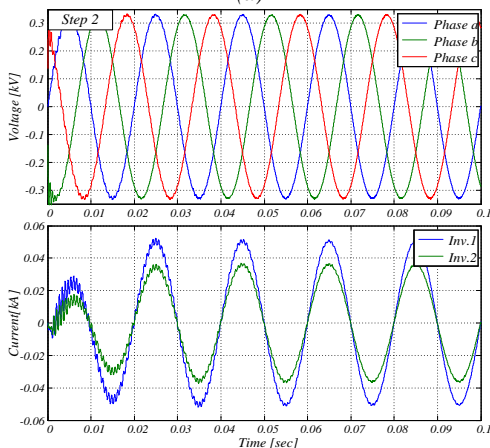


Fig. 3.13 Nyquist diagram of the system at Step 2 for the initial condition (blue) and for the stabilized system with increased damping resistor R_d (green) [C.4].



(a)



(b)

Fig. 3.14 Time domain simulation of the converter voltages (upper) and currents (lower) at node R4 for Step 2: (a) Unstable case; (b) Stabilized case [C.4].

Step 2: The new stabilizing procedure start with other nodes in the network based on statement 2. The Inv.2 connected at node R10 is added to the stable network obtained from the previous step. Then, the minor loop gain for stability evaluation at node R10 is:

$$T_{M2} = \frac{Y_{S2}}{Y_{L2}} \quad (3.18)$$

In Fig. 3.13 is shown the Nyquist plot of the minor loop gain from (3.18). It reveals that the Inv. 2 connected to the network is again unstable (blue) as it encircles $(-1,0j)$. The value of the damping resistor R_d is increased from 1Ω to 1.4Ω in order to stabilize the system. The time domain results are shown in Fig. 3.14(a) and Fig. 3.14(b).

Step 3 ~ 5: The other converters are added to the stable network step by step. Since for these cases the initial conditions are enough to make the system stable, there is no need for additional action for stabilization. The corresponding Nyquist diagrams and time domain waveforms are shown in Fig. 3.15 and Fig. 3.16, respectively. This example demonstrates that the method can obtain a stable network by using the IBSC for multiple connected converters to the same network. However, it shows only one of the many different sequential stabilizing pathways, which may not be the optimal solution. Still, the load admittance can be expanded step by step and the connected converter can be evaluated individually.

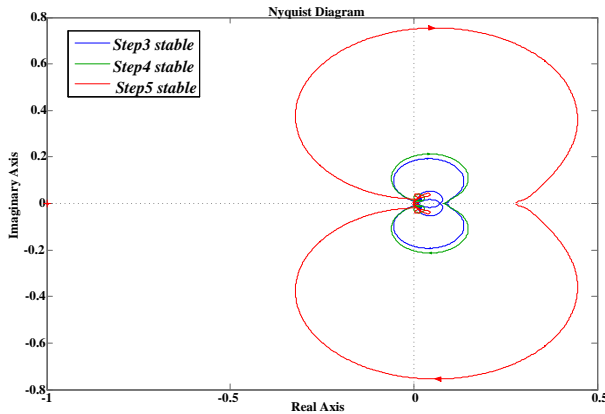


Fig. 3.15 Nyquist diagram of the system at Steps 3 ~ 5 (only the initial condition) [C.4].

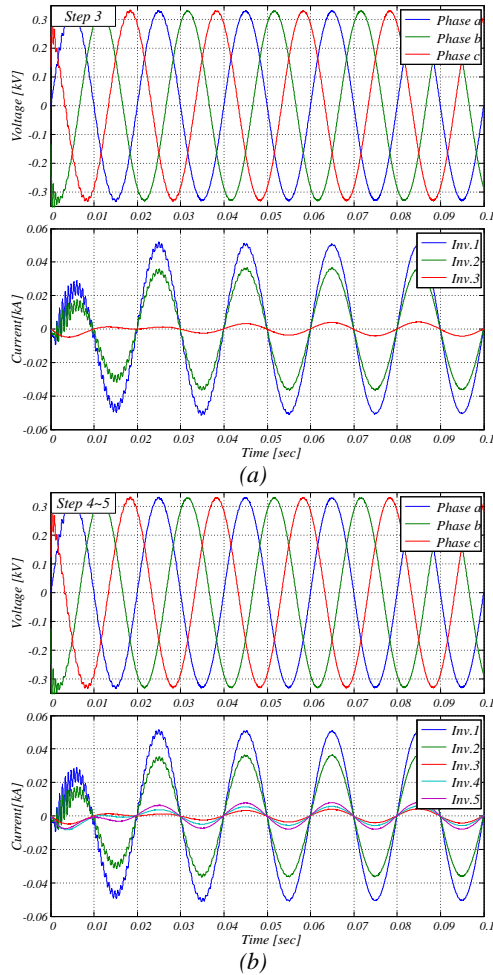


Fig. 3.16 Time domain simulation of the converter voltages (upper) and currents (lower) at node R4 for: (a) Step 3; (b) Step 4 ~ 5 [C.4].

3.6. IMPROVED STABILITY ANALYSIS METHOD TO DEAL WITH COMPLEX DISTRIBUTION SYSTEMS

The sequential stabilizing procedure may become tedious for distribution networks with high share of power electronics based loads/sources. In order to have the node input impedance, the equivalent impedance matrix of the whole network has to be calculated at each procedure, which increases the computational effort. Additionally, the lumped stable network impedance, which contains other converters, may not provide clear information for the coming unstable event. The reason is that all the meaningful nodes are unified and represented as one bulky transfer-function.

Another way of analyzing the stability is to divide the power system in small subsections depending on the geographical constraints of the network. A minimum stability analysis entity can be defined, which can point out the critical nodes where stabilizing efforts are necessary. After the stability of the first entity is obtained, this entity become part of the second(upper) entity's elements. By expanding these entities, it will reach to the distribution feeder and the overall stability analysis will be performed. This method can provide the following advantages:

- “ ▶ Less computational effort
- ▶ Clear about where to start the stability analysis
- ▶ Clear about which node has to be modified to stabilize the system
- ▶ Less susceptible from changes in the network configuration ” [C.50]

3.6.1. THE MINIMAL ENTITY CONCEPT

The connection of the power converters to the distribution network can be achieved by two typical connections as it is illustrated in Fig. 3.17. One way is when the grid is an ideal voltage source V_s directly connected to the network power converters inverters $Y_1 \sim Y_n$ as it is modeled by (3.19). The other way is when a line impedance Z is placed between the ideal voltage source and the paralleled converters as it is modeled by (3.20).

$$\begin{cases} v_a = V_s \\ i_a = v_a(Y_1 + \dots + Y_n) = V_s Y_1 + \dots + V_s Y_n \end{cases} \quad (3.19)$$

$$\begin{cases} v_b = V_s \frac{1}{Z + \frac{1}{Y}} \\ i_b = v_b Y = V_s \frac{1}{Z + \frac{1}{Y}} \end{cases} \quad (3.20)$$

where, $Y = Y_1 + \dots + Y_n$.

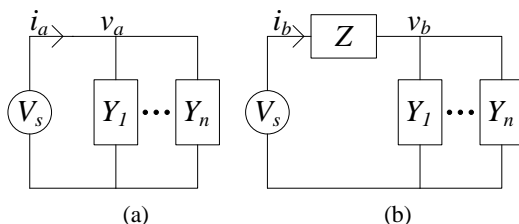


Fig. 3.17 Simple model of the network: (a) Ideal grid with parallel admittance; (b) Ideal grid with series impedance and parallel admittance [C.5].

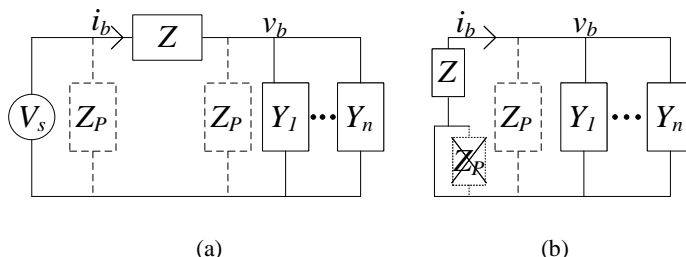


Fig. 3.18 Meaningless parallel compensation from the outside of the unstable node: (a) Full diagram (b) Equivalent diagram [C.5].

The common node voltage across the parallel converters is noted by " v " while the current corresponding to the input voltage V_s is " i ". All the converters are represented by their equivalent output admittance [25].

The stability of the system with an ideal voltage source and paralleled converters is determined by the individual output admittances of the converters $Y_1 \sim Y_n$ as shown in Fig.3.17 (a). If there is any RHP pole in any of the converter's output admittances, the source current i_a will diverge. The stability depends on each of the inverter characteristic.

However, when there is a series impedance Z given by the distribution line that exists in between the ideal voltage source V_s and the parallel admittance of the converters $Y_1 \sim Y_n$, the stability of the system is determined by the characteristic equation $(Z + 1/Y)$ in (3.20). RHZ of $(Z + 1/Y)$, which becomes RHP of the closed loop transfer function, can be created by the algebraic summation of Z and $1/Y$ [53]. Since the line impedance Z is fixed as it is given by the geometry of transmission line, the only way to have access to the system transfer-function is to change Y . The lumped admittance Y needs to be changed by modifying each of output admittance of the converters $Y_1 \sim Y_n$ or by adding additional stabilizing impedance Z_p as it is illustrated in Fig. 3.18 [54]. This stabilizing impedance is commonly connected either in parallel with the ideal voltage source or with the power converter. However, the system instability cannot be solved by the parallel impedance Z_p connected across the ideal voltage source terminal as shown in Fig. 3.18. As result, the stabilizing feature has to be placed in parallel with the power

converter or can be part of the converter itself. This brings the basic concept of the proposed analysis method.

3.6.2. PROPOSED STABILITY ANALYSIS OF THE COMPLEX DISTRIBUTION SYSTEM [C.5]

The stability of complex distribution networks can be evaluated by keeping the instability inside the one of the entities shown in Fig. 3.19. The entities are grouped from bottom to upper feeder as follows. The equivalent load admittances connected to the end bus of the radial network together with the corresponding cable impedance will define the first entity, which is the minimal entity. It should be mentioned that the minimal entity only provides local stability. Therefore, in order to obtain entire system stability, the minimal entity should be expanded to cover the overall network in the same manner as it was previously described.

“However, this method is limited to a very simple case with a line impedance located in series. When the network has multiple series impedances that make several series nodes and each node may contain several branches, the stability analysis becomes more complex. Due to the concept of minimal entity, the stability analysis can be much simpler than the conventional method [C.4]. It groups all the instability problems inside of one entity and there is no need to consider the overall network impedance. All the small regions (entities) can be analyzed separately and the instability of the regional areas becomes clearer to investigate.” [C.5]

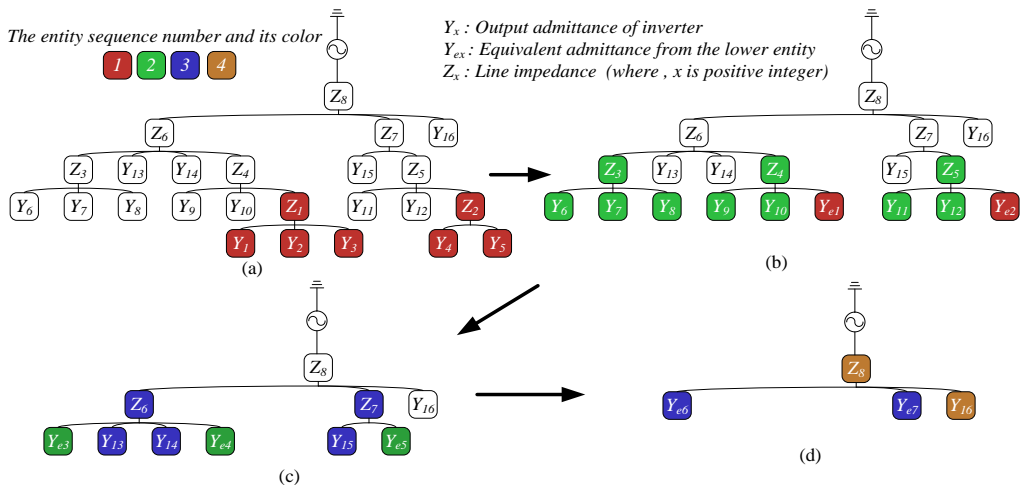


Fig. 3.19 Proposed stability analysis method for a radial grid [C.5].

The stability analysis can be started from the outermost entity (entity number 1) in the network, i.e. the farthest nodes from the feeder, such as $Y_1 + Y_2 + Y_3$ or $Y_4 + Y_5$, as shown in Fig. 3.19 (a). The stability analysis has to be performed for each of the entity group. For example, $Y_1 + Y_2 + Y_3$ is selected for the first entity and the characteristic equation is derived for stability analysis as:

$$Z_1 + \frac{1}{Y} = \frac{Z_1 Y + 1}{Y} \quad (3.21)$$

where, $Y = Y_1 + Y_2 + Y_3$.

According to the Cauchy's argument principle [35], the unstable poles in the first entity can be found. The number of the unstable poles given by the $RHZ(Z_1 Y + 1)$ can be identified by counting the number of N encirclements of the point $(0, j0)$ in the Nyquist plot [53], which can be written as:

$$\begin{aligned} N &= RHZ\left(\frac{Z_1 Y + 1}{Y}\right) - RHP\left(\frac{Z_1 Y + 1}{Y}\right) \\ &= RHZ(Z_1 Y + 1) + RHP(Y) - RHP(Z_1 Y + 1) - RHZ(Y) \\ &= RHZ(Z_1 Y + 1) - RHZ(Y) \\ &= RHZ(Z_1 Y + 1) - RHZ(Y_1 + Y_2 + Y_3) \end{aligned} \quad (3.22)$$

The number of RHZ in the total admittance ($Y_1 + Y_2 + Y_3$) should be known. If the inverters are stable separately and there is no RHZ in the total admittance, the number of unstable poles for the chosen entity becomes the number of the N encirclements given by:

$$RHZ(Z_1 Y + 1) = N + RHZ(Y_1 + Y_2 + Y_3) \quad (3.23)$$

“After each of the first entities have been evaluated, the second entity is analyzed as shown in the Fig. 3.19 (b). The result of the first entity such as Y_{e1} and Y_{e2} will be part of the elements that form the second entities. They can be seen as parallel admittances for the second entity. Therefore, the overall system stability can be analyzed by expending it upwards to include the network as shown in Fig. 3.19 (c) ~ (d). Therefore, each stability analysis does not need the information about the whole network, which is different from the conventional method. This is why this method can be faster than the conventional method. Also, by dividing the stability problems into separated small networks, the cause of instability can be more intuitive than the large transfer function of the conventional method. Additionally, the use of different entities can give an advantage that the stability analysis is more independent from changes in the network topology. In such situations, the model only needs to be checked where the change occurs, while the other entities do not need to be analyzed again.”[C.5]

3.7. SUMMARY

Two essential methods to analyze and evaluate the instability problems between multiple connected VSCs were addressed. The time domain simulation model of the network in PSCAD was explained together with the principle operation of the Electro Magnetic Transient Program (EMTP). The frequency domain model for stability analysis was explained in this section by means of the Impedance Based Stability Criterion (IBSC). By expanding the IBSC it is possible further to reach the new concept of Passivity, which can give a design guide-line for PE based units that can guarantee the stable operation. Some other issues in implementing the IBSC are also mentioned.

CHAPTER 4. STABILIZATION OF SMALL SCALE POWER SYSTEMS

This chapter is based on publications [C.1], [C.2], [C.3].

This chapter discusses about frequency domain analysis and time domain verification in PSCAD/EMTDC of a small scale PE based power distribution system. As it was previously discussed, the accurate IBSC can predict the stability in power systems, while the corresponding response of the power system can be observed in time domain. Four stability assessment studies about a PE based power distribution system will be addressed in the following. One interesting case is investigation of the grid impedance variation and its influence in a PE based power system, where several converters are connected in parallel. They are also shown some scenarios where the configuration of several paralleled connected PE units are changed. Afterwards, several methods to deal with the harmonic instability are described. One of the possible solutions is to implement active damping in the PE units in order to stabilize the network. It is also possible to connect a specialized unit for stabilizing harmonic instabilities, such as an active damper, which becomes more popularly in recent times. For the latter case, it is important to find the most effective location for placing the active damper in the distribution system, fact that is revealed by measuring the required damping resistance of the network by using the IBSC tool.

4.1. STABILITY EVALUATION OF MULTIPLE PARALLELED-CONNECTED CONVERTERS

A PE based distribution system that contains five paralleled-connected three-phase VSCs of different ratings are shown in Fig. 4.1. The converters are operated in grid-connected mode, e.g. are able to inject active or reactive power to the grid. On the DC side of the converters there are connected distributed energy sources, which are modelled as constant DC voltage sources [C.1].

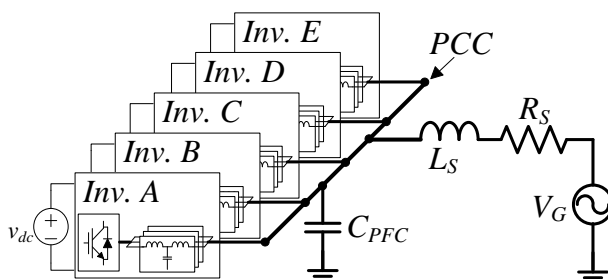


Fig. 4.1 Single line diagram of 3-phase distribution power system with five inverters in parallel [C.1].

There is a three-phase capacitor C_{PFC} connected to the PCC in parallel, which can be used for Power Factor Correction (PFC) for an existing load system like Direct-On-Line (DOL) startup motor application and the default value of the PFC capacitor in this test is $12 \mu F$ [C.1]. The other system ratings are the same as those given in the previous chapter by the Table 3.1. The grid impedance consists of a $400 \mu H$ inductance and a series connected 0.1Ω resistor [C.1].

4.1.1. IMPACT OF THE GRID IMPEDANCE VARIATION

To investigate the impact of the varying grid impedance L_S on the system stability, the equivalent admittance of the grid Y_{SG} and the equivalent admittance of the multiple paralleled-connected converters Y_{LG} are defined as:

$$Y_{SG} = Y_G = \frac{1}{R_S + sL_S} \quad (4.1)$$

$$Y_{LG} = Y_{CPFC} + \sum_{x=A}^E Y_{CLx} = s C_{PFC} + Y_{CLA} + Y_{CLB} + Y_{CLC} + Y_{CLD} + Y_{CLE} \quad (4.2)$$

where, Y_{CPFC} denotes the capacitor admittance of C_{PFC} .

The minor loop gain T_{MG} used for stability analysis is made as:

$$T_{MG} = \frac{Y_{SG}}{Y_{LG}} \quad (4.3)$$

The equivalent inductance of the grid impedance is varied from $100 \mu H$ to $400 \mu H$ and the trajectory of the minor loop gain in the Nyquist plot is represented with red arrows and dotted lines in Fig. 4.2 [C.1]. Since the two trajectories are not encircling the $(-1, j0)$ point, the power system with both the grid inductances are stable [C.1].

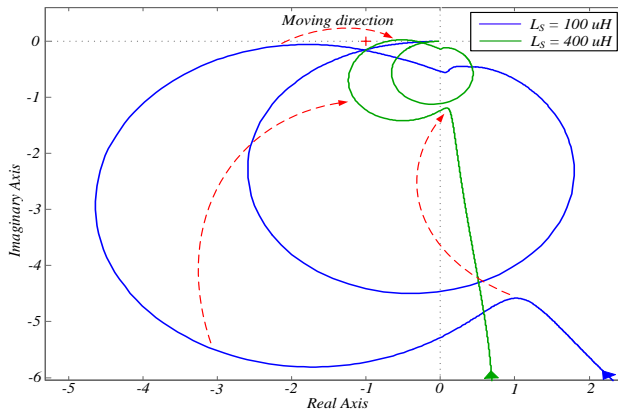


Fig. 4.2 The Nyquist plots of the minor loop gain T_{MG} with the different grid inductance L_S and its moving trajectory as L_S increases [C.1].

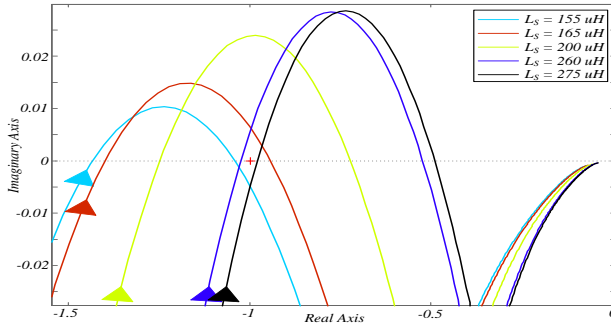


Fig. 4.3 The Nyquist plots for the marginally stable values of L_S [C.1].

However, there is a range of grid inductance values that can make the Nyquist plot of T_{MG} to encircle the $(-1, j0)$ point, as it is illustrated in Fig. 4.3 [C.1]. Some minor loop trajectories are enlarged around the $(-1, j0)$ point to show the range of the grid inductance that lead to instability. It is found that values of ($L_S = 165 \sim 260 \mu H$) makes the power system unstable. Outside this range the stability is ensured.

To demonstrate the validity of the Nyquist plots, time domain simulations are made for the previous parameters of L_S and are illustrated in Fig. 4.4. All the inverters are connected to the PCC and their output current references are set to zero in order to show clearly the effect of instability [C.1]. The parameter values used for the simulation are illustrated in Table 3.1, Section 3.5.3.

When the Nyquist plot shows stable conditions in Fig. 4.2, the voltage waveforms at the PCC does not contain distorted waveforms and the output current of the inverter reaches steady state quickly as it is illustrated in Fig. 4.4 (f) [C.1]. However, when the Nyquist plot moves in the vicinity of $(-1, j0)$ point and there is no encirclement (for example when $L_S = 155 \mu H$), the time domain simulations reveals a slightly longer time to reach the steady state of the current as shown in Fig. 4.4 (a) [C.1].

When the $(-1, j0)$ point is encircled, the system becomes unstable as it is illustrated in Fig. 4.4 (b). It turns into even worse when it goes near to the middle of the unstable region of the grid inductance, e.g. for the $200 \mu H$ grid inductance shown in Fig. 4.3, whose time domain waveforms corresponds to Fig. 4.4 (c).

The Nyquist plot approaches another interception point given by the $260 \mu H$ grid inductance. For this case, the oscillations in the PCC voltage and the inverter currents are more reduced [C.1]. A further increment in the inductance value (from $275 \mu H$ until $400 \mu H$) makes the system stable again as shown in Fig. 4.4 (f) [C.1].

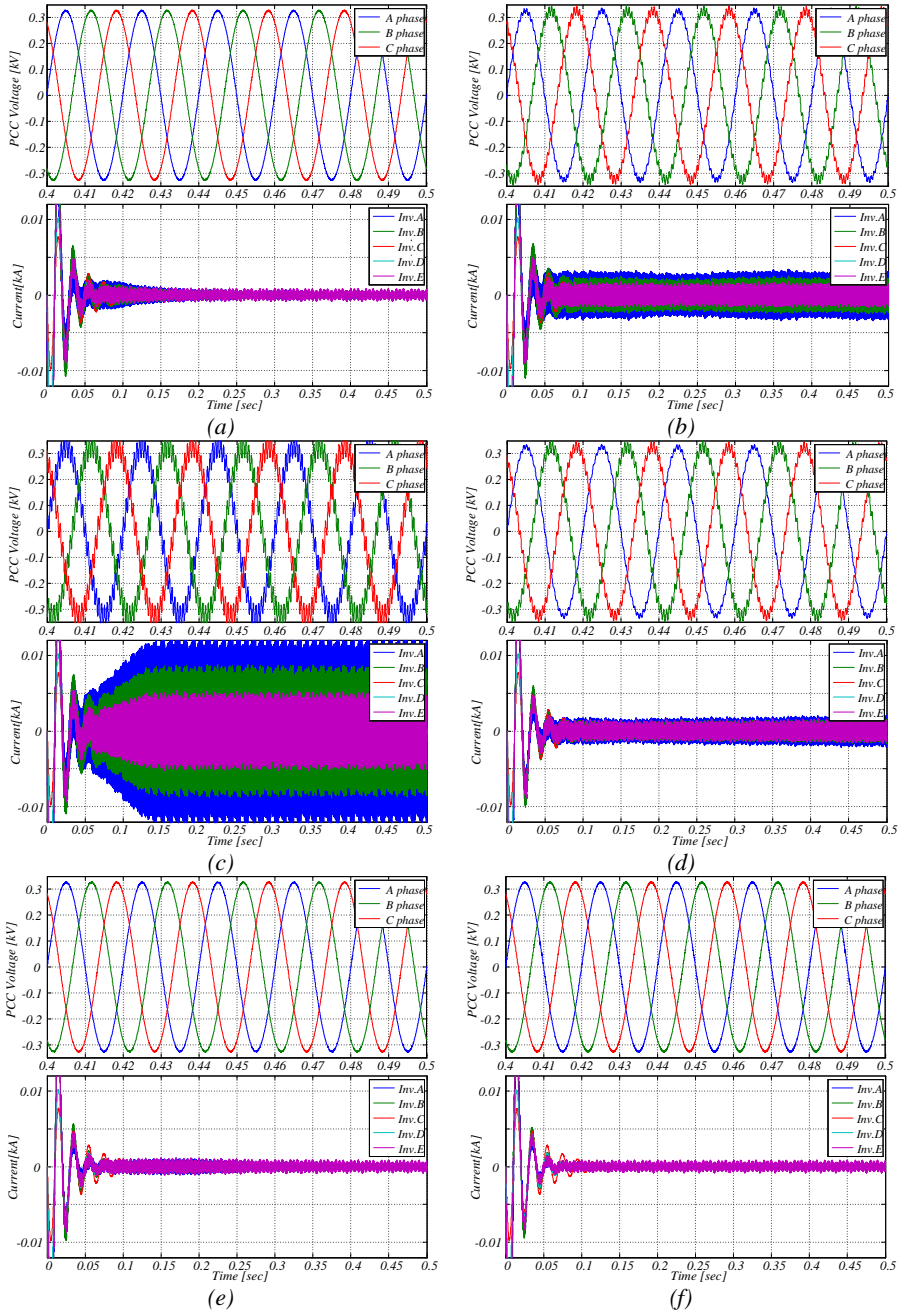


Fig. 4.4 Time-domain simulation for different values of L_S at no-load condition of the PCC voltage (upper) and inverter currents (lower): (a) 155uH; (b) 165uH; (c) 200uH; (d) 260uH; (e) 275uH; (f) 400uH [C.1].

4.1.2. INFLUENCE OF THE CONVERTERS ON STABILITY ANALYSIS

The unstable conditions may also be created when the converters are connected or disconnected in the power system. The reason is that when one or more converters operate in the power system, the load admittance Y_L is changed and the stability of the power system is affected [C.1]. To give an example of such stability analysis, a stable system with $L_S = 400\mu H$ is selected as reference. At first, the stability is evaluated at the output of the inv. A terminals. The source admittance Y_{SA} of the inv. A can be written as:

$$Y_{SA} = Y_{CLA} \quad (4.4)$$

The load admittance, which is seen from the inv. A it will include the equivalent admittances of all the other inverters in the power system and the grid admittance as given by:

$$\text{Case1: } Y_{LA} = Y_G + Y_{CPFC} + Y_{CLB} + Y_{CLC} + Y_{CLD} + Y_{CLE} \quad (4.5)$$

It is worth to consider the influence of some of the connected converters to stability by consequently eliminating some of them from Y_{LA} . This will illustrate different operating scenarios of the network where some different converters are disconnected in the power system. These scenarios are reflected in the equivalent admittance seen from inv. A given by:

$$\text{Case2: } Y_{LA} = Y_G + Y_{CPFC} + Y_{CLB} + Y_{CLC} + Y_{CLD} \quad (4.6)$$

$$\text{Case3: } Y_{LA} = Y_G + Y_{CPFC} + Y_{CLC} + Y_{CLD} + Y_{CLE} \quad (4.7)$$

$$\text{Case4: } Y_{LA} = Y_G + Y_{CPFC} + Y_{CLB} + Y_{CLD} + Y_{CLE} \quad (4.8)$$

$$\text{Case5: } Y_{LA} = Y_G + Y_{CPFC} + Y_{CLB} + Y_{CLE} \quad (4.9)$$

Once the source admittance is known and the scenarios with different load admittances are defined, the stability can be analyzed by the minor loop given by:

$$T_{MA} = \frac{Y_{SA}}{Y_{LA}} \quad (4.10)$$

The results are illustrated in Fig. 4.5 and reveals that there are two unstable scenarios which encircle the $(-1, j0)$ point, which are given by the Case 2 (Inv. E is disconnected) and Case 3 (Inv. B is disconnected). As it is shown in the previous section, the Case 2 is more unstable than the Case 3, since the Nyquist plot of the minor loop gain is encircling farther from the $(-1, j0)$ point.

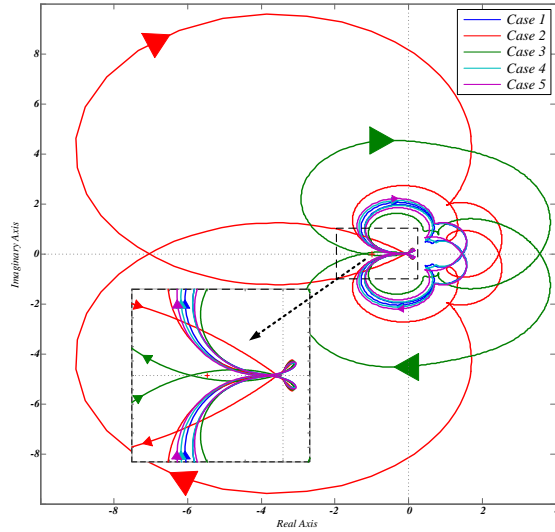


Fig. 4.5 The Nyquist plot of the minor loop gain T_{MA} for different scenarios of the load admittances Y_{LA} [C.1].

In order to verify the Nyquist plots, the time domain analysis is performed and illustrated in Fig. 4.6. The current references are set to the rated value of each converter according to Table 3.1. All the five scenarios are obtained by adjusting the Circuit Breaker (CB) included in each of the converter. In Case 1 with all converters connected, the system is stable. However, when the inv. B or inv. E are disconnected from the network, the system becomes unstable as shown in the Case 2 and Case 3.

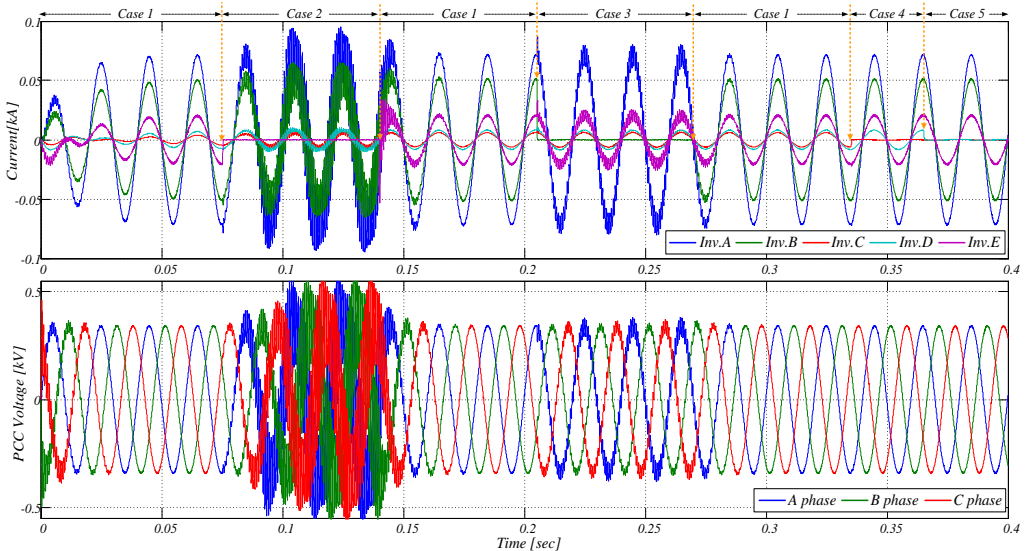


Fig. 4.6 Time-domain simulation with full load condition of the converter showing the inverter phase currents (upper) and the PCC voltage (lower) [C.1].

The inv. C and inv. D don't have significant effect on the system stability, which are related to Case 4 and Case 5.

The presented scenarios illustrate some of the unstable/stable combinations of the power system components. The instabilities are caused by interactions among the controllers and the filter parameters in each inverter.

4.2. NETWORK STABILIZATION WITH ACTIVE DAMPING

Recent research describe the stability of converters mainly by the relation between the LCL filter resonance frequency and the unavoidable time delay from the digital implementation of the controllers [49]. Precise boundaries are defined for the stable region of the LCL-filtered converter without any damping method. It means that the converter can be stable even it has high resonance peak as result of the harmonic filter structure. However, it is valid only for the single converter operation. When the converter is placed somewhere in the distribution network and connected together with other devices, it may not be always stable as result of the equivalent node impedance [25], [37], [54]. Therefore, the resonance peak of the filter may need to be damped in order not to be vulnerable from varying impedances in the network. It is worth to mention that adding a damping for one converter can be useful also to the nearby inverters. One consequence is that not all of the converters in the network are required to have a damping function. To evaluate the benefits of adopting one of the most used damping methods, the Cigré benchmark of a small-scale network with five different converters is adopted as it is illustrated in Fig. 2.2, Section 2.1 [4].

4.2.1. ACTIVE AND PASSIVE DAMPING METHODS

By adopting a damping function, the impedance of the network is changed and it may help the network nearby or other converters to achieve stability. There are mainly two types of damping approaches, one is the passive damping method, which inserts physical resistors in the harmonic filter corresponding to the power converter and may dissipate excessive energy from the resonance [55], [56]. The other approach is to adopt active damping by adding additional control loops and/or feedback signals that emulates the behavior of the physical resistor [57]–[59]. While passive damping methods are simple to be implemented and inexpensive, it may reduce the overall system efficiency, which limits its usage in applications where the emphasis is put on the efficiency, such in the case of PV systems. On the other side, additional sensors for the feedback signal or state estimators may be required to perform active damping. This complicates the overall control structure of the converter and it is also sensitive to the variation in the filter parameters or in the grid impedance. In the following, the active damping method is adopted and its influence for stabilization of the network is explored.

4.2.2. CONVERTER MODEL WITH ACTIVE DAMPING

The source admittance used for stability analysis is given by the output admittance of the converter, which can be found considering the averaged switched model of the grid converter with active damping illustrated in Fig. 4.7. The output admittance of the converter Y_{Sx} can be obtained by rearranging the block diagram [60], which result in:

$$Y_{Sx} = \left. \frac{v_{PCC}}{i_g} \right|_{i_g^* = 0} = \frac{Z_{Lf} + Z_{Cf} + K_{AD}G_d}{Z_{Lf}Z_{Lg} + (Z_{Lf} + Z_{Lg})Z_{Cf} + K_{AD}G_dZ_{Lf} + G_cG_dZ_{Cf}} \quad (4.11)$$

where, K_{AD} is the active damping gain.

The open loop gain T_{OL} of the converter is calculated as:

$$T_{OL} = \frac{G_cG_dZ_{Cf}}{Z_{Lf}Z_{Lg} + (Z_{Lf} + Z_{Lg})Z_{Cf} + K_{AD}G_dZ_{Lf} + G_cG_dZ_{Cf}} \quad (4.12)$$

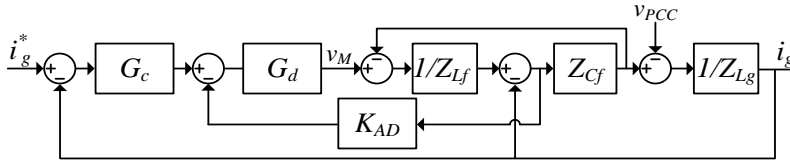


Fig. 4.7 Averaged switching model of an inverter with active damping [C.2].

The implemented time-domain model for the PSCAD/ EMTDC simulation of the grid-connected converter is illustrated in Fig. 4.8.

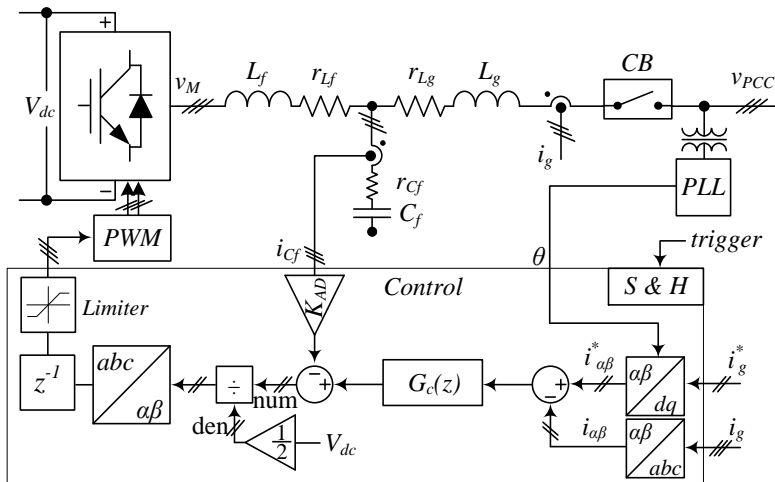


Fig. 4.8 PSCAD implementation of an inverter with active damping [C.2].

In order to implement the digital controller in PSCAD/EMTDC, the sample and hold function is build and the digital resonance controller $G_c(z)$ from (2.9) is used together with the Tustin discretizing method, which results in:

$$G_c = K_p + \frac{K_I \sin(2\pi f_0 T_s)}{2 * 2\pi f_0} \frac{z^2 - 1}{z^2 - 2 \cos(2\pi f_0 T_s) z + 1} \quad (4.13)$$

This controller operates in the stationary reference frame and is driven by an external triggering signal for the sample and hold function.

4.2.3. NETWORK MODEL FOR THE LOAD ADMITTANCE

The source admittance of the converter was obtained in a straightforward manner as given by (4.11). However, the load admittance given by the network impedance needs to be calculated. The problem is that it will include all the other converters connected to that node together with their corresponding line impedances. Therefore, the Kirchoff's Current Law (KCL) admittance matrix is used to solve the admittance relation [54]. The voltage of the reference nodes (the nodes which are to be investigated in the network) are grouped in a voltage vector $[V]$ while the current sources (grid converters) attached to the nodes are grouped in a current vector $[I]$. Afterwards, the relation between the reference node voltages and currents are derived as follows:

$$\begin{array}{c}
 [Y] \\
 \begin{bmatrix} Y_{11} & \dots & Y_{18} \\ \vdots & \ddots & \vdots \\ Y_{81} & \dots & Y_{88} \end{bmatrix}
 \end{array}
 \begin{array}{c}
 [V] \\
 \begin{bmatrix} V_{R6} \\ V_{R10} \\ V_{R18} \\ V_{R16} \\ V_{R15} \\ V_{R3} \\ V_{R4} \\ V_{R9} \end{bmatrix}
 \end{array}
 =
 \begin{array}{c}
 [I] \\
 \begin{bmatrix} I_{inv.1} \\ I_{inv.2} \\ I_{inv.3} \\ I_{inv.4} \\ I_{inv.5} \\ I_{R3} \\ 0 \\ 0 \end{bmatrix}
 \end{array}
 \quad (4.14)$$

All the admittances connected to the reference node are included in the admittance matrix $[Y]$. In order to obtain the node voltages created by the corresponding node currents, the left and right side of (4.14) are multiplied with $[Y]^{-1}$, which results in the impedance matrix $[Z]$:

$$\begin{bmatrix} V \\ V_{R6} \\ V_{R10} \\ V_{R18} \\ V_{R16} \\ V_{R15} \\ V_{R3} \\ V_{R4} \\ V_{R9} \end{bmatrix} = \begin{bmatrix} Z_{11} & \dots & Z_{18} \\ \vdots & \ddots & \vdots \\ Z_{81} & \dots & Z_{88} \end{bmatrix} \begin{bmatrix} I \\ I_{inv.1} \\ I_{inv.2} \\ I_{inv.3} \\ I_{inv.4} \\ I_{inv.5} \\ I_{R3} \\ 0 \\ 0 \end{bmatrix} \quad (4.15)$$

The diagonal elements in $[Z]$ are represented by the equivalent impedances of the reference nodes, which is produced the node voltage and the current of the connected converters. However, these diagonal elements include the output impedance of the converters, which are not identified. Therefore, the stable load admittance can be obtained by subtracting the unidentified source admittance from the inverse of diagonal impedances, which is resulting in:

$$Y_{Lx} = \frac{1}{Z_{xx}} - Y_{Sx} \quad (4.16)$$

where, 'x' indicates the inverter numbering.

4.2.4. CHARACTERIZATION OF THE INDIVIDUAL VSC

As explained in [49], the stable region of the converter with LCL filter is determined by the ratio between the resonance frequency of the LCL filter and the sampling frequency of the converter. If the ratio is higher than 1/6, then the converter is stable without any damping method. For this reason, the harmonic filters are designed according to this stability region as given by the parameters shown in Table 3.1. Taking into considerations the parameters shown in Table 3.1, the open loop characteristics of each individual converter given by (4.12) is shown in Fig. 4.9.

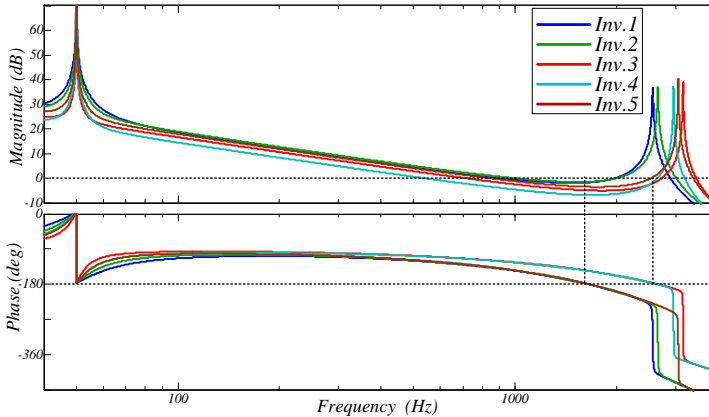


Fig. 4.9 Characteristics of the converters with the parameters given in Table 3.1 [C.2].

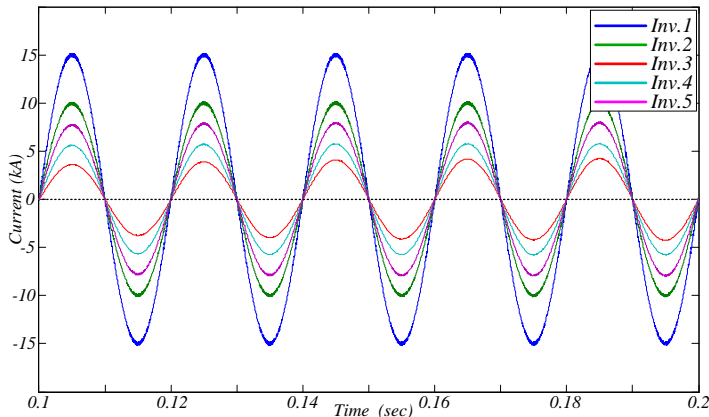


Fig. 4.10 Operation of the converters connected to an ideal grid voltage [C.2].

Since the -180° degrees crossing occurs for negative magnitude, all the converters are designed individually stable. This fact is demonstrated by the time-domain simulation of the converter grid currents under ideal grid voltage (negligible grid impedance), which are illustrated in Fig. 4.10.

4.2.5. STABILITY ANALYSIS OF THE CIGRÉ DISTRIBUTION SYSTEM

In the following, the ideal grid voltage is replaced with the actual Cigré distribution system shown in Fig. 2.2, Section 2.1. The system will be stable if the minor loop gain T_{mx} satisfies the Nyquist stability criterion. T_{mx} is defined as:

$$T_{mx} = \frac{Y_{Sx}}{Y_{Lx}} \quad (4.17)$$

As result of the additional impedance at each node in the Cigré network, the stable operation of the converters cannot be assured. Each node in the test system have its own minor loop gain given by (4.17). The stability of the converters is assessed by the Nyquist stability criterion of the minor loop trajectories illustrated in Fig. 4.11.

It is worth to mention that the minor loops shown in Fig. 4.11 are drawn considering the connection of only one converter at a time in order not to include the effect of the other converters. The interactions between the converters in the Cigré network are presented in the next section. *Inv. 5* is the only stable converter when the grid impedance changes, and the rest of them are unstable. That means that all the converters except the *Inv. 5* may need active damping in order to be stabilized.

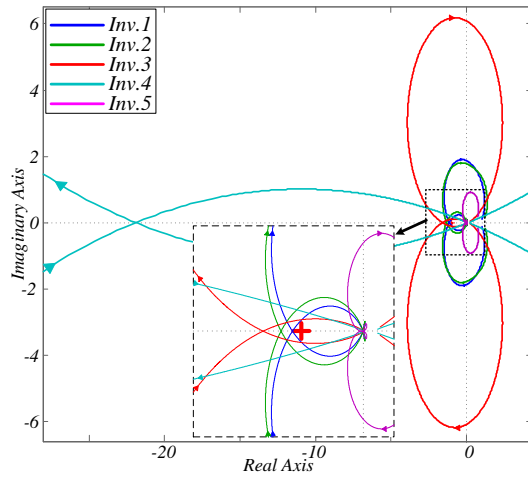


Fig. 4.11 Stability evaluation of the converters without damping [C.2].

4.2.6. STABILIZATION OF THE NETWORK WITH ACTIVE DAMPING

Fig. 4.12 shows the stabilization effect by adding active damping for each of the unstable converters. A comparison between the output currents of the respective unstable and stabilized converters are illustrated in Fig. 4.13.

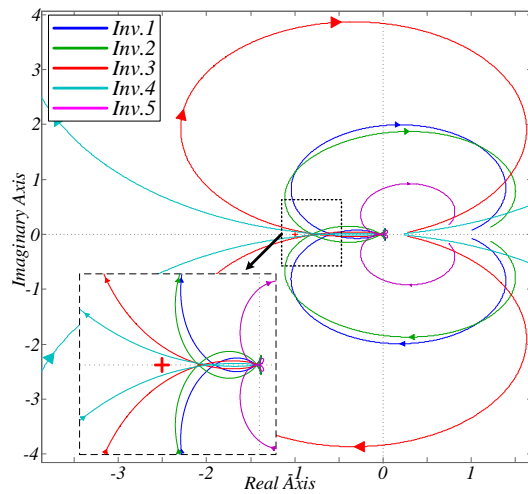


Fig. 4.12 Individually stabilized inverters with active damping [C.2].

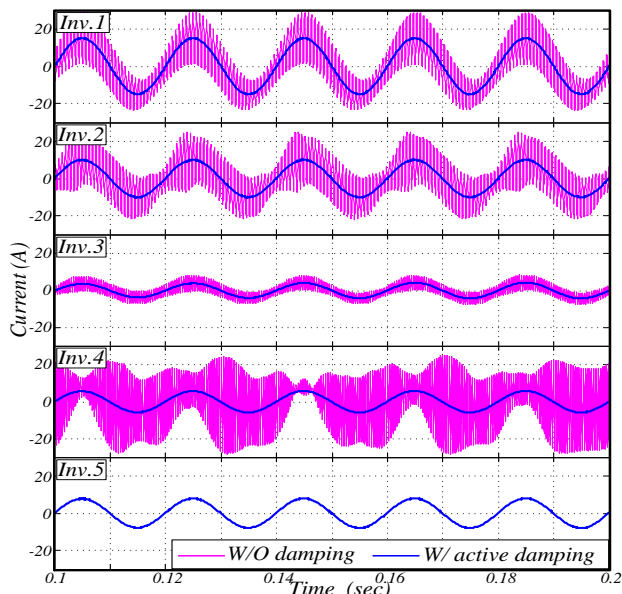


Fig. 4.13 Unstable converter w/o damping and stabilized w/ damping ($K_{AD,Inv.1} = 1$, $K_{AD,Inv.2} = 1$, $K_{AD,Inv.3} = 4$, $K_{AD,Inv.4} = 5$) [C.2].

4.2.7. INTERACTIONS BETWEEN CONVERTERS

Even if the converters are stable when they operate alone, they may easily become unstable when other converters are connected in the network. For example, the *Inv. 1* and *Inv. 2* are becoming unstable when they operate together in the same time as it is illustrated in Fig. 4.14 and Fig. 4.15.

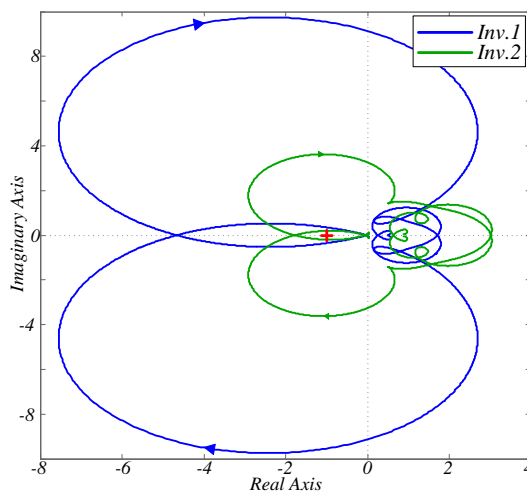


Fig. 4.14 Unstable converters in the network without active damping [C.2].

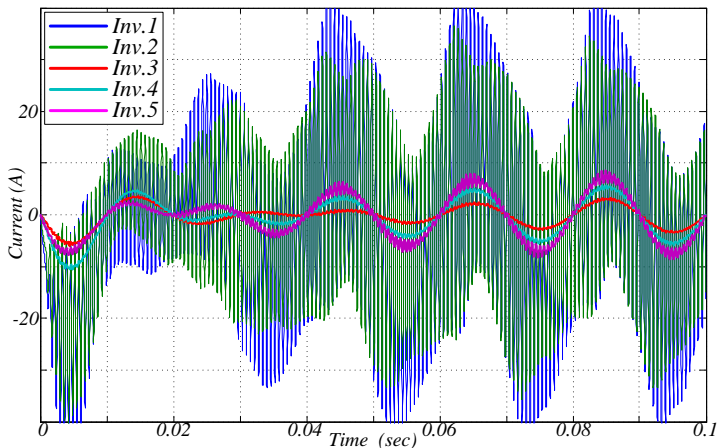


Fig. 4.15 Output current of the converters in case of instability due to interaction between the converters [C.2].

There are several possibilities to stabilize the networks. For this scenario, the active damping gains in the *Inv. 3* and *Inv. 4* are increased in order to stabilize the overall network. The results are shown in Fig. 4.16 together with the adopted values of the active damping gains.

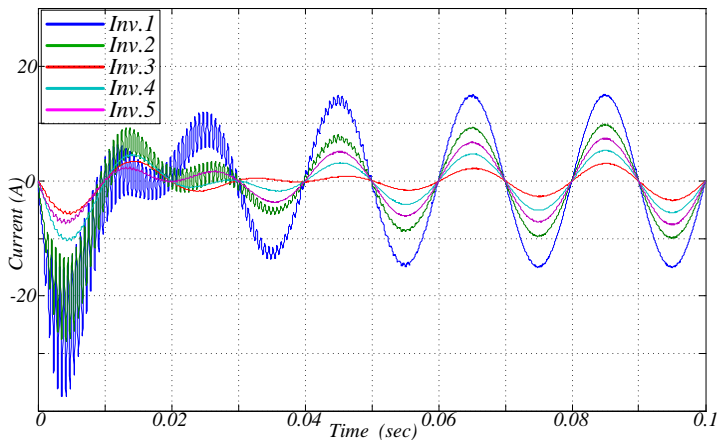


Fig. 4.16 Stabilized converters with increased active damping gains ($K_{AD,Inv.1} = 1$, $K_{AD,Inv.2} = 1$, $K_{AD,Inv.3} = 10$, $K_{AD,Inv.4} = 12$) [C.2].

4.2.8. STABILIZATION OF THE NETWORK WITH REDUCED ACTIVE DAMPING CAPABILITY

Furthermore, the system stability can be obtained by reduced efforts, if the active damping gains are properly chosen. For example, it is possible to achieve the overall

stability only by having active damping functions in the *Inv. 1* and *Inv. 2*. In Fig. 4.17 are shown the stabilized waveforms of converter currents. In comparison with Fig. 4.16, the high frequency transient oscillations are significantly reduced by the proper selection of the active damping gains.

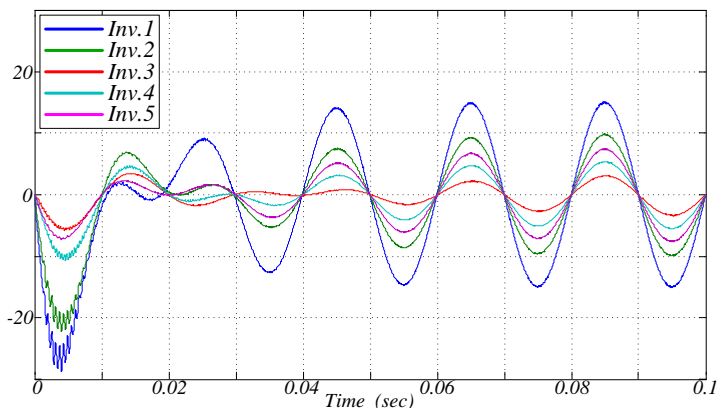


Fig. 4.17 Stabilized network by *Inv. 1* and *Inv. 2* with active damping functions ($K_{AD,Inv.1} = 2$, $K_{AD,Inv.2} = 3$) [C.2].

The result is revealed also by the Nyquist plot of each of the converter minor loop gain illustrated in Fig. 4.18.

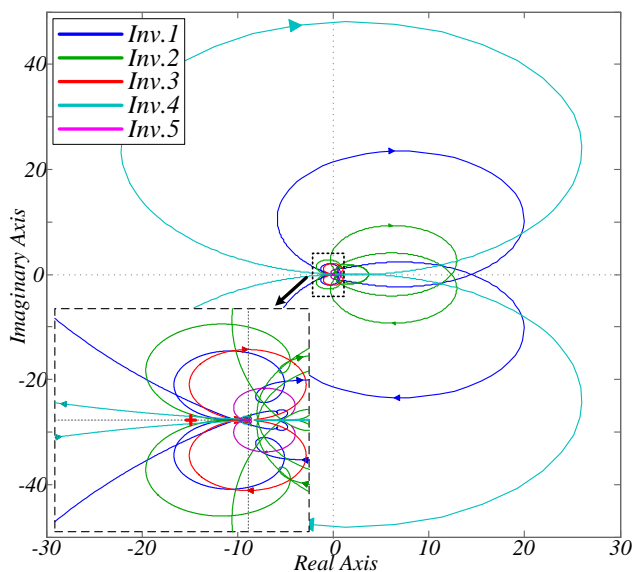


Fig. 4.18 Minor loop gain of the stabilized converters with two active damping functions in the *Inv. 1* and *Inv. 2* [C.2].

4.3. SITE SELECTION OF ACTIVE DAMPER

Another approach to address the network instabilities is to add a specialized damping equipment like an active damper, close to the problematic area [54], [61]. “The active damper, which is a high bandwidth power-electronics based power converter is exclusively designed for harmonic resonance damping has been proposed recently. The active damper is capable of reshaping the equivalent node impedance at the location where it is connected. Therefore, the active damper can be seen as an adjustable frequency dependent resistor. The problem is that complex systems like a distribution power system have many nodes and each node can be a candidate for the placement of the active damper.” [C.3]

In the past, power quality issues in the power system have been addressed with shunt active filters and their placement was shown to be the best at the end terminal of the feeder in a radial distribution system [62]. However, for high frequency harmonic instabilities, this may not lead to the same results, when is to be decided about the active damper placement. the previous research, such as the best place is the end of the radial structure. The optimum place can be found by analyzing the boundary value of the active damper gain or the equivalent resistance at each node in the network needed to ensure the stable network operation.

4.3.1. ACTIVE DAMPER AS A STABILIZER

“The active damper provides a high frequency stabilizing function for the harmonic instabilities by means of adding a frequency dependent dynamic resistive behavior. Its parallel connection makes a plug-and-play capability, which can be placed anywhere in the distribution system.” [C.3]

“Its resistive behavior can be represented as a voltage-controlled current source as shown in Fig. 4.19 (a). In order to avoid the heavy loading from the fundamental frequency, the equivalent resistance of the active damper should not have the same resistance for all frequencies. Therefore, a notch filter $H(s)$ is inserted in the feedback loop of the active damper in order to increase the fundamental frequency resistance, as defined by:

$$H(s) = \frac{s^2 + \omega_n^2}{s^2 + 2\zeta\omega_n s + \omega_n^2} \quad (4.18)$$

where, s is the Laplace operator, ω_n is the notch frequency [rad/sec] and ζ is the damping ratio.” [C.3]

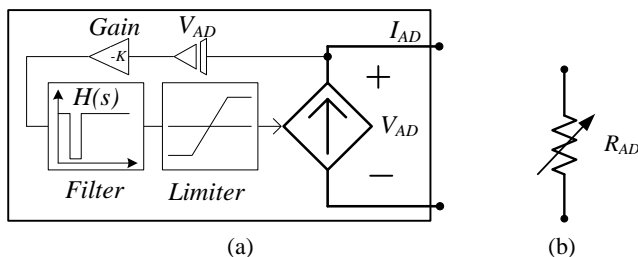


Fig. 4.19 Active damper of distribution line (a) Single-line diagram of the active damper model; (b) Frequency dependent resistor [C.3].

The frequency dependent resistor R_{AD} can be made as follows:

$$R_{AD} = \frac{1}{K \cdot H(s)} \quad (4.19)$$

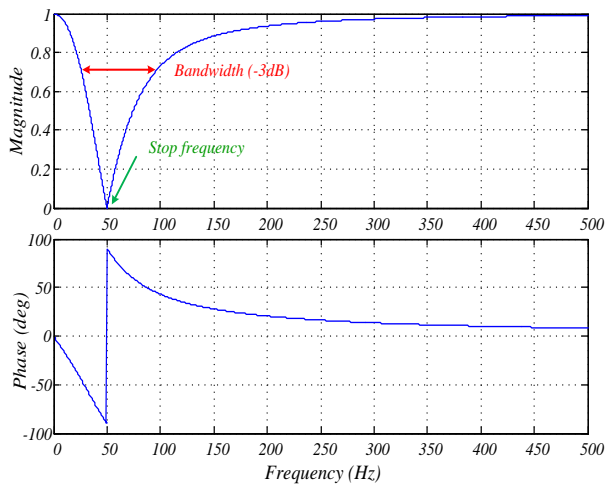
Because, the rated power of the active damper should be in a reasonable range. Therefore, a current limiter is inserted to limit its power rating.

4.3.2. NOTCH FILTER DESIGN FOR AN ACTIVE DAMPER

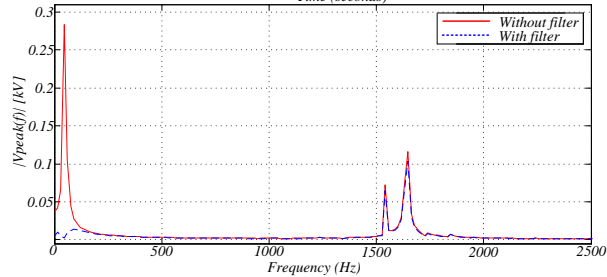
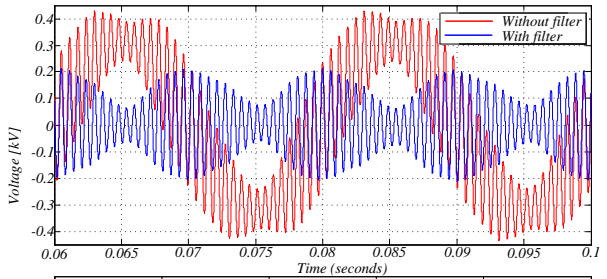
A notch filter is needed to get rid of the needless low frequency harmonics plus the fundamental frequency. Based on (4.18), the design parameters of the notch filter is as follows:

- Notch frequency: 50 [Hz]
- Damping ratio: 0.707
- Bandwidth (-3dB): 70.7 [Hz]

The dynamics of the designed notch filter is demonstrated in the frequency domain with its bode diagram in Fig. 4.20 (a). The filter gain at the stop frequencies moves towards zero, while the desired bandwidth (at -3 dB) of the filter satisfies with the design parameter. In order to see the capability of the notch filter, one exemplary unstable node voltage of the network is used as shown in Fig. 4.20 (b). Therefore, the fundamental frequency waveform is filtered out and the high frequency oscillation is remained only as shown in Fig. 4.20 (b) top figure. The result is also compared in the frequency domain to illustrate the filtering effect as shown in Fig. 4.20 (b) bottom figure.



(a)



(b)

Fig. 4.20 The response of the notch filter: (a) Bode plot; (b) Time domain response (upper) and its FFT (lower) [C.3].

4.3.3. STABILITY ANALYSIS OF THE CIGRÉ DISTRIBUTION NETWORK WITH VARYING GRID IMPEDANCE

In order to verify the stabilizing effects of the active damper, the grid impedance of the Cigré distribution network is increased by three times, which leads to instability. The time-domain simulation of each of the converter output voltage and current are illustrated in Fig. 4.21 for the rated and increased grid impedance. In rated

conditions, each of the converter starts with the oscillations as result of the start-up transients, but they are dampening out within few periods. When the grid impedance is three times larger (weak grid condition), the converters becomes unstable. In this case, the oscillations are maintained during the whole operation of the converters.

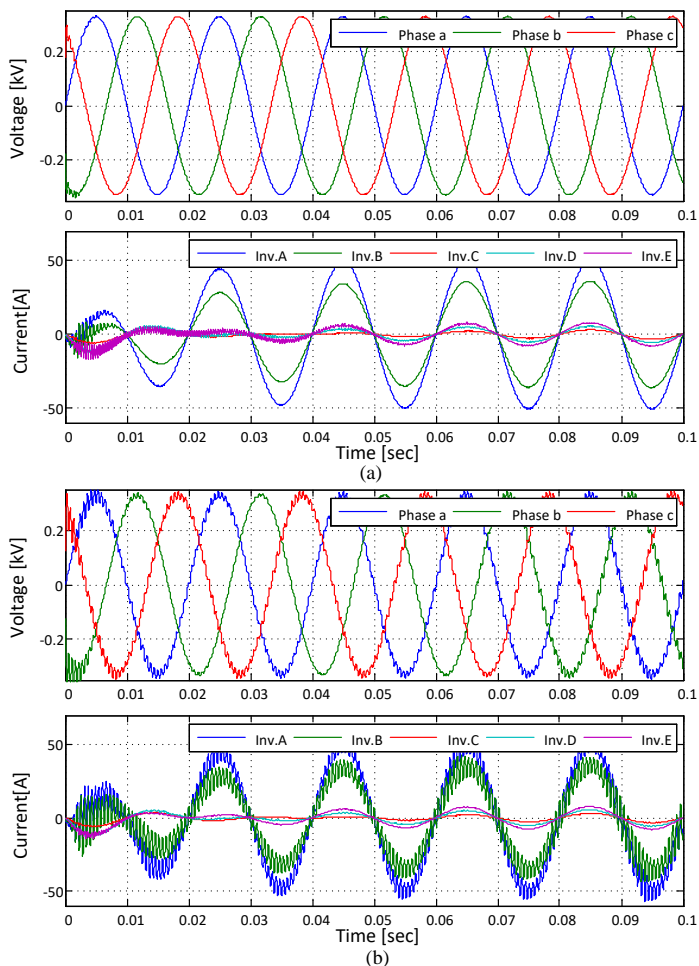


Fig. 4.21 Stable and destabilized distribution system with varying grid impedance: (a) Rated grid impedance; (b) Three times higher grid impedance [C.3].

In order to deal with the weak grid condition, the stability analysis should be performed sequentially in order not to be influenced by an unidentified or a potentially risky system [C.4]. This sequential procedure should be used, if there is more than one non-passive subsystem. The sequential procedure used for the stability analysis of a weak grid condition is illustrated in Fig. 4.22 and explained as follows. From the Inv. A to the Inv. E, all the converters are investigated using the

Z+Z stability criterion which is another example of the IBSC [63]. With this criterion, the $(0, j0)$ point is considered for the point which determines the stability, instead of the $(-1, j0)$ point as used in the conventional approach. If the trajectories in the Nyquist plot encircle the $(0, j0)$ point, then the existence of the possible RHP in the system is found [C.3]. From Fig. 4.22 there is no encirclement in the Nyquist plot. Then, the overall system with the rated grid impedance is stable. However, when the grid impedance gets larger, the system may become unstable [C.3].

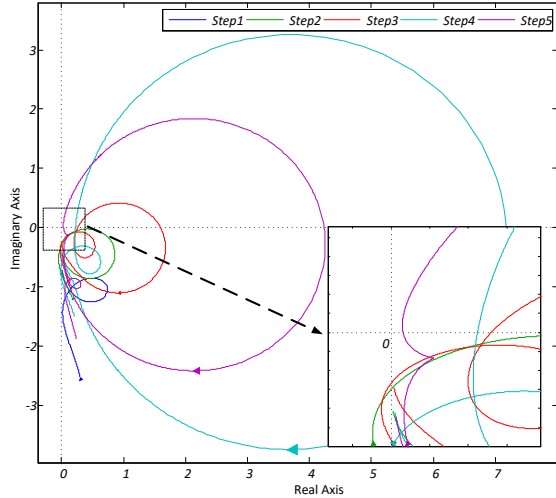


Fig. 4.22 Step by step procedure for analyzing the system stability in the weak grid condition [C.3].

The weak and strong grid conditions are compared by the Nyquist plot in Fig. 4.23.

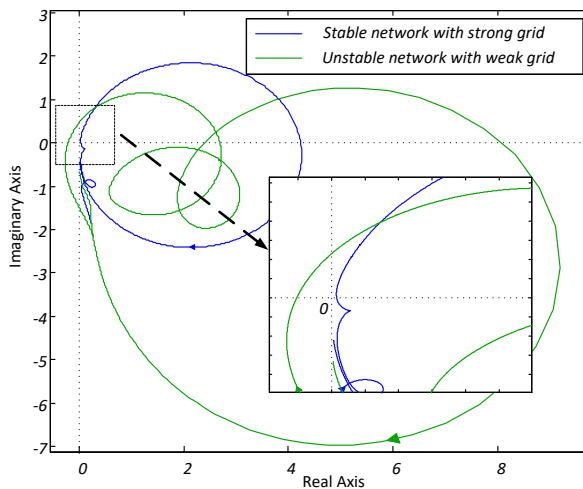


Fig. 4.23 Stability assessment with different grid impedances (step 5) [C.3].

The plot shows that in stiff grid conditions, the Nyquist plot does not encircle the $(0, j0)$ point. Conversely, there is an interaction between the converters when the grid is in a weak condition. There are two stable converters in spite of the change in the grid impedance variation, which are the Inv. A and the Inv. B as illustrated in Fig. 4.24. The other converters in the network (Inv. C, Inv. D and Inv. E) become unstable when the grid impedance is increased. As all are designed stable stand-alone, the converters are stable when they are operated individually, but when converters join together, the system may become unstable. It is caused by the non-passive output admittance of the converters and the effect can be seen in different cases.

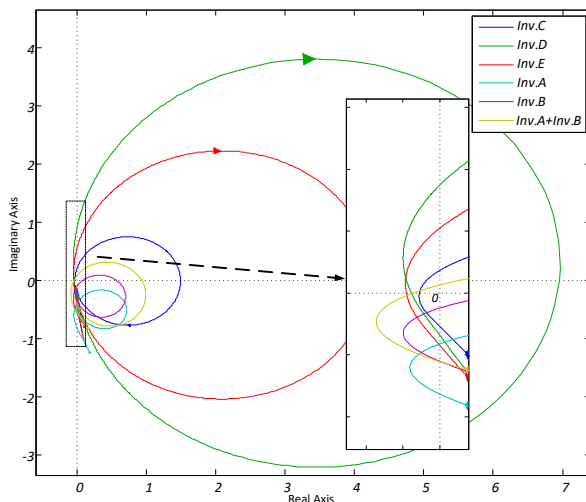


Fig. 4.24 Stability assessment with different grid impedances for individual converters [C.3].

Time domain simulations are illustrated in Fig. 4.25, which demonstrate the instability phenomena shown in the Nyquist plots.

However, up to this point, only the combination of the Inv. A and Inv. B has been shown that may trigger instability with increasing the grid impedance. The other converters are unstable alone when the grid impedance is increased. There may be another unstable or stable conditions, which can result from the different combinations of the converters. All the possible scenarios when there are five different converters in the network is calculated and represented as a summation of the combinational numbers as given by:

$${}_5C_1 + {}_5C_2 + {}_5C_3 + {}_5C_4 + {}_5C_5 = 31 \quad (4.20)$$

All the combinations should be taken into account for a complete evaluation of the network. Afterwards, it is possible to find proper solutions to mitigate the interactions that may lead to instability.

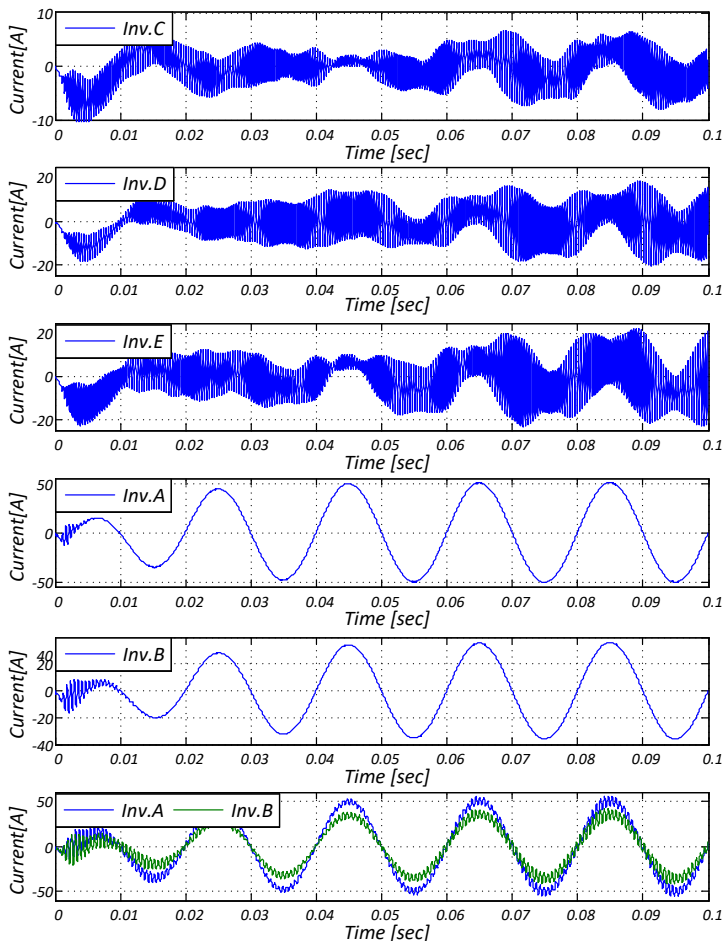


Fig. 4.25 Simulated waveforms of the individual converters output current with increased grid impedances [C.3].

4.3.4. ACTIVE DAMPER PLACEMENT

The active damper can be located at any points in the power system due to its parallel structure. This brings a high degree of freedom when deciding about its location to mitigate the network instabilities. However, it may bring confusions to us about its location from many possibilities. For an active damper, the best location may be a place where the least effort is required to cover all the instabilities. The effort or the capacity of the active damper will be the amount of injected or absorbed current needed to obtain the stable operation of the network.

In order to decide the place where the minimum damping is required, the parameter sweep method is used. By varying the damping resistor in the active damper, the

boundary values needed for stabilizing the network can be obtained at each node. In Fig. 4.26, the resistance is increased from 1 Ω to 30 Ω at node R4. The stability measurement point is the node R4 while the active damper is placed at node R16. The system becomes unstable when the resistance becomes larger.

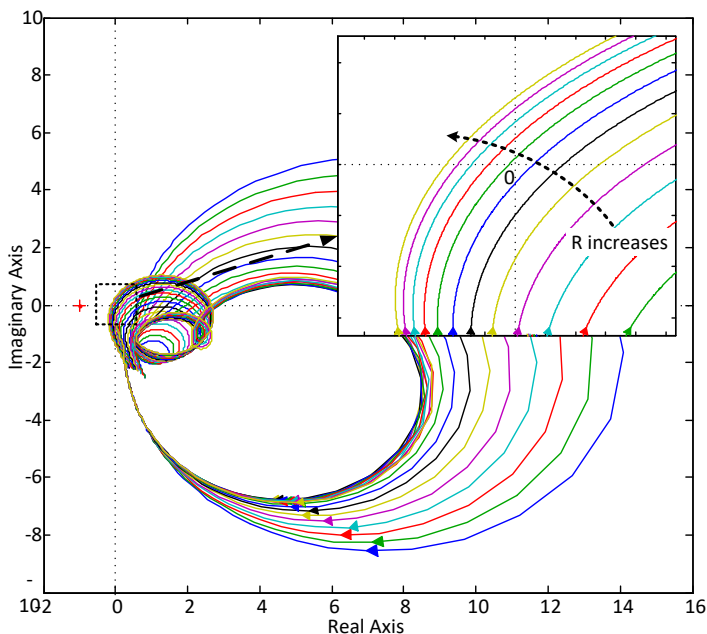


Fig. 4.26 Stability at node R4, when the active damper is placed at node R16 with different values of the resistance (from 1 Ω to 30 Ω) [C.3].

All of the nodes and various converter operating conditions are considered at the same time. Therefore, some of the representative cases are illustrated in Table 4.1.

Table 4.1 Required damping resistance [Ω] for unstable network [C.3].

Maximum R [Ω]		Node name							
		R3	R4	R6	R9	R10	R15	R16	R18
Converters combination	{E}	5.0	7.2	7.2	7.2	7.2	21.0	7.2	7.2
	{D}	5.0	8.6	14.7	12.3	12.3	7.2	25.0	12.3
	{C}	2.9	6.0	8.6	17.5	20.9	4.2	8.6	30.0
	{A,B}	5.0	7.2	14.7	21.0	25.1	7.2	14.7	25.1
	{C, D, E}	3.5	5.1	7.2	10.3	10.3	8.6	10.3	12.3
	{A, B, C, D, E}	4.2	7.2	12.3	17.5	21.0	7.2	12.3	21.0
	{A}	Stable							
	{B}	Stable							
Ranking		8	7	5	3	2	6	4	1

In Table 4.1, the rows show the combinations of joining converters in the test grid and the columns show the active damper place. The numbers in the table represent the maximum value of the resistance that is necessary to ensure the overall system stability. For example, when only the Inv. E is seen in the system, the node R15 needs the minimum effort for stabilizing them. Instead, the node R3 is required the most effort. In order to give comparisons, all the data are grouped and sorted based on the effectiveness of the damping efforts [C.3]. Each row is ranked separately and their rankings are summed up and represented in the bottom row. The results show that the active damper connected on the node R18 has the lowest effort. An equivalent damping resistance value of 7.2Ω or less is needed to ensure a stable network for all operating conditions.

In general, it may be expected that the best place for placement of the active damper is the node where the interacting converter is located or the closest location from the unstable converter; e.g., the node R15 for Inv. E, the node R16 for Inv. D or the node R18 for Inv. C. Moreover, there is a trend that the stabilizing effort become effective when the active damper location is getting far from the feeder. It is becoming more effective when it moves towards the terminal of the distribution network. This might be reasonable since the aforementioned nodes are located in between the interacting converters. Therefore, it may easily dampen the oscillations in between them. Fig. 4.27 shows the time domain simulation results that corresponds to the scenarios defined in Table 4.1. At first, the simulations are made with and without the active damper connected to the node R18. The corresponding damping resistor value for the damper is set to 7.2Ω and the output current waveforms are shown in correspondence with the analyzed results. As it is expected in the table 4.1, only the individual operations of the Inv. A and Inv. B are stable without the active damper as shown in the upper plot. Also, the entire system becomes stable with an active damper with 7.2Ω equivalent resistance.

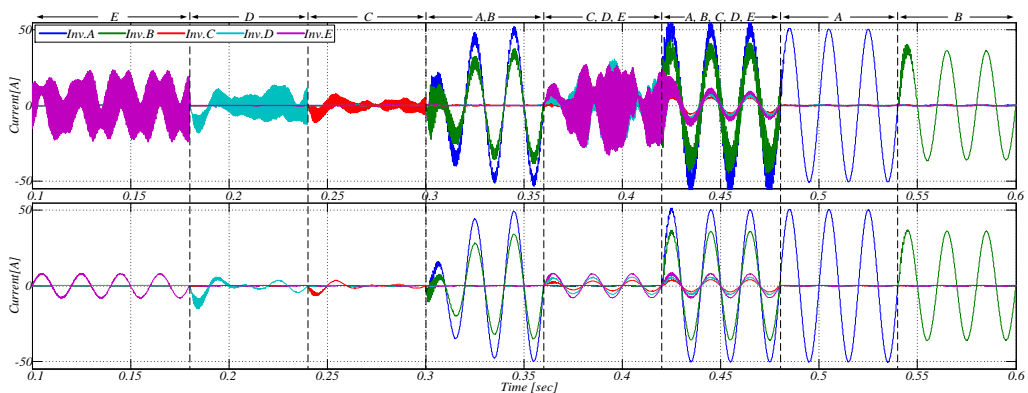


Fig. 4.27 Time domain simulations of the converters output current when: No active damper is connected (upper); The active damper is placed at node R18 (lower) [C.3].

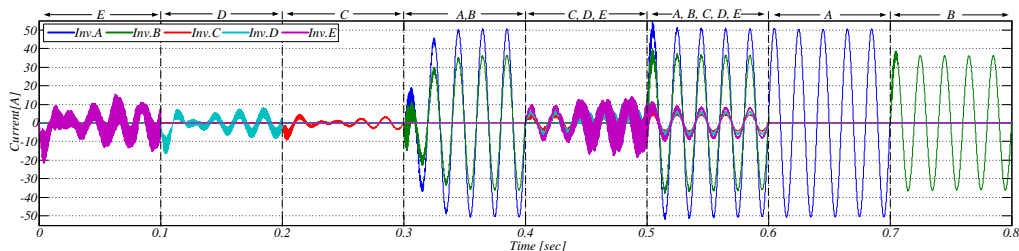


Fig. 4.28 Time domain simulations of the converters output current when the active damper is placed at node R9 with the damping resistance value set to 17.5Ω [C.3].

In order to verify the validity of the simulation, the effect of an active damper at node R9 is simulated also. In this case, the selected damping resistance for the active damper is $17.5\ \Omega$. As shown Table 4.1, there exist three unstable cases of the converters, which are {D}, {E} and {C, D, E}. The respective stable and unstable operating conditions are depicted in Fig. 4.28.

The parameter sweep method for analyzing the required equivalent damping resistance of active damper used to stabilize the power distribution system shows a reasonable accuracy and can find out the effective location for the active damper placement. However, the computation burden on the sweeping method will become heavy when the complexity of the network is increased largely. Therefore, a method to reduce the calculation efforts needs to be taken into consideration.

4.4. SUMMARY

The stability assessments for some case studies are given. Firstly, the unstable operations of the paralleled converters are investigated and secondly, a more realistic benchmark case has been adopted and the stability analysis is performed. There are several ways to stabilize the unstable system by introducing additional damping into the system such as passive damping, active damping methods and/or a specialized harmonic frequency damping unit, such as the active damper are discussed. The relative stability of the network is investigated by measuring the required damping for all nodes in the network. The most adequate location in the network for the placement of the stabilization unit, which is the most unstable point in the network, is found. This shows the stability risky indexes of the network, which can be used to avoid the resonance condition in the network, by adding necessary damping function.

CHAPTER 5. EXTENDED MODEL FOR HARMONIC STABILITY STUDY

This chapter is based on publication [J.2].

The influence of the harmonic filter model in stability analysis is shown in this chapter. First, the control interaction of the power converters with harmonic filter is given. A hypothesis is drawn, such as the converter side inductance in the harmonic filter can be the main cause for mismatch in stability analysis, fact that is supported by the high loss characteristic of the converter side inductance, which account for the majority of loss in the harmonic filter. This makes the equivalent damping of the inductor unknown. A Jiles-Atherton hysteresis model is investigated and implemented in order to overcome the drawbacks of the more simplified inductor models, which are given mainly by a pure inductance in series with a resistor. This reveals a very different behavior of the harmonic filter than otherwise expected and which cannot be revealed by the conventional modeling approach. The stability analysis of the grid-connected converter with improved harmonic filter model conclude this chapter.

5.1. INTRODUCTION

Power electronics based sources raises new challenges to the power system stability, given by the closed loop response of the converter with the interfaced harmonic filter [64]. The main cause of instability is a reduced phase and gain margin of the closed loop system due to the resonant behavior of the filter [65]. Methods that addresses resonance damping of the filter with the view to improve stability are well documented in literature and may include among others, active damping [66]–[68] and/or passive damping methods [33], [69]. There is also the possibility to avoid passive or active damping methods by a proper placement of the resonance frequency of the filter depending on the position of the current sensor used for the current reference signal [C.6].

To illustrate the stability phenomena in practical applications, a 10 kW power converter connected to the utility grid is illustrated in Fig. 5.1 together with the measured grid current waveforms, which approaches the instability of the power converter. The unstable condition is obtained by increasing deliberately the proportional gain of the current regulator until the resonance of the whole system is excited [70]. Therefore, the lack of damping around the resonance frequency of the filter may trigger instability. It can be summarized that the stability of a power electronics based system depends on the impedance of the filter, impedance of the network at PCC and the current controller parameters. From the three factors, the

design of the current controllers and the impedance of the network are relatively well addressed in literature [71]–[73].

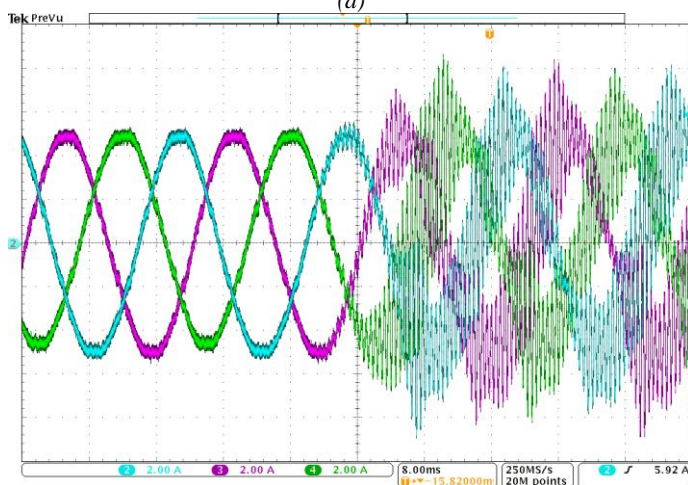
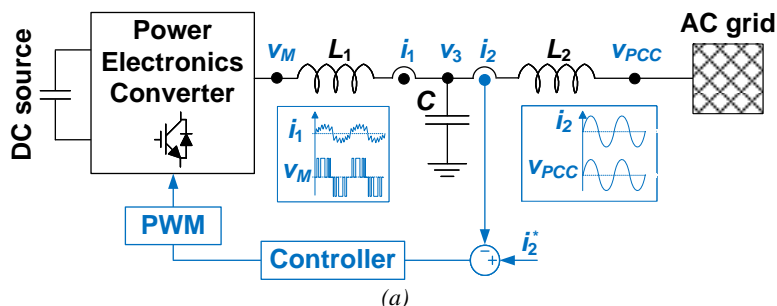


Fig. 5.1 Stability phenomena in power electronics based power system: (a) Circuit diagram of a power converter connected to the AC grid through an LCL filter, where L_1 and L_2 are the filter inductors on the converter and grid side, respectively and C accounts for the filter capacitance. The measured variables can be the converter and grid current (i_1 and i_2), converter modulated voltage (v_M), capacitor voltage (v_C) and the voltage at PCC (v_{PCC}); (b) Grid current waveforms (i_2) approaching instability [J.2].

The only thing, which is not completely understood is the impedance of the harmonic filter. For example, the converter side inductor of the harmonic filter (LCL filter) is excited with high-frequency rectangular voltages, which leads to significant losses as a result of the skin effect and dynamic hysteresis minor loops given by the high switching frequency ripple [29]. It means that the main losses of the harmonic filter are distributed in the converter side inductor and these losses are changing with the operating condition of the converter [30], [74].

5.2. DESCRIPTION OF HARMONIC INSTABILITY

The influence of the harmonic filter impedance on the harmonic stability is explored in the following.

5.2.1. FILTER MODEL

There are different methods of modeling the filter impedances, given by Z_1 , Z_2 and Z_3 . The simplest method is to consider the pure parameter values alone, which disregards the parasitic components. This is useful for the worst case evaluation of the system and it helps to find simple useful analytical solutions for filter and the controller design [75]. However, it neglects the existing damping of the passive components, which improve the stability of the interconnected system.

Another modeling method is to use serial or parallel resistors to mimic the average power loss in the component, which are used further to emulate the damping effect (for a given power loss in the component). A series resistor representation, which accounts for the loss in passive components is illustrated in Fig. 5.2. Then, the corresponding filter impedances result as follows:

$$Z_1 = R_1 + sL_1 \quad (5.1)$$

$$Z_2 = R_2 + sL_2 \quad (5.2)$$

$$Z_3 = R_3 + \frac{1}{sC} \quad (5.3)$$

where, R_1 , R_2 and R_3 are the equivalent lumped resistors, which account for the average losses in the passive components.

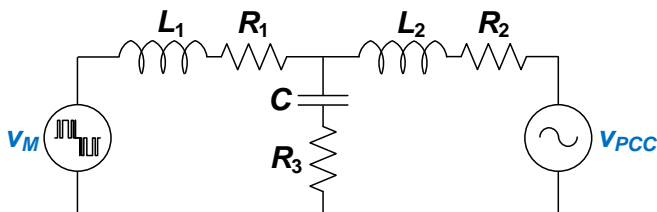


Fig. 5.2 Single-phase small signal model of the grid inverter with LCL filter including its parasitic resistances [J.2].

However, the effect of the damping may not be represented as a constant for all the operating condition if we consider how the loss in the magnetic inductor is created, e.g. it is dependent on the excitation voltage, its frequency and the current bias [29].

Therefore, the lumped parameter may not be able to model properly the damping behavior of the filter, which may still lead to have a mismatch in practice.

5.2.2. CONTROLLER DESIGN

The current controller can be deterministically designed optimally according to [76], assuming that the harmonic filter parameters are known. Then, the main controller parameters are as follows [76]:

$$\omega_c \approx \frac{\pi - \theta_m}{T_d} \quad (5.4)$$

$$k_p \approx \frac{\omega_c(L_1 + L_2)}{V_{dc}} \quad (5.5)$$

$$k_i \approx k_p \frac{\omega_c}{10} \quad (5.6)$$

where, the current controller proportional and integral gains are selected as a function of the desired crossover frequency ω_c and phase margin θ_m . The resulting designed system parameters are given in Table 5.1, which are derived considering the ratings of the *Inv. A* connected in the Cigré distribution network illustrated in Fig. 2.2, Section 2.1.

Table 5.1 System parameters for stability studies.

Symbol	Electrical Constant	Value
V_g	Grid voltage	400 V
f_1	Grid fundamental frequency	50 Hz
f_s	Switching/sampling frequency	10 kHz
V_{dc}	Converter dc-link voltage	700 V
S	Converter power rating	35 kVA
Δi_{max}	Converter current ripple	15%
L_1	LCL filter - converter-side inductance	0.71 mH
R_1	Parasitic resistance of L1	0.2035 Ω
L_2	LCL filter - grid-side inductance	0.22 mH
R_2	Parasitic resistance of L2	0.15 Ω
C	LCL filter - capacitance	22 μ F
R_3	Parasitic resistance of C	1 Ω
k_p	Proportional gain	5
k_i	Integral gain	1000

5.2.3. EVALUATION OF STABILITY MARGIN BY ROOT LOCUS

For stability analysis, it is suitable to consider only the proportional gain of the current controller [C.6]. Then, it is easy to be followed from (5.5) that the system stability is mainly influenced by the total inductance in the system. To illustrate this, the open loop gain root locus $T(s)$ of the grid-connected converter with LCL filter using Zero-Order Hold (ZOH) discretization is shown in Fig. 5.3.

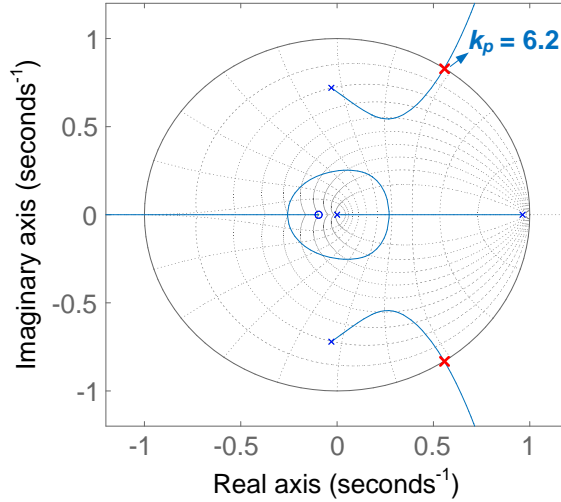


Fig. 5.3 Root locus of the discretized $T(s)$ in z -domain showing the stability margin of the power converter [J.2].

The proportional gain that leads to marginal instability is also illustrated (the proportional gain is placed at the unity circle). Recalling Fig. 5.1, a proportional gain above this value will cause the excitation of the filter resonant poles, which lead to instability. Even for a stable proportional gain, such as illustrated in Table 5.1, the system could approach instability if the total inductance ($L_1 + L_2$) in the system is changing.

The problem of the aforementioned stability analysis approach is that it assumes that the harmonic filter parameters are known. However, the impedance of the filter inductances given in (5.1) – (5.2) does not consider the inductor nonlinearity given by the magnetic hysteresis phenomena. This aspect is subject of discussion in the next sections.

5.3. INDUCTOR CHARACTERIZATION

5.3.1. LOSS IN THE FILTER INDUCTORS

In general, the inductor loss can be grouped into winding loss and core loss. The winding loss is created by the electrical resistance of the winding with the current flowing inside. As the frequency of the current increases, it causes a reduction in the effective conduction area of the winding, also called skin effect, which is highly dependent on the frequency [77], [78].

The core loss is composed of two major parts: one is the hysteresis loss and the other is the eddy current loss. Both are caused by the changing magnetic flux in the magnetic core. The hysteresis loss is known to be created by the magnetic domain wall movement in a core during the magnetizing and demagnetizing processes [79]. The eddy current loss is created by the induced voltage from the magnetic flux variation and it is frequency dependent as well, similar to the winding loss [77]. The consequence is that there are many factors combined together that makes it unclear which losses are related to the system damping and how it finally contributes to the converter stability. Therefore, only the influence of the hysteresis loss is considered in the following in order to decouple the effect of different loss mechanism that exists in the magnetic components and thereby the winding loss is neglected.

5.3.2. JILES-ATHERTON MODEL (JAH) FOR THE MAGNETIC HYSTERESIS

There are several implementation models of the magnetic hysteresis in the literature [80]–[83]. Unfortunately, there is no ready available model which can be used in common simulation platforms. The Jiles-Atherton hysteresis model (JAH) has gained more and more acceptance, because it includes the behavior of the magnetization process in a mathematical form [79]. Its accuracy have been demonstrated for several magnetics materials [84]–[86].

Since the existence of magnetic hysteresis behavior was discussed in [87], there have been various attempts to explain and explore the understanding of the hysteresis phenomena [80]–[83]. An idea about a frictional resistance to the spin of the magnetic domain (as the material is magnetized or demagnetized), is accepted as a possible reason of the hysteresis and it became the theoretical basis of JAH model [79]. It assumes there exist two different ways of magnetization; one is the reversible magnetization, which does not create loss and it is caused by the domain wall bulging; the other is the irreversible magnetization caused by displacements in the magnetic domain, resulting from their pinning sites and which exhibit loss that gives the well-known hysteresis characteristic.

There is an ideal magnetization characteristic called anhysteresis, which shows only the status of saturation under the magnetic field equivalent to a lossless hysteresis. It has a zero value when the magnetic field is zero and reach the saturation value as the magnetic field tends to infinity. In the following, a typical example of the anhysteresis magnetization M_{an} characteristic as a function of the effective magnetic field H_e is given, which shows the actual magnetic field experienced by the magnetic domain in the medium [79].

$$M_{an}(H_e) = M_s \left(\coth\left(\frac{H_e}{a}\right) - \frac{a}{H_e} \right) \quad (5.7)$$

where, $H_e = H + \alpha M$; M_s is the saturation magnetization; H is the applied magnetic field; a is a saturation slope factor; M is the magnetization of the medium and α a parameter for the inter-domain coupling [79].

This anhysteresis magnetization plays an important role in the JAH model. At each state of magnetization M and effective magnetic field H_e , the anhysteresis magnetization M_{an} becomes a reference point for the rate of change in M in the medium, which determines the trajectory of the B-H curve. It works for both irreversible magnetization M_{irr} and reversible magnetization M_{rev} in a differential form as follows:

$$\frac{dM_{irr}}{dH} = \frac{1}{\frac{\delta k}{\mu_0} - \alpha(M_{an} - M)} (M_{an} - M) \quad (5.8)$$

where, k is the irreversible magnetization coefficient. The coefficient δ takes the value 1 when H increases in the positive direction ($dH/dt > 0$), and -1 when H increases in the negative direction ($dH/dt < 0$), ensuring that the pinning oppose changes in the magnetization.

$$\frac{dM_{rev}}{dH} = c \left(\frac{dM_{an}}{dH} - \frac{dM}{dH} \right) \quad (5.9)$$

where, c is the magnetization coefficient and it is smaller than 1.

By summing (5.8) and (5.9), it leads to:

$$\frac{dM}{dH} = \frac{1}{(1+c)} \frac{1}{\frac{\delta k}{\mu_0} - \alpha(M_{an} - M)} (M_{an} - M) + \frac{c}{(1+c)} \frac{dM_{an}}{dH} \quad (5.10)$$

By replacing the above equation variables with the geometrical information of the core, such as the core cross-sectional area A_c , the mean magnetic field length l and the number of turns N , the terms in (5.10) can be related to the electrical quantities.

$$B = \mu_0 (H + M) \quad (5.11)$$

$$H l = N i \quad (5.12)$$

$$v = N \frac{d\phi}{dt} = N A_c \frac{dB}{dt} \quad (5.13)$$

where, i is the current passing the inductor winding, v is the voltage across the winding terminals, ϕ is the magnetic flux and B is the magnetic flux density.

5.3.3. IMPLEMENTATION OF THE INDUCTOR HYSTERESIS IN PSCAD/EMTDC

The Dommel's inductor model is illustrated in Fig. 5.4. Here, g_L is the equivalent conductance term and $I_L(t - \Delta t)$ is the history term containing the previous voltage $v_L(t - \Delta t)$ and $i_L(t - \Delta t)$.

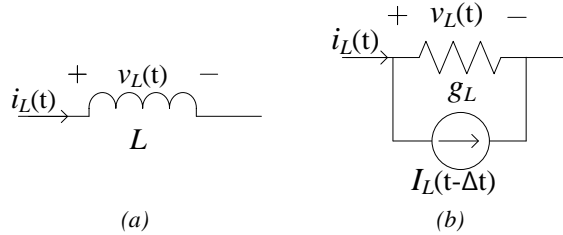


Fig. 5.4 Dommel's equivalence of an inductor: (a) Ideal inductor; (b) Practical inductor [J.2].

The inductor current relation can be derived as follows:

$$i_L(t) = g_L v_L(t) + I_L(t - \Delta t) \quad (5.14)$$

$$\text{where, } g_L = \frac{\Delta t}{2L} \text{ and } I_L = i_L(t - \Delta t) + g_L v_L(t - \Delta t)$$

The nonlinear term can be included by adding an additional current source in parallel with the component as a compensation source [40].

The relation between the magnetization and the magnetic field intensity is established in a differential equation form in (5.10) and the connections between the electrical quantities are listed (5.11) - (5.13). In order to implement the JAH model in PSCAD/EMTDC, the nonlinear differential equation has to be simplified in the form of a difference equation and it has to be updated for each simulation time step Δt . The underlying idea for this method, called the initial value problem, is to rewrite the variables, dy and dx into a differential equation $\frac{dy(x)}{dx} = f(x, y)$, with finite steps Δy and Δx . This gives algebraic formulas for the change in the functions when the independent variable x is "stepped" by one "stepsize" Δx . A good

approximation can be obtained by decreasing the step size to a very small value and by adding a small increment to the function at each step [88]. Therefore, (5.10) can be treated as a constant parameter β , which is determined at the time $(t - \Delta t)$ and the relations (5.11) - (5.13) are converted into difference equations and by applying the trapezoidal rule, they can be calculated iteratively [89].

$$\beta(t - \Delta t) = \frac{\Delta M}{\Delta H} = \frac{1}{(1+c)} \frac{1}{\delta k / \mu_0 - \alpha(M_{an} - M)} (M_{an} - M) + \left(\frac{c}{1+c} \right) \frac{dM_{an}}{dH} \quad (5.15)$$

$$\Delta H l = N \Delta i = N(i(t) - i(t - \Delta t)) \quad (5.16)$$

$$\frac{v(t) + v(t - \Delta t)}{2} = N A_c \frac{\Delta B}{\Delta t} \quad (5.17)$$

$$\frac{\Delta B}{\Delta H} = \mu_0 \left(1 + \frac{\Delta M}{\Delta H} \right) \quad (5.18)$$

By substituting (5.15) - (5.17) to (5.18) and isolate for $i(t)$ leads to,

$$i(t) = Q(t - \Delta t) v(t) + Q(t - \Delta t) v(t - \Delta t) + i(t - \Delta t) \quad (5.19)$$

$$\text{where, } Q(t - \Delta t) = \frac{1}{2} \frac{\Delta t l}{\mu_0 A_c N^2 (\beta(t - \Delta t) + 1)}$$

Therefore, the history term and the equivalent conductance term $Q(t - \Delta t)$ for the JAH inductor model are determined.

5.4. HARMONIC STABILITY SCENARIO WITH IMPROVED INDUCTOR MODEL

The improved version of the JAH is adopted and implemented in PSCAD/EMTDC. The developed model allows evaluating the actual behavior of the closed loop response of the power converters, which include the harmonic filter and its equivalent damping as result of the filter losses.

5.4.1. INDUCTOR HYSTERESIS MODEL SPECIFICATIONS

An arbitrary nonlinear inductor based on the JAH model is implemented in PSCAD/EMTDC with the main parameters given in Table 5.2. The coefficients of the JAH model can be found based on the considerations discussed in [84], [85]. The dimensions of the magnetic core and the number of turns are calculated in such a way to obtain a 0.71 mH inductance at rated current, as indicated in Table 5.1 (for the LCL filter converter side inductance). The resulting B-H dependencies of the implemented inductor hysteresis model are illustrated in Fig. 5.5 for sinusoidal and PWM voltage excitation.

The presence of the small dynamic minor hysteresis loops, which are superimposed to the main hysteresis loop (in the case of pulse excitation), leads to significant losses in the core compared with sinusoidal excitation [30], [74]. These core losses can be used to find a lumped resistance of the core, which accounts for the average core losses in the filter inductor, given by:

$$R_c = \frac{2P_c}{I_0^2} = 2P_c \left(\frac{N}{H_0 l} \right)^2 \quad (5.20)$$

where, R_c is the core resistance, P_c is the average core loss, and I_0 and H_0 are the rms output current and magnetic field strength, respectively. For the considered operating conditions of the power converter, the average core losses in the converter side inductance are around 112 W, which it translates into a 0.2035 Ω lumped core resistance.

Table 5.2 Inductor hysteresis model parameters for inductor L_1 [J.2].

Symbol	Meaning	Value
M_s	Saturated magnetization	1.6 E+6
a	JAH coefficient 1	5676.9
k	JAH coefficient 2	0.02
α	JAH coefficient 3	1 E-5
c	JAH coefficient 4	0.79
N	Number of turns	61
A_c	Cross-section area of the core	0.0018 m ²
l	Mean magnetic flux path length	0.2742 m

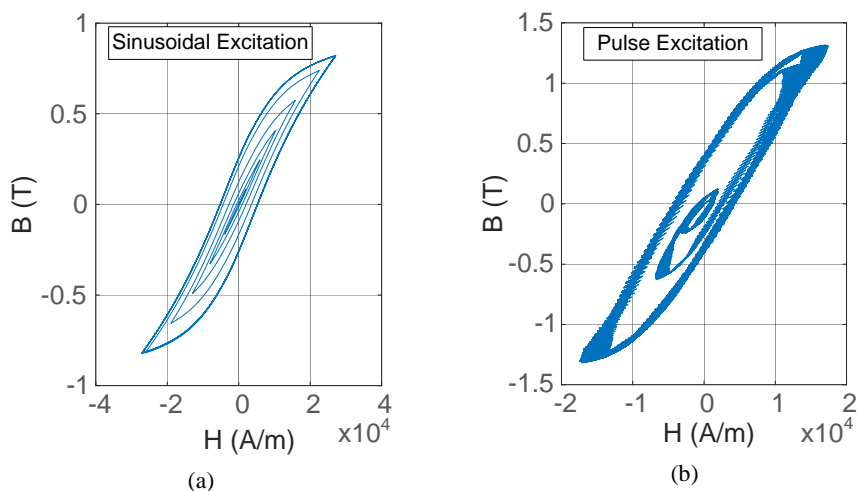


Fig. 5.5 B-H characteristics of the implemented inductor under: (a) Sinusoidal voltage excitation; (b) PWM voltage excitation [J.2].

5.4.2. INFLUENCE OF THE INDUCTOR HYSTERESIS MODEL ON THE STABILITY ANALYSIS

To investigate the differences between the hysteresis inductor model and the lumped inductor model, the calculated lumped core resistance can be used to ensure that the two inductor models have the same average power loss. Then, the stability analysis of the grid-connected power converter using the hysteresis and lumped model of the inductors are illustrated in Fig. 5.6.

The proportional gain of the current controller is increased to be marginal stable according to the analysis given in Section II. The results illustrated in Fig. 5.6 show that the power converter is unstable with the lumped inductor, which match the previous analysis.

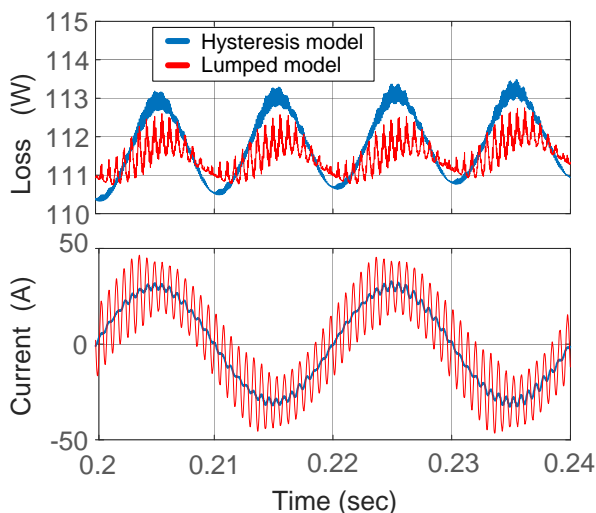


Fig. 5.6 Actual damping effect of the inductor hysteresis on the grid current waveforms for the hysteresis and lumped model of the converter side inductor ($k_p = 6.2$) [J.2].

However, the power converter is stable with the hysteresis inductor model, which shows how the actual core resistance has a frequency dependent damping behavior, which cannot be described with the lumped inductor model. Therefore, the stability analysis previously given in Section 5.2.3 cannot accurately describe the resonance interactions between the power converter and the utility grid, because the loss caused by the nonlinearity of the harmonic filter is not completely known. In short, even if the inductor hysteresis model and the lumped model have the same average power loss, the loss distribution is different, which leads to an increased damping effect from the inductor hysteresis model.

5.4.3. TRANSIENT RESPONSE OF THE VSC WITH HYSTERESIS MODEL OF THE FILTER INDUCTOR

The previous result considers the scenario where the proportional gain, which leads to marginal stability, was adopted in order to show that there is a better stability margin from the VSC with a hysteresis inductor model. However, when the system uses the designed proportional gain according to Table 5.1, both the inductor hysteresis and inductor lumped models will lead to stable output current waveforms at the PCC.

To illustrate the difference between the two models, the dynamic response of the VSC with hysteresis and lumped inductor models is illustrated in Fig. 5.7 with a load-step in the current. It shows that even the two models are stable, the overshoot during a load-step in the current is much higher for the lumped inductor model, which reveals again that the loss caused by the nonlinearity of the passive filter is not known and different results can be obtained compared to what is expected. The reason is that the small dynamic minor hysteresis loops, which cause significant losses cannot be modeled with a lumped resistance.

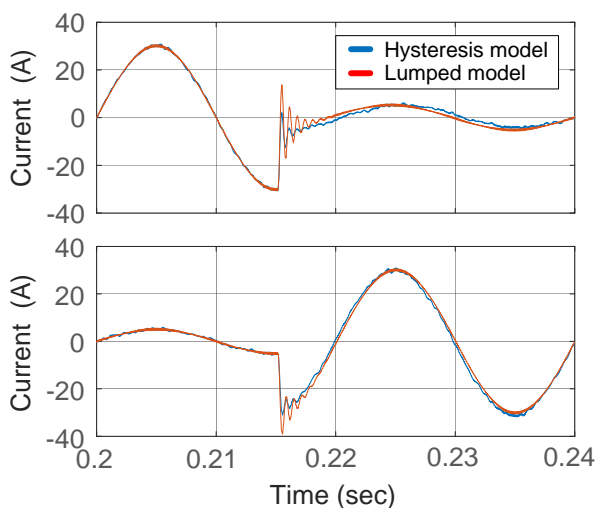


Fig. 5.7 Dynamic response of the grid-connected converter with hysteresis and lumped model of the converter side inductor ($k_p = 5$) [J.2].

5.5. SUMMARY

The importance of a more detailed representation of the converter side inductance in harmonic filters like the LCL filter was addressed in this chapter. It provides a more accurate stability evaluation for connection of modern power electronics based converters to the utility grid. The reason is that the converter side inductance is

excited with rectangular voltages, which result in small dynamic minor hysteresis loops of significant losses. To illustrate and describe the phenomena, a Jiles-Atherton hysteresis inductor model has been implemented in PSCAD/EMTDC to show the importance of the magnetic hysteresis. It reveals that the core loss in the converter side inductance provides more damping and therefore, increased stability margin for the power converter, compared with the conventional lumped resistor representation, which accounts for the same average power loss. Additionally, the dynamic response of the power converter with inductor hysteresis model and lumped inductor model reveals that the plant of the system given by the harmonic filter is not completely known during the design process of the current controllers. However, only the influence of the core loss given by the magnetic hysteresis has been under investigation. Since the JAH model has previously proved to model and describe the hysteresis accurately, the results presented here should be valid. For complete validation is required in the future to model also the frequency dependent winding loss and eddy current losses created by the induced voltage from the magnetic flux variation in order to have a full inductor model.

CHAPTER 6. CONCLUSIONS

The main conclusions of this work are given in this chapter. The purpose of this study was to find out the possible interaction problems among the interconnected VSCs in nowadays' power distribution system. Then, several contributions in this field are given.

6.1. SUMMARY

Possible instability scenarios, which are caused by the non-passive region of the VSCs, are investigated in this work and several solutions are discussed. Further, the optimal point for addressing the instability problem in the network is also found. In the end, a detailed model of the filter inductor in the VSC shows that the inherent damping in the inductor can diminish the interaction problem drastically.

In Chapter 1, the background, motivation and the objectives of this study are shown for given limitations of the system.

In Chapter 2, each element in the benchmark network is explained before proceeding to the main instability issues. The aim for this chapter is to focus more on the instability issues related among VSCs in the distribution network only and not to be mixed or coupled with other factors, such as the subharmonic oscillations or imbalanced loading condition. The three phase load is assumed to be balanced load and the positive sequence impedance of the transmission line (cable) is considered. The essential parts of the VSC are included in the model such as the PLL, current controller and harmonic filters.

In Chapter 3, two essential methods to analyze and evaluate the instability problem among multiple VSCs are addressed. The time domain simulation model of the network is explained in PSCAD as well as the principle operation of the Electro Magnetic Transient Program (EMTP). The frequency domain model for stability analysis is explained in this section by means of the Impedance Based Stability Criterion (IBSC). By expanding the IBSC it is possible further to approach the concept of Passivity, which can give a design guide-line for PE based units that can guarantee the stable operation of the network. Several other issues in implementing the IBSC are also mentioned.

In Chapter 4, the stability assessments for several scenarios are given. Firstly, the unstable operations of the paralleled converters are investigated and secondly, a more realistic benchmark network has been adopted and the stability analysis is performed. There are several ways to stabilize the unstable system by introducing additional damping into the system such as passive damping and active damping methods, and/or a specialized harmonic frequency damping unit called the active

damper. Also, the relative stability of the network is investigated by measuring the required damping at all nodes. The most adequate location for the stabilization of the network, which is the most unstable point in the network, can be found. This may show the risky index of the network.

In Chapter 5, the importance of a more detailed representation of the converter side inductance in harmonic filters like the LCL filter was addressed. It provides a more accurate stability evaluation for connection of modern power electronics based converters to the utility grid. The reason is that the converter side inductance is excited with rectangular voltages, which result in small dynamic minor hysteresis loops of significant losses. To illustrate and describe the phenomena, a Jiles-Atherton hysteresis inductor model has been implemented in PSCAD/EMTDC to show the importance of the magnetic hysteresis. It reveals that the core loss in the converter side inductance provides more damping and therefore, increased stability margin for the power converter, compared with the conventional lumped resistor representation, which accounts for the same average power loss. Additionally, the dynamic response of the power converter with inductor hysteresis model and lumped inductor model reveals that the plant of the system given by the harmonic filter is not completely known during the design process of the current controllers.

In Chapter 6, the main conclusions and contributions of the work are highlighted.

6.2. CONTRIBUTIONS

The contributions of this study can be summarized as follows.

- Identification of the unstable conditions among the multi-paralleled VSCs in the power system: interaction problem caused by the parallel VSCs with LCL filters are found in time domain simulation. The reasonable behavior of the LCL filter in the VSC may bring other VSCs connected to the same network to be unstable. Resonances in the grid impedance can also bring the VSC to become unstable.
- Modeling and investigation of the harmonic interaction problems of power electronics based power systems: by using the IBSC approach, those unstable cases among the parallel VSCs are identified in the frequency domain. The Nyquist stability criterion can help us to find a possible cause of the unstable closed loop poles based on the impedance relations in the system.
- Stabilization methods to deal with the high frequency resonance interactions at system level: the effect of existing damping solutions in the test system are evaluated and include passive or active damping methods of the VSC, and/or the use of an external damping unit, called active

damper.

- A stability map of the network for a more effective stabilization: by adopting the IBSC for all nodes in the network, the relative stability of the individual node is compared. By introducing one of the damping solutions to the most unstable node, the unstable system can be effectively stabilized.
- Influence of the filter inductor hysteresis on stability analysis: the damping effect on system stability from the loss of the magnetic hysteresis in the filter inductor is discussed. Time domain simulation based on the Jiles-Atherton hysteresis model is performed and a comparison with the conventional lumped loss model has been made.

6.3. FUTURE WORKS

Newly obtained research questions in relation to this study can be:

- In stability analysis of a small scale power distribution system, the the IBSC may not be able to predict the harmonic instabilities unless a full degree of inherent system damping is considered.
 - Generalized hysteresis modeling for anisotropic materials is needed. There are many anisotropic magnetic materials which are widely used in PE application. In order to include those hysteresis characteristics into the stability analysis, a generalized model of JAH should be adopted.
 - Copper loss is also an important damping element of the system. Losses created inside of the conductor also have a significant effect in the stability analysis. The main reasons are the proximity effect and the skin effect of the conductor.
- Load is also an important part of the power system stability analysis as it is also a PE based power unit. Many of them are having the constant power load characteristic which violates the passivity theorem inherently and it may also be the reason of instability in the system as well.

LITERATURE LIST

- [1] F. Blaabjerg, Z. Chen, and S. B. Kjaer, "Power Electronics as Efficient Interface in Dispersed Power Generation Systems," *IEEE Trans. Power Electron.*, vol. 19, no. 5, pp. 1184–1194, Sep. 2004.
- [2] EU, "2030 Energy Strategy." [Online]. Available: <https://ec.europa.eu/energy/en/topics/energy-strategy/2030-energy-strategy>.
- [3] Frankfurt School-UNEP Centre/BNEF. 2016., "GLOBAL TRENDS IN RENEWABLE ENERGY INVESTMENT 2016," 2016.
- [4] T. Force, "Benchmark Systems for Network Integration of Renewable and Distributed Energy Resources," no. April, p. 63, 2014.
- [5] E. J. Coster, J. M. A. Myrzik, B. Kruimer, and W. L. Kling, "Integration Issues of Distributed Generation in Distribution Grids," *Proc. IEEE*, vol. 99, no. 1, pp. 28–39, Jan. 2011.
- [6] M. Glinkowski, J. Hou, and G. Rackliffe, "Advances in Wind Energy Technologies in the Context of Smart Grid," *Proc. IEEE*, vol. 99, no. 6, pp. 1083–1097, Jun. 2011.
- [7] J. H. R. Enslin and P. J. M. Heskes, "Harmonic Interaction Between a Large Number of Distributed Power Inverters and the Distribution Network," *IEEE Trans. Power Electron.*, vol. 19, no. 6, pp. 1586–1593, Nov. 2004.
- [8] HOPEWIND, "Several Key Technical Problems of Grid-Connected Inverter," *China wind Power Center*. [Online]. Available: <http://www.cwpc.cn/cwpp/files/1314/1050/5552/6.-.pdf>.
- [9] T. Tsanova, "Germany's DolWin2 offshore link is off for repairs," 2016. [Online]. Available: <http://renewables.seenews.com/news/germanys-dolwin2-offshore-link-is-off-for-repairs-529905>.
- [10] I. Shumkov, "Dong's Anholt offshore wind farm shuts down due to new cable fault," 2015. [Online]. Available: <http://renewables.seenews.com/news/dongs-anholt-offshore-wind-farm-shuts-down-due-to-new-cable-fault-464750>.
- [11] T. Tsanova, "Denmark's Anholt offshore wind farm back online with fixed cable," 2015. [Online]. Available: <http://renewables.seenews.com/news/denmarks-anholt-offshore-wind-farm-back-online-with-fixed-cable-502705>.

- [12] A. Oliveira, “Third-party cable fault keeps WindFloat 1 power off grid,” 2016. [Online]. Available: <http://www.rechargenews.com/wind/1423623/third-party-cable-fault-keeps-windfloat-1-power-off-grid>.
- [13] E. Möllerstedt and B. Bernhardsson, “Out of control because of harmonics. An analysis of the harmonic response of an inverter locomotive,” *IEEE Control Syst. Mag.*, vol. 20, no. 4, pp. 70–81, 2000.
- [14] L. Harnefors, A. G. Yepes, A. Vidal, and J. Doval-Gandoy, “Passivity-Based Stabilization of Resonant Current Controllers With Consideration of Time Delay,” *IEEE Trans. Power Electron.*, vol. 29, no. 12, pp. 6260–6263, Dec. 2014.
- [15] P. M. Anderson, B. L. Agrawal, and J. E. Van Ness, Eds., *Subsynchronous resonance in power systems*. New York: IEEE PRESS, 1990.
- [16] “Photovoltaic Power Systems in Theory and Practice (PVPS).” Aalborg University, 2016.
- [17] F. F. da Silva and C. L. Bak, *Electromagnetic Transients in Power Cables*, vol. 72. 2013.
- [18] H.-D. Fulop, K. Didriksen Lund, and Y. W. Foo, “EPSH 2-831 Distribution Cable Modelling,” 2015.
- [19] International Electrotechnical Commission, “IEC 62040-3:2011.” IEC, 2011.
- [20] D. G. Holmes and T. A. Lipo, *Pulse Width Modulation for Power Converters: Principles and Practice*. John Wiley & Sons, 2003.
- [21] “IEEE Recommended Practice and Requirements for Harmonic Control in Electric Power Systems,” *IEEE Std 519-2014 (Revision of IEEE Std 519-1992)*. IEEE Standards Association, New York, pp. 1–29, 2014.
- [22] S. K. Chaudhary, “PhD Course: An Introduction to HVDC and MTDC Transmission System.” Aalborg University, 2016.
- [23] V. Kaura and V. Blasko, “Operation of a phase locked loop system under distorted utility conditions,” *IEEE Trans. Ind. Appl.*, vol. 33, no. 1, pp. 58–63, 1997.
- [24] R. Teodorescu, M. Liserre, and P. Rodriguez, *Grid Converters for Photovoltaic and Wind Power Systems*. Wiley, 2011.

- [25] X. Wang, F. Blaabjerg, and P. C. Loh, "An Impedance-Based Stability Analysis Method for Paralleled Voltage Source Converters," in *Proc. The 2014 International Power Electronics Conference*, 2014, pp. 1529–1535.
- [26] L. Harnefors, a G. Yepes, a Vidal, and J. Doval-Gandoy, "Passivity-Based Controller Design of Grid-Connected VSCs for Prevention of Electrical Resonance Instability," vol. 62, no. 2, pp. 702–710, 2015.
- [27] D. Dong, B. Wen, D. Boroyevich, P. Mattavelli, and Y. Xue, "Analysis of Phase-Locked Loop Low-Frequency Stability in Three-Phase Grid-Connected Power Converters Considering Impedance Interactions," *IEEE Trans. Ind. Electron.*, vol. 62, no. 1, pp. 310–321, Jan. 2015.
- [28] V. Blasko and V. Kaura, "A new mathematical model and control of a three-phase AC-DC voltage source converter," *IEEE Trans. Power Electron.*, vol. 12, no. 1, pp. 116–123, 1997.
- [29] T. Shimizu and S. Iyasu, "A practical iron loss calculation for AC filter inductors used in PWM inverters," *IEEE Trans. Ind. Electron.*, vol. 56, no. 7, pp. 2600–2609, 2009.
- [30] J. Muhlethaler, M. Schweizer, R. Blattmann, J. W. Kolar, and A. Ecklebe, "Optimal Design of LCL Harmonic Filters for Three-Phase PFC Rectifiers," *IEEE Trans. Power Electron.*, vol. 28, no. 7, pp. 3114–3125, Jul. 2013.
- [31] M. S. Rylko, K. J. Hartnett, J. G. Hayes, and M. G. Egan, "Magnetic Material Selection for High Power High Frequency Inductors in DC-DC Converters," in *Proc. of IEEE Applied Power Electronics Conference and Exposition*, 2009, pp. 2043–2049.
- [32] Y. Jiao and F. C. Lee, "LCL Filter Design and Inductor Current Ripple Analysis for a Three-Level NPC Grid Interface Converter," *IEEE Trans. Power Electron.*, vol. 30, no. 9, pp. 4659–4668, Sep. 2015.
- [33] R. N. Beres, X. Wang, M. Liserre, F. Blaabjerg, and C. L. Bak, "A Review of Passive Power Filters for Three-Phase Grid-Connected Voltage-Source Converters," *IEEE J. Emerg. Sel. Top. Power Electron.*, vol. 4, no. 1, pp. 54–69, Mar. 2016.
- [34] H. Dommel, "Digital Computer Solution of Electromagnetic Transients in Single-and Multiphase Networks," *IEEE Trans. Power Appar. Syst.*, vol. PAS-88, no. 4, pp. 388–399, Apr. 1969.

- [35] R. C. Dorf and R. H. Bishop, *Modern control systems, 10th edition*, 10th ed. Prentice Hall, 2005.
- [36] R. D. Middlebrook, "Input filter considerations in design and application of switching regulators," in *Proc. IEEE Ind. Appl. Soc. Annu. Meeting*, 1976, pp. 91–107.
- [37] J. Sun, "Impedance-Based Stability Criterion for Grid-Connected Inverters," *IEEE Trans. Power Electron.*, vol. 26, no. 11, pp. 3075–3078, Nov. 2011.
- [38] L. H. L. Z. M. Bongiorno, L. Harnefors, L. Zhang, and M. Bongiorno, "Frequency-domain passivity-based current controller design," *IET Power Electron.*, vol. 1, no. 4, p. 455, 2008.
- [39] R. A. Decarlo and P.-M. Lin, *Linear Circuit Analysis : Time Domain, Phasor, and Laplace Transform Approaches*. Oxford Press, 2001.
- [40] A. M. Gole, "Power Systems Transient Simulation." University of Manitoba, p. Course Notes, 1998.
- [41] J. Sun, "Small-Signal Methods for AC Distributed Power Systems—A Review," *IEEE Trans. Power Electron.*, vol. 24, no. 11, pp. 2545–2554, Nov. 2009.
- [42] J. Wyatt, L. Chua, J. Gannett, I. Goknar, and D. Green, "Energy concepts in the state-space theory of nonlinear n-ports: Part I—Passivity," *IEEE Trans. Circuits Syst.*, vol. 28, no. 1, pp. 48–61, Jan. 1981.
- [43] H. Bai, X. Wang, P. C. Loh, and F. Blaabjerg, "Passivity Enhancement of Grid-Tied Converter by Series LC-Filtered Active Damper," in *7th IEEE Energy Conversion Congress and Exposition, ECCE 2015*, 2015.
- [44] I. Queinnec, L. Martinez-Salamero, C. Alonso, A. Cid-Pastor, R. Leyva, and S. Tarbouriech, "Passivity-based integral control of a boost converter for large-signal stability," *IEE Proc. - Control Theory Appl.*, vol. 153, no. 2, pp. 139–146, Mar. 2006.
- [45] A. Riccobono and E. Santi, "Comprehensive Review of Stability Criteria for DC Power Distribution Systems," *IEEE Trans. Ind. Appl.*, vol. 50, no. 5, pp. 3525–3535, Sep. 2014.
- [46] D. C. Youla, L. J. Castriota, and H. J. Carlin, "Bounded Real Scattering Matrices and the Foundations of Linear Passive Network Theory," *IRE Trans. Circuit Theory*, vol. 6, no. 1, pp. 102–124, 1959.

- [47] A. Riccobono and E. Santi, "A novel Passivity-Based Stability Criterion (PBSC) for switching converter DC distribution systems," *Proc. IEEE 27th Appl. Power Electron. Conf. Expo.*, pp. 2560–2567, Feb. 2012.
- [48] X. Wang, F. Blaabjerg, and P. C. Loh, "Proportional derivative based stabilizing control of paralleled grid converters with cables in renewable power plants," in *2014 IEEE Energy Conversion Congress and Exposition (ECCE)*, 2014, pp. 4917–4924.
- [49] S. G. Parker, B. P. McGrath, and D. G. Holmes, "Regions of Active Damping Control for LCL Filters," *IEEE Trans. Ind. Appl.*, vol. 50, no. 1, pp. 424–432, Jan. 2014.
- [50] M. Huang, X. Wang, P. C. Loh, and F. Blaabjerg, "LLCL-Filtered Grid Converter with Improved Stability and Robustness," *IEEE Trans. Power Electron.*, vol. PP, no. 99, pp. 1–1, 2015.
- [51] Y. Tang, W. Yao, P. Loh, and F. Blaabjerg, "Design of LCL-Filters with LCL Resonance Frequencies beyond the Nyquist Frequency for Grid-Connected Converters," *IEEE J. Emerg. Sel. Top. Power Electron.*, vol. PP, no. 99, pp. 1–1, 2015.
- [52] L. Corradini, P. Mattavelli, M. Corradin, and F. Polo, "Analysis of Parallel Operation of Uninterruptible Power Supplies Loaded Through Long Wiring Cables," *IEEE Trans. Power Electron.*, vol. 25, no. 4, pp. 1046–1054, Apr. 2010.
- [53] F. Liu, J. Liu, H. Zhang, and D. Xue, "Stability Issues of Z+Z Type Cascade System in Hybrid Energy Storage System (HESS)," *IEEE Trans. Power Electron.*, vol. 29, no. 11, pp. 5846–5859, Nov. 2014.
- [54] X. Wang, F. Blaabjerg, M. Liserre, Z. Chen, J. He, and Y. Li, "An Active Damper for Stabilizing Power-Electronics-Based AC Systems," *IEEE Trans. Power Electron.*, vol. 29, no. 7, pp. 3318–3329, Jul. 2014.
- [55] W. Wu, Y. He, T. Tang, and F. Blaabjerg, "A New Design Method for the Passive Damped LCL and LLCL Filter-Based Single-Phase Grid-Tied Inverter," *IEEE Trans. Ind. Electron.*, vol. 60, no. 10, pp. 4339–4350, Oct. 2013.
- [56] R. Peña-Alzola, M. Liserre, F. Blaabjerg, R. Sebastián, J. Dannehl, and F. W. Fuchs, "Analysis of the Passive Damping Losses in LCL-Filter-Based Grid Converters," *IEEE Trans. Power Electron.*, vol. 28, no. 6, pp. 2642–2646, Jun. 2013.

- [57] D. Pan, X. Ruan, C. Bao, W. Li, and X. Wang, "Capacitor-Current-Feedback Active Damping With Reduced Computation Delay for Improving Robustness of LCL-Type Grid-Connected Inverter," *IEEE Trans. Power Electron.*, vol. 29, no. 7, pp. 3414–3427, Jul. 2014.
- [58] C. Bao, X. Ruan, X. Wang, W. Li, D. Pan, and K. Weng, "Step-by-Step Controller Design for LCL-Type Grid-Connected Inverter with Capacitor–Current-Feedback Active-Damping," *IEEE Trans. Power Electron.*, vol. 29, no. 3, pp. 1239–1253, Mar. 2014.
- [59] M. Liserre, R. Teodorescu, and F. Blaabjerg, "Stability of photovoltaic and wind turbine grid-connected inverters for a large set of grid impedance values," *IEEE Trans. Power Electron.*, vol. 21, no. 1, pp. 263–272, Jan. 2006.
- [60] X. Wang, X. Ruan, S. Liu, and C. K. Tse, "Full Feedforward of Grid Voltage for Grid-Connected Inverter With LCL Filter to Suppress Current Distortion Due to Grid Voltage Harmonics," *IEEE Trans. Power Electron.*, vol. 25, no. 12, pp. 3119–3127, Dec. 2010.
- [61] H. Bai, X. Wang, P. Loh, and F. Blaabjerg, "Passivity Enhancement of Grid-Tied Converters by Series LC-Filtered Active Damper," *IEEE Trans. Ind. Electron.*, pp. 1–1, 2016.
- [62] H. Akagi, "Control strategy and site selection of a shunt active filter for damping of harmonic propagation in power distribution systems," *IEEE Trans. Power Deliv.*, vol. 12, no. 1, pp. 354–363, 1997.
- [63] L. Fangcheng, L. Jinjun, Z. Haodong, X. Danhong, H. S. Ul, and Z. Linyuan, "Stability issues of Z+Z or Y+Y type cascade system," *2013 IEEE Energy Convers. Congr. Expo.*, no. 2, pp. 434–441, Sep. 2013.
- [64] A. M. Hava, T. A. Lipo, and W. L. Erdman, "Utility interface issues for line connected PWM voltage source converters: a comparative study," in *Proc. of IEEE Applied Power Electronics Conference and Exposition*, 1995, pp. 125–132.
- [65] M. Liserre, F. Blaabjerg, and S. Hansen, "Design and Control of an LCL-Filter-Based Three-Phase Active Rectifier," *IEEE Trans. Ind. Appl.*, vol. 41, no. 5, pp. 1281–1291, Sep. 2005.
- [66] M. Malinowski and S. Bernet, "A Simple Voltage Sensorless Active Damping Scheme for Three-Phase PWM Converters With an LCL Filter," vol. 55, no. 4, pp. 1876–1880, 2008.

- [67] J. Dannehl, M. Liserre, and F. W. Fuchs, "Filter-Based Active Damping of Voltage Source Converters With LCL Filter," *IEEE Trans. Ind. Electron.*, vol. 58, no. 8, pp. 3623–3633, Aug. 2011.
- [68] M. Liserre, a. Dell'Aquila, and F. Blaabjerg, "Genetic Algorithm-Based Design of the Active Damping for an LCL-Filter Three-Phase Active Rectifier," *IEEE Trans. Power Electron.*, vol. 19, no. 1, pp. 76–86, Jan. 2004.
- [69] T. C. Y. Wang, Z. Ye, G. Sinha, and X. Yuan, "Output filter design for a grid-interconnected three-phase inverter," in *Proc. of IEEE 34th Annual Conference on Power Electronics Specialist, 2003. PESC '03.*, 2003, vol. 2, pp. 779–784.
- [70] M. Liserre, S. Member, F. Blaabjerg, and R. Teodorescu, "Grid Impedance Estimation via Excitation of LCL -Filter Resonance," vol. 43, no. 5, pp. 1401–1407, 2007.
- [71] E. Twining and D. G. Holmes, "Grid current regulation of a three-phase voltage source inverter with an LCL input filter," *IEEE Trans. Power Electron.*, vol. 18, no. 3, pp. 888–895, May 2003.
- [72] M. Liserre, F. Blaabjerg, and A. Dell'Aquila, "Step-by-step design procedure for a grid-connected three-phase PWM voltage source converter," *Int. J. Electron.*, vol. 91, no. 8, pp. 445–460, Aug. 2004.
- [73] M. Liserre, R. Teodorescu, and F. Blaabjerg, "Stability of photovoltaic and wind turbine grid-connected inverters for a large set of grid impedance values," *IEEE Trans. Power Electron.*, vol. 21, no. 1, pp. 263–272, Jan. 2006.
- [74] R. Beres, X. Wang, and F. Blaabjerg, "Evaluation of Core Loss in Magnetic Materials Employed in Utility Grid AC Filters," 2016, pp. 3051–3057.
- [75] S. G. Parker, B. P. McGrath, D. G. Holmes, S. Member, B. P. McGrath, and D. G. Holmes, "Regions of Active Damping Control for LCL Filters," *IEEE Trans. Ind. Appl.*, vol. 50, no. 1, pp. 424–432, Jan. 2014.
- [76] D. G. Holmes, T. a. Lipo, B. P. McGrath, and W. Y. Kong, "Optimized Design of Stationary Frame Three Phase AC Current Regulators," *IEEE Trans. Power Electron.*, vol. 24, no. 11, pp. 2417–2426, Nov. 2009.

- [77] N. Igarashi, M. Uozumi, T. Kosuge, and A. Sato, "Pure Iron Based Soft Magnetic Composite Core That Enables Downsizing Automotive Reactors," pp. 98–103.
- [78] R. W. Erickson and D. Maksimović, *Fundamentals of Power Electronics*. Boston, MA: Springer US, 2001.
- [79] D. C. Jiles and D. L. Atherton, "Theory of ferromagnetic hysteresis," *J. Magn. Magn. Mater.*, vol. 61, no. 1–2, pp. 48–60, Sep. 1986.
- [80] G. Wildermann, "Magnetic Researches," *Philos. Mag. J. Sci.*, vol. 22, no. 5, p. 50, 1886.
- [81] J. Brauer, "Simple equations for the magnetization and reluctivity curves of steel," *IEEE Trans. Magn.*, vol. 11, no. 1, pp. 81–81, Jan. 1975.
- [82] J. Rivas, J. Zamarro, E. Martin, and C. Pereira, "Simple approximation for magnetization curves and hysteresis loops," *IEEE Trans. Magn.*, vol. 17, no. 4, pp. 1498–1502, Jul. 1981.
- [83] M. Rahman, M. Poloujadoff, R. Jackson, J. Perard, and S. Gowda, "Improved algorithms for digital simulation of hysteresis processes in semi hard magnetic materials," *IEEE Trans. Magn.*, vol. 17, no. 6, pp. 3253–3255, Nov. 1981.
- [84] A. Ramesh, D. C. Jiles, and Y. Bi, "Generalization of hysteresis modeling to anisotropic materials," *J. Appl. Phys.*, vol. 81, no. 8, p. 5585, 1997.
- [85] R. Szewczyk, "Validation of the anhysteretic magnetization model for soft magnetic materials with perpendicular anisotropy," *Materials (Basel)*, vol. 7, no. 7, pp. 5109–5116, 2014.
- [86] D. C. Jiles, J. B. Thoenke, and M. K. Devine, "Numerical determination of hysteresis parameters for the modeling of magnetic properties using the theory of ferromagnetic hysteresis," *IEEE Trans. Magn.*, vol. 28, no. 1, pp. 27–35, 1992.
- [87] J. C. Maxwell, *A Treatise on Electricity and Magnetism*. Oxford, 1873.
- [88] W. H. Press, S. A. Teukolsky, W. T. Vetterling, and B. P. Flannery, *Numerical recipes: The art of scientific computing*, 3rd ed. Cambridge University Press, 2007.

- [89] U. D. Annakkage, P. G. McLaren, E. Dirks, R. P. Jayasinghe, and A. D. Parker, "A current transformer model based on the Jiles-Atherton theory of ferromagnetic hysteresis," *IEEE Trans. Power Deliv.*, vol. 15, no. 1, pp. 57–61, 2000.

Appendix A. Code for JAH model

The source code of the implemented subroutine of the JAH model in the PSCAD/EMTDC is given in the following.

```

=====
SUBROUTINE MYSUB_CFG_DEBUG(SS,NBR)

    INTEGER SS ! Subsystem number
    INTEGER NBR ! Branch number

    CALL CURRENT_SOURCE2_CFG(NBR,SS)! Sets DEFRRDBR to TRUE and
    GEQ to 0.0
END
=====
SUBROUTINE MYSUB_EXE_DEBUG(SS,NBR,D1,D2,D3,D4,D5)
!
INCLUDE 'nd.h'
INCLUDE 's0.h'
INCLUDE 's1.h'
INCLUDE 'branches.h'
INCLUDE 'rtconfig.h'
INCLUDE 'emtstor.h'
INCLUDE 'warn.h'
INCLUDE 'emtconst.h'

!!!!!!!!!!!!!!!!!!!!!!!!LOCAL VARIABLES!!!!!!!!!!!!!!!!!!!!!!!!
REAL c,k,mu0,alfa,Ms,a,N,Ac,l
REAL V0,I0,dMdH0,H0,M0,He0,Hea0,Man0,dMandH0,Q0,G0,V_1
REAL dMdH_1,H_1,M_1,delM,del,INEW
REAL D1,D2,D3,D4,D5

INTEGER SS ! Subsystem number
INTEGER NBR ! Branch number

INTEGER MYSTORF

MYSTORF = NSTORF
NSTORF = NSTORF + 4

!!!!!!!!!!!!!!!!!!!!!!!!Constants!!!!!!!!!!!!!!!!!!!!!!!!!!!!
c = 0.15
k = 0.5
mu0 = 4.0*PI_*1.0E-7

```

APPENDIX A. CODE FOR JAH MODEL

```

alfa = 3.0E-2
Ms = 1.6E6
a = 1100.0
N = 100.0
Ac = 0.0005
l = 0.25
!!!!!!!!!!!!!!!!!!!!!!!!!!!!!!!!!!!!!!!!!!!!!!!!!!!!!!!!!!!!!!

IF (TIMEZERO) THEN
STORF(MYSTORF) = 0.0
STORF(MYSTORF+1) = 0.0
STORF(MYSTORF+2) = 0.0
STORF(MYSTORF+3) = 0.0
STORF(MYSTORF+4) = 0.0
ENDIF

H_1 = STORF(MYSTORF)
M_1 = STORF(MYSTORF+1)
B_1 = STORF(MYSTORF+2)
V_1 = STORF(MYSTORF+3)

V0 = VBRANCH(SS,NBR)
I0 = CBR(NBR,SS)

B0 = (V0+V_1)/(2.0*Ac*N)*DELT+B_1 !Trapezoidal method
H0 = N/l*I0
M0 = B0/mu0-H0

He0 = M0*alfa+H0
Hea0 = He0/a

xrng = 0.002236068865 ! For tolerance range := 0.1e-5

IF ((Hea0.LT.-xrng).OR.(Hea0.GT.xrng)) THEN
Man0 = Ms * (1.0/TANH(Hea0)-1.0/Hea0)
dMandH0 = Ms/a*(1.0 - 1.0/(TANH(Hea0)**2.0)+ 1.0/Hea0**2.0)
ELSE
Man0 = 0.0
dMandH0 = Ms/a/3.0 !!! dManH0 can be approximated as one value for limiting its
range.
ENDIF

IF (((Man0.GT.M0).AND.(H0.LT.H_1)).OR.((Man0.LT.M0).AND.(H0.GE.H_1)))
THEN

```

```

delM = 0.0
ELSE
delM = 1.0
ENDIF

IF (H0 .LT. H_1) THEN
del = -1.0
ELSE
del = 1.0
ENDIF
dMdH0=delM*(Man0-M0)/((1.0+c)*(del*k/mu0-alfa*(Man0-
M0)))+c*dMandH0/(1.0+c)
Q0 = mu0*(dMdH0+1.0)

G0 = DELT*I/(Q0*N**2.0*Ac)*0.5
INEW = G0*V0 + I0

STORF(MYSTORF) = H0
STORF(MYSTORF+1) = M0
STORF(MYSTORF+2) = B0
STORF(MYSTORF+3) = V0

D1 = G0
D2 = Man0
D3 = dMdH0
D4 = B0
D5 = H0
!
CALL CURRENT_SOURCE2_EXE(NBR,SS,G0,INEW)
RETURN
END

```


ISSN (online): 2446-1636
ISBN (online): 978-87-7112-861-1

AALBORG UNIVERSITY PRESS